# Studies on Thioether Oxidation Under Light Irradiation and Electrochemical Transformation of Alkenes

**PIJUSH KANTI ROY**

**2023**

# Studies on Thioether Oxidation Under Light Irradiation and Electrochemical Transformation of Alkenes

PIJUSH KANTI ROY

Student ID: 1416212701

Department of Applied Chemistry

Graduate School of Science and Engineering

Doshisha University, Japan

2023

# PREFACE

Light energy constitutes a renewable, clean, and economical source of power. It is indispensable for photosynthesis in plants, contributing to oxygen production, a gas vital for human respiration. Additionally, light energy is harnessed in many technologies, pharmaceutical developments, and diverse research endeavors, positioning it as a superior green energy source to alternatives such as thermal energy and biofuels. Photocatalysis leverages photon energy to generate chemical energy, a process employed in water splitting, decomposition of organic pollutants, reduction of carbon dioxide, organic synthesis, and selective oxidation. Heterocyclic compounds, recognized for their potent physiological activities, require innovative and efficient chemical transformations to synthesize complex cyclic structures from simple starting materials. Radical addition and cyclization methodologies are a formidable strategy in synthesizing heterocyclic compounds, offering advantages over overreactions such as the aza-Diels-Alder, exemplified by the synthesis of tetrahydropyridines.

Furthermore, epoxides are crucial intermediates in producing numerous chemical products, including epoxy resins and pharmaceuticals, typically synthesized through oxygen-atom transfer reactions with olefins. The conventional epoxidation of alkenes often involves using peroxides, such as *tert*-butyl hydroperoxide, peracetic acid, or *m*-chloroperoxybenzoic acid, or is carried out via chlorohydrin. These methods, however, are fraught with handling challenges and generate undesired stoichiometric by-products. Such drawbacks can be circumvented by synthesizing an active oxidizing agent in situ.

In this study, I focused on the two novel methodologies have been discovered for generating thioalkyl radicals through one-electron oxidation followed by deprotonation from thioanisole through blue light irradiation. The first approach involves irradiating an electron donor acceptor (EDA) complex formed between electron donor thioanisole and an electron-deficient alkene benzylidenemalononitrile (BMN) under blue light irradiation, leading to form the carbon-carbon bonds of donor and acceptor molecules. Secondly, the reaction rate was accelerated in the presence of titanium dioxide. It occurs through charge transfer from thioanisole to the conduction band of titanium dioxide photocatalyst upon blue light irradiation. When maleimides were employed, an annulation reaction with thioanisole derivatives under blue light irradiation yielded thiochromenopyrrolediones in the presence of $TiO_2$, C–C bond formation can be achieved without the formation of an EDA complex. In addition, it was investigated the aerobic oxidation of thioanisole derivatives under irradiation by a 370 nm wavelength ultraviolet LED lamp.

Moreover, inspired by Tanaka's work, another method has examined the electrochemical epoxidation via in situ electrochemical generation of percarbonate by using manganese-salen complex as a mediator in an organic solvent-aqueous carbonate two-phase system in a simple undivided cell. As I expected, electrochemical epoxidation of styrene derivatives proceeded when a BDD was used as an anode.

Kyoto, Japan
November, 2023                                                                                      **Pijush Kanti Roy**

# CONTENTS

# GENERAL INTRODUCTION

Light energy is a renewable power source and a fundamental pillar in driving advancements across many scientific disciplines. Its critical role in photosynthesis extends beyond facilitating oxygen production to underpinning the sustenance of life. Beyond essential photosynthetic functions, light energy's exploitation is pivotal at the vanguard of innovations in technology, pharmaceuticals, and a wide array of research endeavors, firmly establishing it as an unrivaled source of green energy.

In photocatalysis, photon energy is skillfully transformed into chemical energy, driving essential reactions such as water splitting, degradation of organic pollutants, carbon dioxide reduction, and complex organic syntheses. These applications underscore the integral role of light energy in the progression of green chemistry.

Substantial research has explored novel functionalization techniques for thioethers, given their prevalence in natural products, agrochemicals, pharmaceuticals, materials, and oxidized congeners. Researchers have been fascinated by using visible light as a trigger to transform chemical processes to create a greener way in synthetic chemistry.[1,2] Photochemical reaction open up a new avenue in compound synthesis, comparing efficiently with traditional thermal methods.[3] Recently, some research groups have developed many photocahemical methods and dramatically changed the situation, which is the toolbox of modern synthetic chemistry.[4] Advances in the field have been mainly motivated by photoredox catalysis.[5] This technique relies on the presence of colored photocatalysts to generate radical species[6] that absorb visible light energy under mild reaction conditions.[7] In recent years, synthetic chemists have reported photochemical reactions in the absence of photoredox catalysts following electron donor-acceptor (EDA) complexes. The association of an electron-rich donor and an electron-deficient acceptor compounds can form a new aggregate of molecules in the ground state called an EDA complex.[8] This EDA complex absorb visible light but the two precursors do not. A single electron transfer (SET) upon visible light irradiation is used as a trigger to generate radical intermadiates under mild photoreaction conditions.[9] The photochemical generation of radicals for carbon-carbon bond formation has been the subject of intense recent scrutiny. Some methods of generating radical species using electron donor-acceptor (EDA) complexes have been reported. In some cases, a mixture of an electron-rich donor and one with an electron-deficient acceptor forms an EDA complex. The EDA complex was formed between

an electron-deficient alkene and benzothiazoline derivatives acting as a radical transfer reagent.[10] Irradiation of visible light on the charge transfer band created a radical pair, followed by irreversible radical (R·) generation through C-C bond scission of cation radical species of the benzothiazoline derivatives. The anion radical, derived from the alkene, combines with the radical (R·) to give the hydroalkylation products by protonation (Scheme 1).
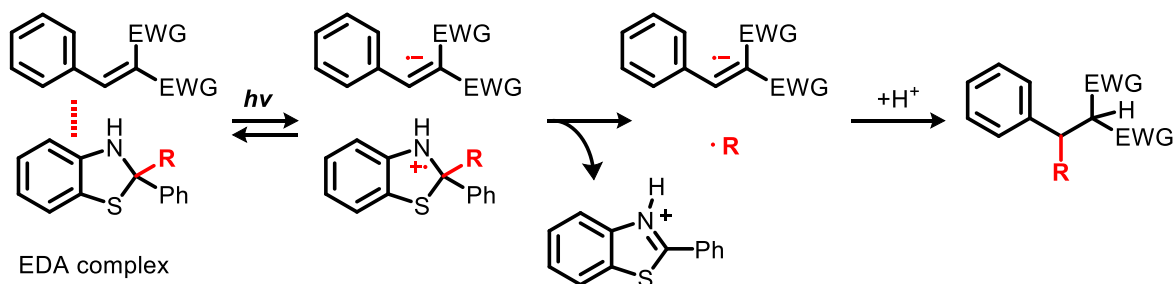


**Scheme 1**. Radical formation via C-C bond cleavage of cation radical species of benzothiazoline derivatives.

In 2019, Zhang and Yu synthesized α-amino ketones derivatives from imines and α-ketoacids via an electron-donor-acceptor pathway leading to decarboxylative acylation under visible-light irradiation.[11] A mixture of imine and α-ketoacids reversibly forms an EDA complex. Shining light on this EDA complex produces a pair of radicals. Decarboxylation from the carboxylic radical then occurs, combining acyl radical with an α-aminoalkyl radical to form α-amino ketones derivatives (Scheme 2). This protocol was adapted for amide, cyanide, ester, ether, halides, and heterocycle substrates.
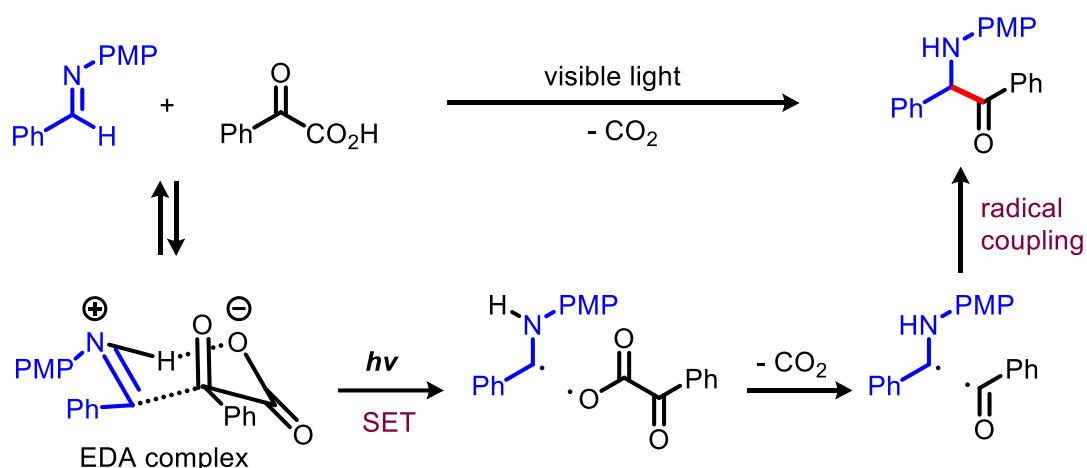


**Scheme 2**. Synthesis of α-amino ketones from an electron donor-acceptor complex.

On the other hand, Fu *et al*. have reported another modification of the EDA complexation technique in which triphenylphosphine, *N*-(acyloxy)phthalimide, and sodium iodide were used as a catalytic donor, an electron-deficient acceptor and an additive, respectively. Upon light irradiation on the EDA complex, radical pairs were formed, and then the bond between the substrate and the radical species was formed, and the donor regenerated through the reduction of an electron, as shown in Scheme 3.[12]
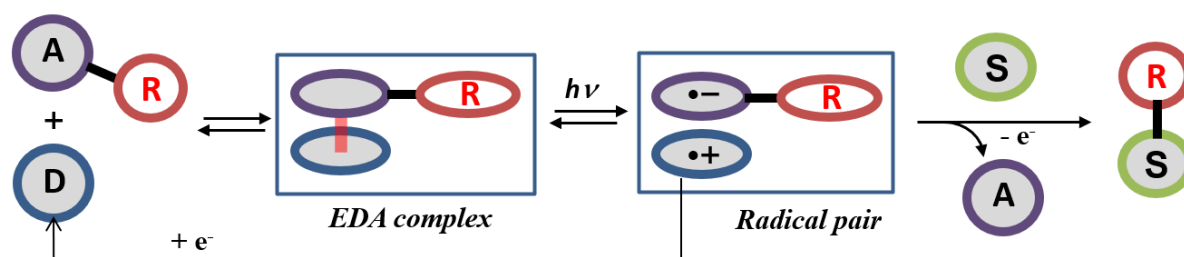


**Scheme 3**. Catalytic electron donor-acceptor systems. A: Acceptor, D: Donor, R: Radical, S: Substrate.

Radicals can form under mild conditions upon selective photoexcitation events in a controllable manner from electron donor-acceptor (EDA) complexes. However, reactions that occur through EDA complexes are less effective due to the back electron transfer. Stephenson and his team have promoted C-H trifluoromethylation and alkylation of (hetero) arenes from EDA complexes using 2-methoxynaphthalene and acylated ethyl isonicotinate *N*-oxide as donor and acceptor, respectively, under visible light irradiation.[13] The EDA complex (II) can be formed by π-stacking interactions in a mixture of 2-methoxynaphthalene donor (I) and acylated ethyl isonicotinate *N*-oxide acceptor. Visible light irradiation of EDA complex (II) followed by single electron transfer generates reactive radical species (R·) and 2-methoxynaphthalene radical cation (III). This reactive radical species (R·) can be trapped with an arene and generate the desired C-H trifluoromethylated product through an oxidation and deprotonation process, and simultaneously forming 2-methoxynaphthalene (I) to complete the catalytic cycle (Scheme 4).

a)
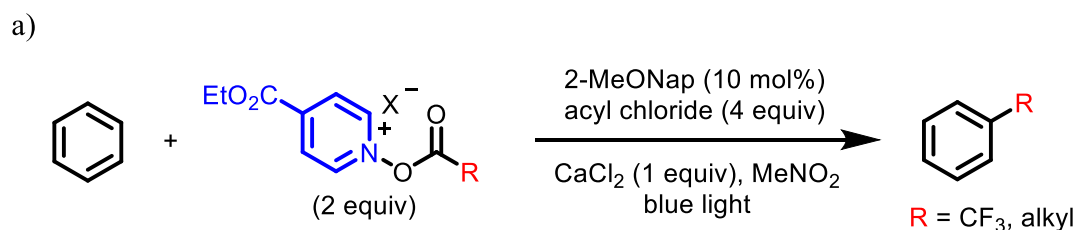
b)
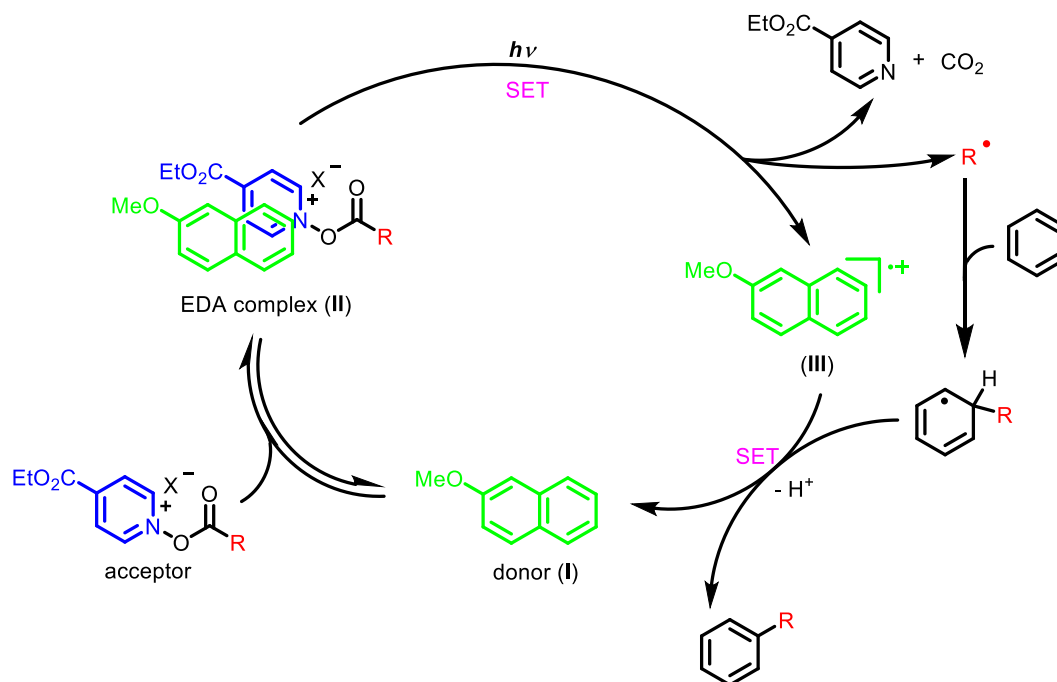


**Scheme 4**. C-C bond formation reaction via catalytic electron donor-acceptor complex (a), and the plausible reaction mechanism (b).

Similarly, Li and co-workers achieved C-H perfluoroalkylation of arenes from triarylamines and $\alpha$-perfluorosulfonylpropiophenone reagents used as catalytic donors and an acceptor, respectively, to form EDA complexes under visible light irradiation.[14] In this proposed mechanism, a mixture of triphenylamine and the perfluoroalkylating reagent containing sulfonylpropiophenone forms the EDA complex. Upon light irradiation of the EDA complex, a single electron transfer technique generated a radical pair of the triphenylaminium radical cation and the radical anion of the propiophenone-containing perfluoroalkylating reagent. Because of the weak C-S bond of the radical anion perfluoroalkylating reagent, the radical anion cleaves to form the perfluoroalkyl radical, a resonance-stabilized enolate and $SO_2$ molecule. This perfluoroalkyl radical reacts with the arenes substrate to form an intermediate radical oxidized by the triphenylaminium radical cation, yielding the functional product and the triphenylamine catalyst (Scheme 5).

a)



4

b)
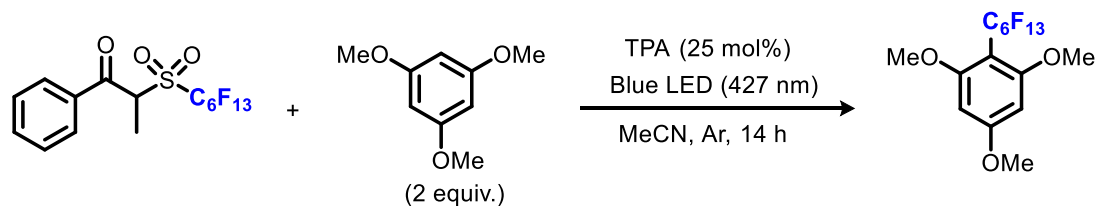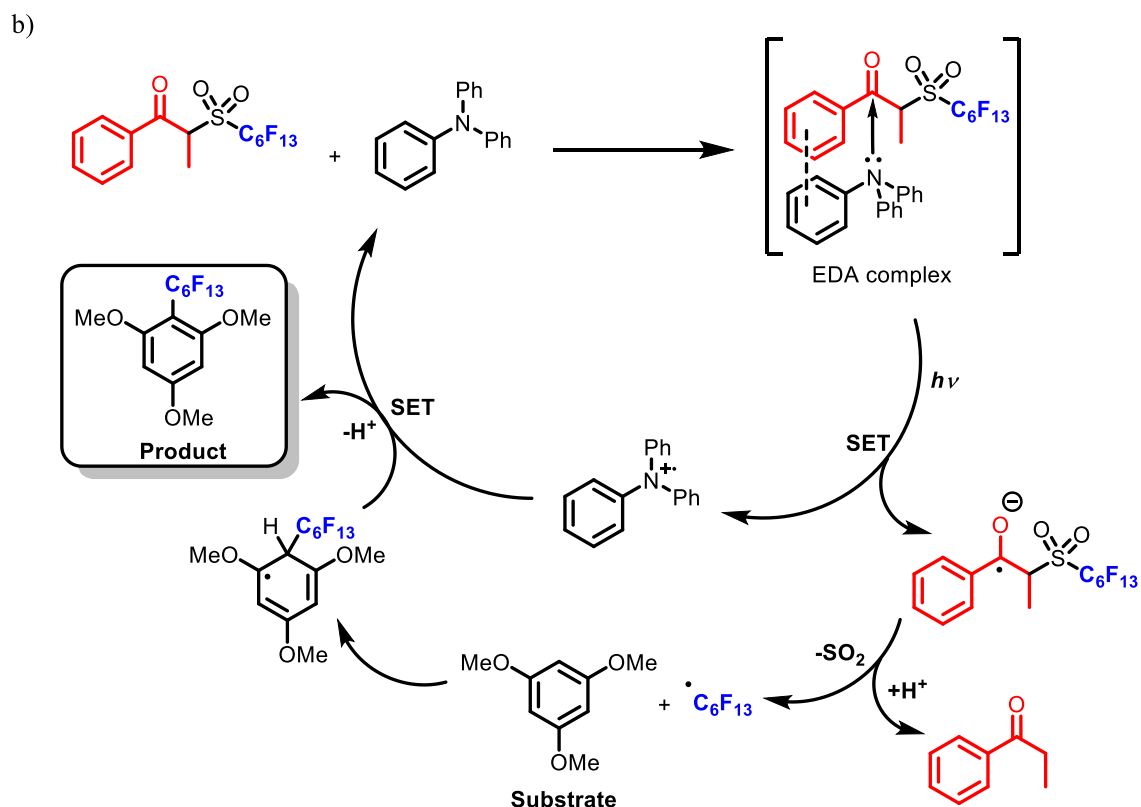


**Scheme 5**. C-C bond-forming reaction used triarylamines as catalytic donors under light-mediated EDA complexes (a), and the plausible reaction mechanism (b).

In 2023, Takizawa and his team synthesized selective C-N bond formation by hydroamination of styrene and naphthylamine under UV light irradiation in an oxygen atmosphere.[15] Naphthylamine and dioxygen on UV light irradiation formed EDA complex that generated N cation radical and superoxide anion by single electron transfer from naphthylamine to dioxygen. This N cation radical reacts with styrene to form the N-C bond formation of the desired product via a reduction and hydrogen atom transfer strategy (Scheme 6).

a)

b)
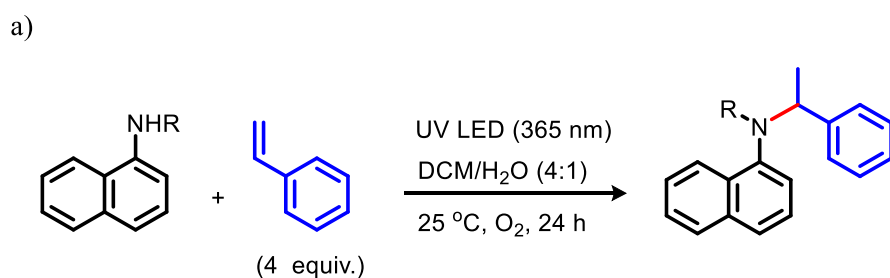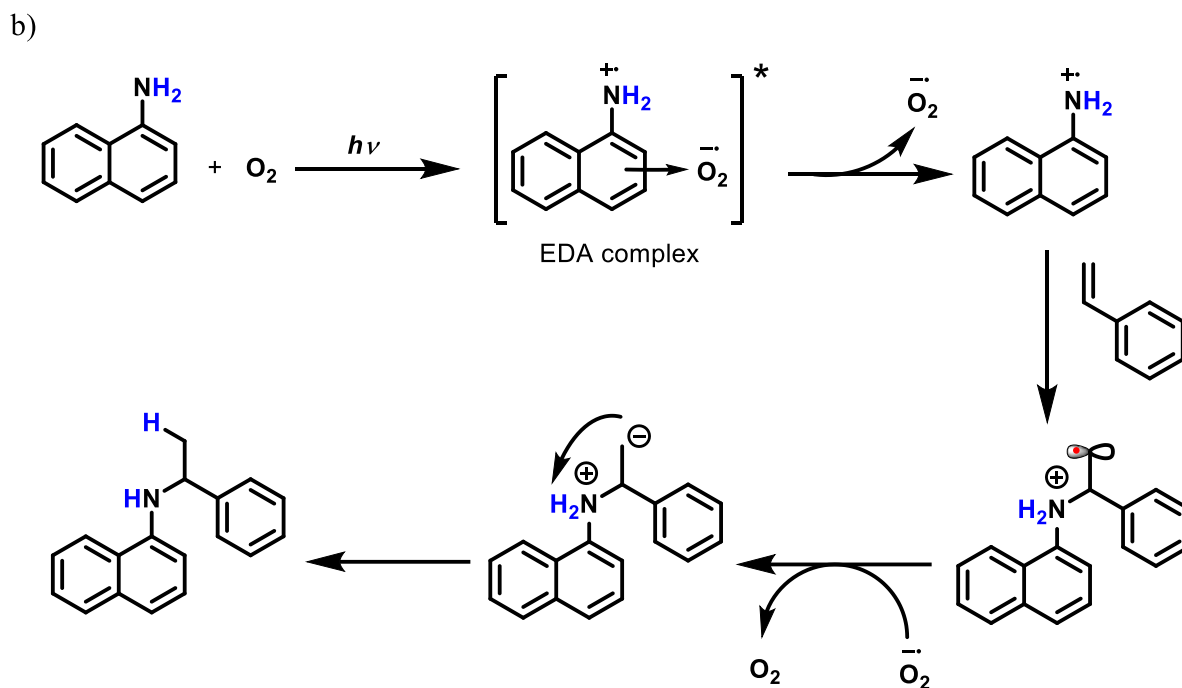


**Scheme 6**. Aerobic N-C bond formation of arylamines and styrene through electron donor-acceptor complex under UV LED irradiation (a), and the plausible reaction mechanism (b).

Organosulfur compounds and higher oxidation state syngenetic sulfoxides [S(II)] and sulfones [S(IV)] are prevalent in pharmaceutivals, natural products, agrochemicals, and materials.[16-18] Several research groups have reported that, higher oxidation states of sulfur containing compounds such as sulfoxides and sulfones are synthesized from thioethers. Particular focus has been placed on reactions forming carbon-carbon bonds via α-thioalkyl radical intermediates exhibiting remarkable nucleophilic properties. These radicals have been generated predominantly through one-electron oxidation of sulfur-containing compounds with α-electrofuge groups, such as trimethylsilyl, carboxylic acids, and trifluoroborates. Alternatively, α-thioalkyl radicals can be formed from thioethers using either a hydrogen atom transfer (HAT) catalyst or a photoredox catalyst.

α-Thioalkyl radicals are an important intermediate for making other chemicals. It can create them by oxidizing sulfur compounds with a single electron transfer and breaking apart thioethers that have an α-electrofuge group, like trimethylsilyl, carboxylic acid, and trifluoroborates (Scheme 7).[19-24]
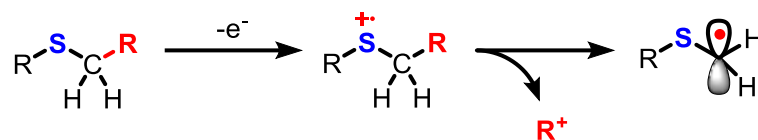
**R** = SiMe$_3$, CO$_2$H, and BF$_3$K

**Scheme 7**. Formation of α-thioalkyl radicals through single electron oxidation and fragmentation of thioethers comprising an α-electrofuge group.

Koike and Akita showed how to make α-thioalkyl radicals from alkyl- and aryl-thioalkylation of olefins using the corresponding organotrifluoroborates as starting materials, and the key point of this technique was deboronation (Scheme 8).[21] At the same time, Alfonzo and Hande found a way to create them directly through C-H activation (Scheme 9),[25] with the help of weak Brønsted bases (CF$_3$CO$_2$Na). These examples use photoredox catalysts to generate α-thioalkyl radicals and create new C-C bonds.
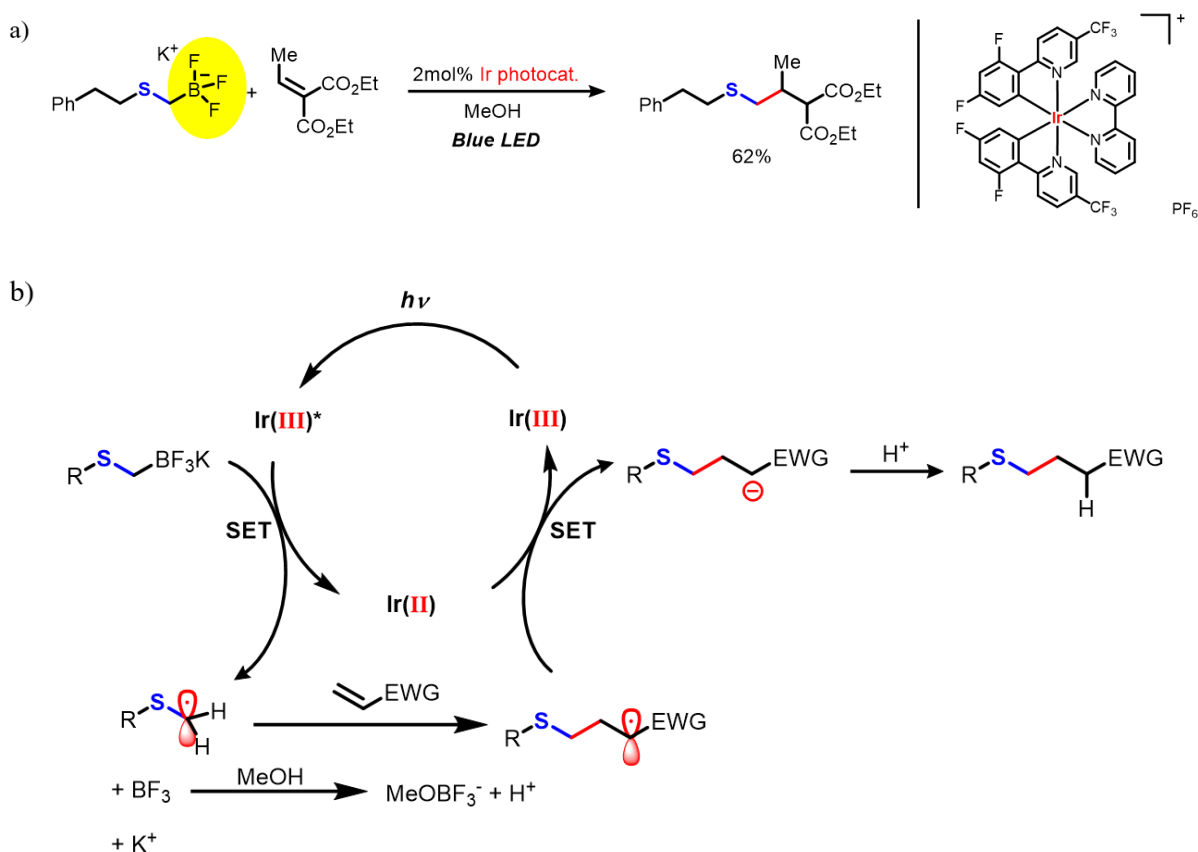


**Scheme 8**. C-C bond formation reaction through α-thioalkyl radicals (a), and the plausible reaction mechanism of this reaction (b).

In modern photocatalysis, an innovation of the C-H activation reaction has more significant advantages such as higher selectivity and milder reaction conditions than other conventional C-H activation reactions due to the low energy photons used as energy sources.[26] From C-H activation to C-C bond formation to compounds with biological activity, these techniques are highly selective and stepatom economical reactions.[27-29] *α*-Amino functionalization reactions produce nucleophilic *α*-amino radicals via C-H activation reactions that form C-C bonds in the presence of electron-poor multiple bond species.[30] In this approach, Nicewicz and co-workers generated *α*-amino radicals by one-electron oxidation and subsequient deprotonation using an acridinium photocatalyst.[31,32] In 2018, Jui et al have synthesized *α*-alkylation of amines such as unnatural *γ*-amino acids[31,33] and peptides[31,34] by single-electron transfer and deprotonation techniques under visible light irradiation in the presence of irradium photocatalyst.

However, recent developments have focused on directly activating the *α*-C-H bond of the sulfur in thioethers to generate nucleophilic α-thioalkyl radicals, utilizing these radical species to functionalize thioethers. This method has garnered attention for expanding the synthetic scope of organosulfur compounds. For instance, MacMillan and colleagues have successfully generated α-thioalkyl radicals from thioethers using a triple catalytic combination (Organo-, nickel-, and photoredox catalysts).[35] It has been demonstrated that α-thioalkyl radicals can arise from one-electron oxidation with subsequent proton abstraction by co-occurring weak Brønsted bases. The formation of carbon-carbon bonds via the charge separation state in irradiated charge transfer complexes has been extensively investigated. Nevertheless, similar to the generation of α-thioalkyl radicals, a leaving group is often essential for the irreversible formation of the desired radical, preventing back electron transfer and regeneration of the original charge transfer complex.

a)

b)
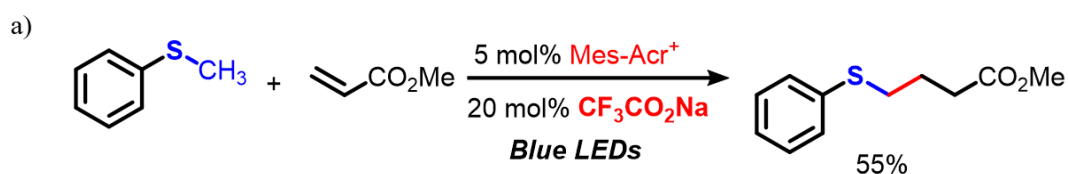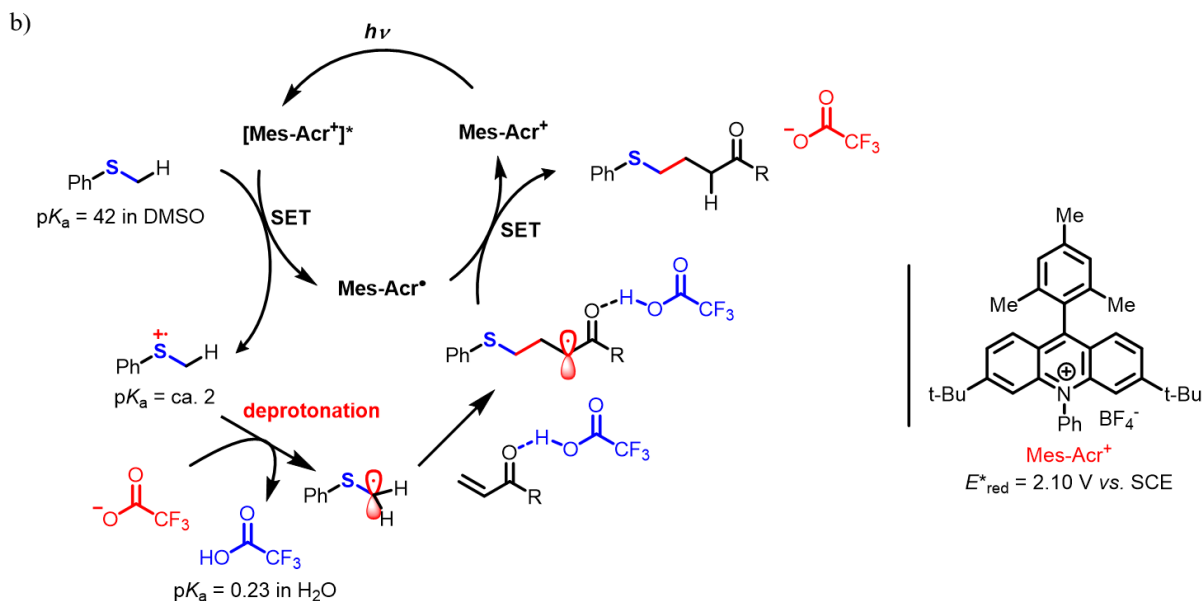


**Scheme 9**. C-C bond formation reaction through C-H activation of thioanisole to α-thioalkyl radicals (a), and the plausible reaction mechanism (b).

The domain of heterocyclic compounds, recognized for their significant biological activities, has witnessed the advent of novel and efficient synthetic methodologies. Many research groups have reported on the inherent complexity of generating elaborate cyclic structures from more basic molecules by employing radical addition and cyclization techniques. This strategy broadens the array of synthetic methods and enhances yield and selectivity, particularly in synthesizing tetrahydropyridines, thus presenting a formidable challenge to the traditionally preferred aza-Diels-Alder reaction.[36] The work of Hoffmann *et al.* and Yu *et al.* involved synthesizing tetrahydroquinoline derivatives from *N,N*-dimethylaniline and electron-deficient alkenes through a radical addition/cyclization methodology, utilizing titanium dioxide and a ruthenium complex photocatalyst, respectively.[37,38] In addition, Walton *et al.* synthesized annulation involving anisole or thioanisole derivatives via one-electron oxidation and decarboxylation of aryl acetate to produce *α*-oxygen methyl radicals or *α*-thiomethyl radicals through radical addition/cyclization pathway.[39,40]

Sulfoxide-containing compounds play a remarkable role in organic synthesis,[41] medicinal[42] and polymer chemistry.[43] Several sulfoxides exhibit a dominant physiological activity and are used as drugs. Various methods for the selective synthesis of sulfoxide-containing molecules have been reported worldwide. However, many research groups use light as an energy source to develop environmentally friendly protocols, such as photochemistry, which plays an important role in the selective synthesis of sulfoxides from sulfides (Table 1).

9

**Table 1**. Selective oxidation of methyl phenyl sulfide into methyl phenyl sulfoxide with $O_2$.
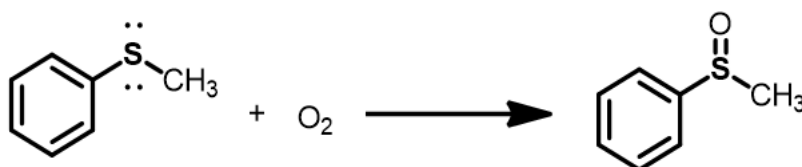


| Photocatalyst (mg) | Light sources | Atmosphere | Solvent | Substrate (mmol) | t (h) | Conv. (%) | Ref. |
|---|---|---|---|---|---|---|---|
| TiO$_2$ (Degussa P25) (40) | 300 W Xe lamp (400 nm) | O$_2$ | CH$_3$OH | 0.3 | 10 | 84 | [44] |
| ARS-TiO$_2$ (9.6) | 300 W Xe lamp (450 nm) | O$_2$ | CH$_3$OH | 0.3 | 3 | 84 | [45] |
| CdS/C$_3$N$_4$ (5) | 30 W × 3, white LEDs (420 nm) | O$_2$ | CH$_3$OH | 0.3 | 6 | 62 | [46] |
| Bi$_4$O$_5$Br$_2$ (20) | 30 W blue LED | O$_2$ | H$_2$O | 0.2 | 6 | 99 | [47] |
| NNU-45 (4) | 300 W Xe lamp | Air | CHCl$_3$ + CH$_3$OH | 0.4 | 4 | 99 | [48] |
| BN@TTCOP-2 (10) | 3 W × 30, white LEDs | O$_2$ | CH$_3$OH | 0.2 | 8 | 100 | [49] |
| SFC-CMP (5) | 3 W × 4, Blue LEDs (460±10) | O$_2$ | CH$_3$OH | 0.3 | 0.75 | 93 | [50] |

On the other hand, epoxides are intermediates in manufacturing many chemical products, including epoxy resins and pharmaceuticals. An oxygen-atom transfer reaction to the olefins generally produces these epoxides. Most epoxidation reactions of alkenes are performed with peroxides such as *tert*-butyl hydroperoxide, peracetic acid, *m*-chloroperoxybenzoic acid, or with the chlorohydrin method.[51-53] Such reagents are challenging to handle and also produce undesirable stoichiometric by-products.[54,55] Those problems can be avoided if an active oxidizing agent can be synthesized in situ.[56-63] Consequently, research has been conducted on

the electrolytic epoxidation of alkene using water as the oxygen source. An elegant method for the indirect electrochemical epoxidation of olefins, employing bromide ions as mediators, has been reported.[56] Torii *et al.* reported electrochemical alkene epoxidation reactions using the $CH_3CN$-water-NaBr system.[57] In this system, the electrolysis of NaBr in water produces NaOBr, and water is an oxygen source for the epoxide. Moreover, the use of $Fe_2O_3$ as a photoelectrode for alkene epoxidation has also been reported.[64] In this method, epoxidation of aliphatic alkenes was not very efficient, and produced ketones and bromine-substituted by-products. The indirect electrochemical epoxidationof propylene, with chloride ion serving as the mediator, has been developed.[65] Tanaka and co-workers subsequently reported electrochemical epoxidation of styrene derivatives using *N,N'*-bis(3,5-di-tert-butylsalicylidene)-1,2-cyclohexanediaminomanganese(III) chloride in a $CH_2Cl_2$-water-NaCl system.[66] In this system, the electrolysis of NaCl in water produces NaOCl, and Jacobsen's catalyst promotes the epoxidation reaction of styrene derivatives with NaOCl in the $CH_2Cl_2$-water biphasic system. This reaction employs styrene derivatives as substrates. When applied to cycloalkenes, my investigations revealed that, in addition to epoxidation, allylic chlorination also proceeds. This necessitated the search for electrolyte mediators other than chloride ions. Consequently, I decided to prepare peroxycarbonate ions using carbonate ions as the electrolyte mediator, given their known efficacy in facilitating alkene epoxidation.[67-69] Percarbonate is a more active oxidant than $H_2O_2$, which is generated by the equilibrium reaction between carbonate ions and $H_2O_2$.[70] Therefore, carbonates have often been used as an activator for the oxidation reactions with $H_2O_2$, including epoxidation reactions.[67,68,71-73] Several research groups have recently explored olefin epoxidation via electrochemical methods, employing in situ electrochemical generation of chemical oxidants such as hydrogen peroxide, active halogens, or peroxodicarbonate to convert olefin substrates to their corresponding epoxides. Direct oxidation of water using manganese oxide nanoparticle ($Mn_3O_4$ NPs) used as catalyst to epoxidize alkenes has also been reported.[74] I focus on boron-doped diamond (BDD) stems from its broad potential window, which allows for the oxidation of carbonate ions without oxidizing water.[75-80]


**Outline of the Present Thesis**

In Chapter 1 of Part 1, The study delves into innovative methods for generating α-thioalkyl radicals through one-electron oxidation followed by deprotonation from thioanisole

derivatives triggered by visible light irradiation. The initial method encompasses the irradiation with the blue light of a charge transfer complex formed between benzylidenemalononitrile (BMN), an electron-deficient alkene, and thioanisole. This process facilitates an electron transfer from thioanisole to BMN, producing a BMN anion radical that is a weak Brønsted base. This base aids in the proton transfer from the one-electron-oxidized thioanisole, leading to the formation of α-thioalkyl radicals, which are subsequently involved in carbon-carbon bond formation with alkenes. The findings highlight the crucial role of deprotonation, the impact of specific electron-donating substituents in thioanisole, and the effectiveness of weak Brønsted bases in enhancing the reactions' efficiency and yield. This mechanism's ability to generate α-thioalkyl radicals presents a promising avenue for more efficient synthesis processes.

Chapter 2 of Part 1 introduces a novel approach for the generation of α-thioalkyl radicals through one-electron oxidation and subsequent deprotonation of thioanisole, facilitated by titanium dioxide photocatalysts under blue light irradiation. The proposed mechanism suggests a charge transfer from thioanisole to the conduction band of titanium dioxide upon exposure to blue light, leading to thioanisole's one-electron oxidation and the eventual formation of α-thioalkyl radicals via deprotonation. Incorporating titanium dioxide significantly enhances the reaction rate of thioanisole derivatives with the alkene BMN. The study investigates a variety of 4-substituted thioanisoles and N-substituted maleimides as precursors, yielding moderate to high yields through radical addition/cyclization reactions. This method underscores the efficiency of heterogeneous titanium dioxide photocatalysts in accelerating complex syntheses within thioether chemistry.

In Chapter 3 of Part 1, the focus shifts to the selective oxidation of thioanisole derivatives employing 2,2,2-trifluoroethanol solvent and green oxidants like dioxygen under a 370 nm ultraviolet LED lamp. The technique's practical utility is demonstrated through a gram-scale reaction, yielding the desired product with excellent efficiency.

In Chapter 1 of Part 2, drawing inspiration from Tanaka's seminal research, this part explores the electrochemical epoxidation through the in situ generation of percarbonate, utilizing a manganese-salen complex as a catalyst within an organic solvent-aqueous carbonate biphasic system and employing a simple undivided cell. The process is optimized when using a boron-doped diamond (BDD) electrode as the anode, leading to the efficient epoxidation of styrene derivatives.

**References**

(1)     G. Ciamician, *Science* **1912**, *36*, 385−394.

(2)     D. M. Schultz, T. P. Yoon, *Science* **2014**, *343*, 1239176.

(3)     V. Balzani, P. Ceroni, A. Juris, *Photochemistry and Photophysics, Eds., Wiley-VCH*, **2014**.

(4)     G. E. M. Crisenza, D. Mazzarella, P. Melchiorre, *J. Am. Chem. Soc.* **2020**, *142*, 5461−5476.

(5)     M. H. Shaw, J. Twilton, D. W. C. MacMillan, *J. Org. Chem.* **2016**, *81*, 6898−6926.

(6)     M. Yan, J. C. Lo, J. T. Edwards, P. S. Baran, *J. Am. Chem. Soc.* **2016**, *138*, 12692−12714.

(7)     D. A. DiRocco, K. Dykstra, S. Krska, P. Vachal, D. V. Conway, M. Tudge, *Angew. Chem., Int. Ed.* **2014**, *53*, 4802−4806.

(8)     R. Foster, *J. Phys. Chem.* **1980**, *84*, 2135−2141.

(9)     S. V. Rosokha, J. K. Kochi, *Acc. Chem. Res.* **2008**, *41*, 641−653.

(10)    T. Uchikura, T. Fujii, K. Moriyama, T. Akiyama, *Bull. Chem. Soc. Jpn.* **2021**, *94*, 2962-2966.

(11)    H.-H. Zhang, S. Yu, *Org. Lett.* **2019**, *21*, 3711-3715.

(12)    M.-C. Fu, R. Shang, B. Zhao, B. Wang, Y. Fu, *Science* **2019**, *363*, 1429-1434.

(13)    E. J. McClain, T. M. Monos, M. Mori, J. W. Beatty, C. R. J. Stephenson, *ACS Catal.* **2020**, *10*, 12636-12641.

(14)    D. J. Castillo-Pazos, J. D. Lasso, E. Hamzehpoor, J. Ramos-Sanchez, J. M. Salgado, G. Cosa, D. F. Perepichka, C.-J. Li, *Chem. Sci.* **2023**, *14*, 3470-3481.

(15)    D. Fan , A. Sabri , H. Sasai, S. Takizawa, *Molecules* **2023**, *28*, 365.

(16)    K. A. Scott, J. T. Njardarson, *Top. Curr. Chem.* **2018**, *376*, 5.

(17)    D. A. Boyd, *Angew. Chem., Int. Ed.* **2016**, *55*, 15486−15502.

(18)    P. Devendar, G.-F. Yang, *Top. Curr. Chem.* **2017**, *375*, 82.

(19)    M. Mella, M. Freccero, E. Fasani, A. Albini, *Chem. Soc. Rev.* **1998**, *27*, 81-89.

(20)    E. Hasegawa, M. A. Brumfield, P. S. Mariano, U. C. Yoon, *J. Org. Chem.* **1988**, *53*, 5435-5442.

(21)    Y. Li, K. Miyazawa, T. Koike, M. Akita, *Org. Chem. Front.* **2015**, *2*, 319-323.

(22)    E. Baciocchi, T. Del Giacco, F. Elisei, A. Lapi, *J. Org. Chem.* **2006**, *71*, 853-860.

(23)    C. Silva-Cuevas, E. Paleo, D. F. León-Rayo, J. A. Lujan-Montelongo, *RSC Advances* **2018**, *8*, 24654-24659.

(24)    R. A. Garza-Sanchez, T. Patra, A. Tlahuext-Aca, F. Strieth-Kalthoff, F. Glorius, *Chem. Eur. J.* **2018**, *24*, 10064-10068.

(25)    E. Alfonzo, S. M. Hande, *ACS. Catal.* **2020**, *10*, 12590-12595.

(26)    P. Bellotti, H.-M. Huang, T. Faber, F. Glorius, *Chem. Rev.* **2023**, *123*, 4237−4352.

(27)    J. Choi, G. C. Fu, *Science* **2017**, *356*, eaaf7230.

(28)    Z. Chen, M.-Y. Rong, J. Nie, X.-F. Zhu, B.-F. Shi, J.-A. Ma, *Chem. Soc. Rev.* **2019**, *48*, 4921−4942.

(29)    J. D. Lasso, D. J. Castillo-Pazos, C.-J. Li, *Chem. Soc. Rev.* **2021**, *50*, 10955−10982.

(30)    F. Parsaee, M. C. Senarathna, P. B. Kannangara, S. N. Alexander, P. D. E. Arche, E. R. Welin, *Nat. Rev. Chem.* **2021**, *5*, 486−499.

(31)    N. A. Romero, D. A. Nicewicz, *Chem. Rev.* **2016**, *116*, 10075−10166.

(32)    J. B. McManus, N. P. R. Onuska, M. S. Jeffreys, N. C. Goodwin, D. A. Nicewicz, *Org. Lett.* **2020**, *22*, 679− 683.

(33)    K. Lang, J. W.Chin, *Chem. Rev.* **2014**, *114*, 4764−4806.

(34)    R. A. Aycock, C. J. Pratt, N. T. Jui, *ACS Catal.* **2018**, *8*, 9115−9119.

(35)    C. Le, Y. Liang, R. W. Evans, X. Li, D. W. C. MacMillan, *Nature* **2017**, *547*, 79-83.

(36)    M.-H. Cao, N. J. Green, S.-Z. Xu, *Org. Biomol. Chem.* **2017**, *15*, 3105-3129.

(37)    S. Marinković, N. Hoffmann, *Eur. J. Org. Chem.* **2004**, *2004*, 3102-3107.

(38)    X. Ju, D. Li, W. Li, W. Yu, F. Bian, *Adv. Synth. Catal.* **2012**, *354*, 3561-3567.

(39)    D. W. Manley, R. T. McBurney, P. Miller, R. F. Howe, S. Rhydderch, J. C. Walton, *J. Am. Chem. Soc.* **2012**, *134*, 13580-13583.

(40)    D. W. Manley, A. Mills, C. O'Rourke, A. M. Z. Slawin, J. C. Walton, *Chem. Eur. J.* **2014**, *20*, 5492-5500.

(41)    B. Ferber, H. B. Kagan, *Adv. Synth. Catal.* **2007**, *349*, 493-507.

(42)    M. Feng, B. Tang, S. H. Liang, X. Jiang, *Curr. Top. Med. Chem.* **2016**, *16*, 1200-1216.

(43)    X. Xu, X. Huang, Y. Chang, Y. Yu, J. Zhao, N. Isahak, J. Teng, R. Qiao, H. Peng, C.-X. Zhao, *Biomacromolecules* **2020**, *22*, 330-339.

(44)    X. Lang, W. Hao, W. R. Leow, S. Li, J. Zhao, X. Chen, *Chem. Sci.* **2015**, *6*, 5000-5005.

(45)    X. Lang, J. Zhao, X. Chen, *Angew. Chem. Int. Ed.* **2016**, *128*, 4775-4778.

(46)    Y. Xu, Z.-C. Fu, S. Cao, Y. Chen, W.-F. Fu, *Catal. Sci. Technol.* **2017**, *7*, 587-595.

(47)    W. Zhao, C. Yang, J. Huang, X. Jin, Y. Deng, L. Wang, F. Su, H. Xie, P. K. Wong, L. Ye, *Green Chem.* **2020**, *22*, 4884-4889.

(48)  H. Wei, Z. Guo, X. Liang, P. Chen, H. Liu, H. Xing, *ACS Appl. Mater. Interfaces* **2019**, *11*, 3016-3023.

(49)  X. Lan, Q. Li, Y. Zhang, Q. Li, L. Ricardez-Sandoval, G. Bai, *Appl. Catal. B: Environ.* **2020**, *277*, 119274.

(50)  X. Dong, H. Xu, H. Hao, W. Sheng, X. J. Lang, *J. Coll. Interface Sci.* **2022**, *608*, 882-892.

(51)  R. H. Holm, *Chem. Rev.* **1987**, *87*, 1401-1449.

(52)  Q.-H. Xia, H.-Q. Ge, C.-P. Ye, Z.-M. Liu, K.-X. Su, *Chem. Rev.* **2005**, *105*, 1603-1662.

(53)  M. Yan, Y. Kawamata, P. S. Baran, *Chem. Rev.* **2017**, *117*, 13230-13319.

(54)  V. G. Dryuk, *Tetrahedron* **1976**, *32*, 2855-2866.

(55)  C. Kim, T. G. Traylor, C. L. Perrin, *J. Am. Chem. Soc.* **1998**, *120*, 9513-9516.

(56)  S. Torii, K. Uneyama, M. Ono, H. Tazawa, S. Matsunami, *Tetrahedron Lett.* **1979**, *20*, 4661-4662.

(57)  S. Torii, K. Uneyama, H. Tanaka, T. Yamanaka, T. Yasuda, M. Ono, Y. Kohmoto, *J. Org. Chem.* **1981**, *46*, 3312-3315.

(58)  H. Nishihara, K. Pressprich, R. W. Murray, J. P. Collman, *Inorg. Chem.* **1990**, *29*, 1000-1006.

(59)  S. Funyu, T. Isobe, S. Takagi, D. A. Tryk, H. Inoue, *J. Am. Chem. Soc.* **2003**, *125*, 5734-5740.

(60)  D. Shen, C. Saracini, Y.-M. Lee, W. Sun, S. Fukuzumi, W. Nam, *J. Am. Chem. Soc.* **2016**, *138*, 15857-15860.

(61)  B. Chandra, K. K. Singh, S. S. Gupta, *Chem. Sci.* **2017**, *8*, 7545-7551.

(62)  D. Tatsumi, T. Tsukamoto, R. Honna, S. Hoshino, T. Shimada, S. Takagi, *Chem. Lett.* **2017**, *46*, 1311-1314.

(63)  K. Jin, J. H. Maalouf, N. Lazouski, N. Corbin, D. Yang, K. Manthiram, *J. Am. Chem. Soc.* **2019**, *141*, 6413-6418.

(64)  Y. Zhao, M. Duan, C. Deng, J. Yang, S. Yang, Y. Zhang, H. Sheng, Y. Li, C. Chen, J. Zhao, *Nature Com.*, **2023**, *14*, 1943.

(65)  M. R. Rifi, F. H. Covitz, Introduction to Organic Electrochemistry, Marcel Dekker: New York, 1974.

(66)  H. Tanaka, M. Kuroboshi, H. Takeda, H. Kanda, S. Torii, *J. Electroanal. Chem.* **2001**, *507*, 75-81.

(67)  H. Yao, D. E. Richardson, *J. Am. Chem. Soc.* **2000**, *122*, 3220-3221.

(68)     B. S. Lane, M. Vogt, V. J. DeRose, K. Burgess, *J. Am. Chem. Soc.* **2002**, *124*, 11946-11954.

(69)     A.-K. Seitz, P. J. Kohlpaintner, T. V. Lingen, M. Dyga, F. Sprang, M. Zirbes, S. R. Waldvogel, L. J. Gooßen, *Angew. Chem. Int. Ed.* **2022**, *61*, e202117563.

(70)     D. E. Richardson, H. Yao, K. M. Frank, D. A. Bennett, *J. Am. Chem. Soc.* **2000**, *122*, 1729-1739.

(71)     H. H. Monfared, V. Aghapoor, M. Ghorbanloo, P. Mayer, *Appl. Catal. A. Gen.* **2010**, *372*, 209-216.

(72)     B. Hincapie, S. M. Llano, H. F. Garces, D. Espinal, S. L. Suib, L. Garces, *Adsorpt. Sci. Technol.* **2018**, *36*, 9-22.

(73)     A. M. Garcia, V. Moreno, S. X. Delgado, A. E. Ramírez, L. A. Vargas, M. A. Vicente, A. Gil, L. A. Galeano, *J. Mol. Catal. A: Chem.* **2016**, *416*, 10-19.

(74)     K. Jin, J. H. Maalouf, N. Lazouski, N. Corbin, D. Yang, K. Manthiram, *J. Am. Chem. Soc.* **2019**, *141*, 6413-6418.

(75)     Irkham, A. Fiorani, G. Valenti, N. Kamoshida, F. Paolucci, Y. Einaga, *J. Am. Chem. Soc.* **2020**, *142*, 1518−1525.

(76)     M. S. Saha, T. Furuta, Y. Nishiki, *Electrochem. Commun.* **2004**, *6*, 201–204.

(77)     S. Velazquez-Peña, C. Sáez, P. Cañizares, I. Linares-Hernández, V. Martínez-Miranda, C. Barrera-Díaz, M. A. Rodrigo, *Chem. Eng. J.* **2013**, *230*, 272–278.

(78)     M. S. Saha, T. Furuta, Y. Nishiki, *Solid-State Lett.* **2003**, *6*, D5.

(79)     Y. Einaga, *Acc. Chem. Res.* **2022**, *55*, 3605−3615.

(80)     Y. Einaga, *Electrochem.* **2022**, *90(10)*, 101002.

# PART 1


# Photochemistry of Thioanisole Derivatives

# Chapter 1

# A Simple Method for the Formation of α-Thioalkyl Radicals and the Promotion of Carbon-Carbon Bond Formation by Photoirradiation of Electron Donor-Acceptor Complexes

## Abstract

This study documents the formation of an electron donor-acceptor complex between thioanisole and benzylidenemalononitrile. Upon irradiation, the electron donor-acceptor complex generates α-thioalkyl radicals, facilitating carbon-carbon bond formation. Mechanistic investigations underscore the crucial roles of both one-electron oxidation and deprotonation processes in achieving a reaction yield up to 43%.

## Introduction

Thioethers and their oxidized counterparts, such as sulfoxides and sulfones, are ubiquitously found in natural products, pesticides, and pharmaceuticals.[1] This ubiquity has driven substantial research into synthesizing structures incorporating thioethers and functionalizing thioether compounds. As part of this endeavor, the generation of α-thioalkyl radicals, known for their pronounced nucleophilicity, for use in carbon-carbon bond-forming reactions has been explored. α-thioalkyl radicals can be yielded through the one-electron oxidation of thioethers that bear α-electrofuge groups, such as trimethylsilyl, carboxylic acid, and trifluoroborate, which subsequently dissociate to produce α-thioalkyl radicals (Scheme 1a).[2-7]

In a seminal study conducted in 2017, MacMillan and his team proficiently executed the α-C(sp$^3$)–H alkylation of thioethers with alkyl bromides using a confluence of photoredox catalysts, nickel catalysts, and hydrogen atom transfer catalysts.[8,9] Additionally, Alfonzo and

Hande demonstrated the generation of α-thioalkyl radicals via the C–H activation of thioethers, enabled by photoredox catalysts and weak base catalysts, which then interacted with electron-deficient olefins (Scheme 1b),[10] and *N*-methoxyheteroarenium salts.[11] A stereoselective α-C($sp^3$)–H functionalization reaction of thioethers was adeptly performed by Tan and colleagues, employing a chiral gallium(III)-*N,N'*-dioxide complex as a catalyst, in conjunction with isatin, which served both as a photoredox catalyst and a coupling partner.[12]

*Previous works*
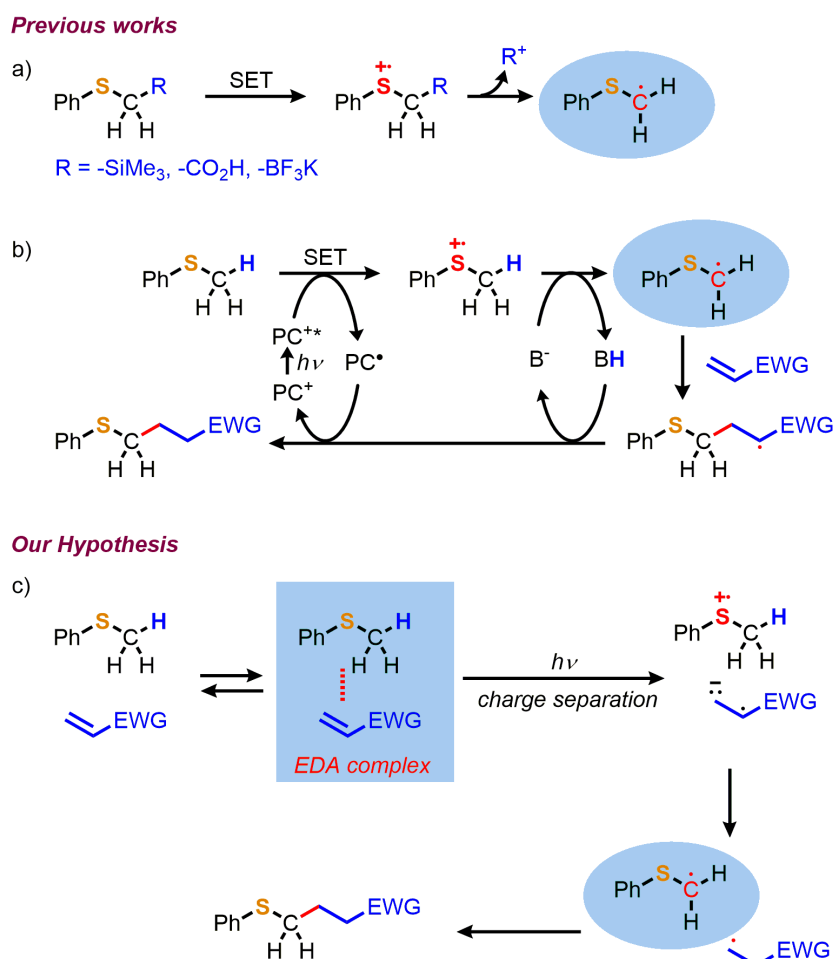


**Scheme 1.** Strategy for the Generation of α-Thioalkyl Radicals for Use in C–C Bond Formation.

While the examples above delineate the generation of α-thioalkyl radicals through single-electron oxidation facilitated by photoredox catalysts, it is also established that photo-irradiation of electron-donor-acceptor (EDA) complexes, also known as charge-transfer (CT) complexes, can similarly catalyze the generation of various radical species of donor molecules.[13] Given the conjectural generation of α-thioalkyl radicals from thioethers via photoirradiation of an EDA complex (Scheme 1c), I investigated with thioanisole serving as the electron donor within the EDA complex, followed by photoirradiation experiments. I

present the formation of an EDA complex between a fundamental thioanisole derivative and an electron-deficient alkene. Furthermore, I noticed that upon photoirradiation of the EDA complex's CT band, the process of carbon-carbon bond formation was initiated.

## Results and discussion

Initially, I verified whether thioanisole **1a** forms EDA complexes with a range of alkenes (**2a**-**2j**), which possess a theoretically estimated electron affinity ranging from 1.6 to 3.2 eV (Figure 1, and Table 1). Only benzylidenemalononitrile (**2a**), the most electron-deficient alkene, turned yellow when mixed with **1a** in acetonitrile, as illustrated in Figures 2A and 3. By employing the absorption intensity of the CT band of the EDA complex between **1a** and **2a**, with 1.0 M total concentration of **1a** and **2a** in acetonitrile, I established a Job's plot and noted a comparatively gentle curve peaking at a 1:1 ratio (Figure 2B). Through curve fitting, using the equation positing the formation of a 1:1 complex, the association constant was ascertained as $K = 0.34 \pm 0.01$ M$^{-1}$, closely aligning with the reported association constant for similar EDA complexes.[14,15] Noncovalent interaction plot[16] of a computationally optimized structure of the EDA complex between **1a** and **2a** further suggested the existence of attractive interactions (Figure 2C). It is worth mentioning that the involvement of thiophenols as donors in EDA complex formation has previously been documented, where they were exploited for visible-light-promoted C-S cross-coupling.[17]
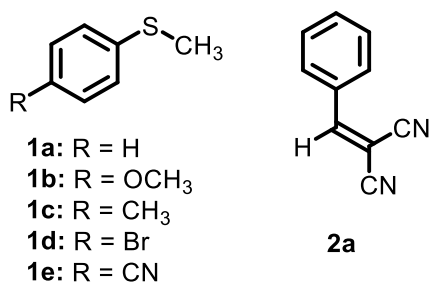


**1a:** R = H
**1b:** R = OCH$_3$
**1c:** R = CH$_3$
**1d:** R = Br
**1e:** R = CN

**2a**

**Figure 1.** Thioanisole derivatives (**1a**–**1e**) and an electron-deficient alkene (**2a**) used for this study.

**Table 1.** Electron affinity of **2a-2j**.

| Acceptor molecule | Electron affinity (eV)[a] |
|---|---|
| benzylidenemalononitrile (**2a**) | 3.20 |
| fumaronitrile (**2b**) | 3.06 |
| dimethyl fumarate (**2c**) | 3.06 |
| dimethyl maleate (**2d**) | 2.72 |
| styrene (**2e**) | 1.62 |
| *N*-phenylmaleimide (**2f**) | 3.06 |
| maleimide (**2g**) | 3.03 |
| *N*-benzylmaleimide (**2h**) | 2.97 |
| *N*-ethylmaleimide (**2i**) | 2.96 |
| diethyl benzylidenemalonate (**2j**) | 2.51 |

[a] Vertical electron affinity (in eV) was calculated at M062X/(ma-)def2-TZVP/CPCM(acetonitrile) using Orca 5.0.
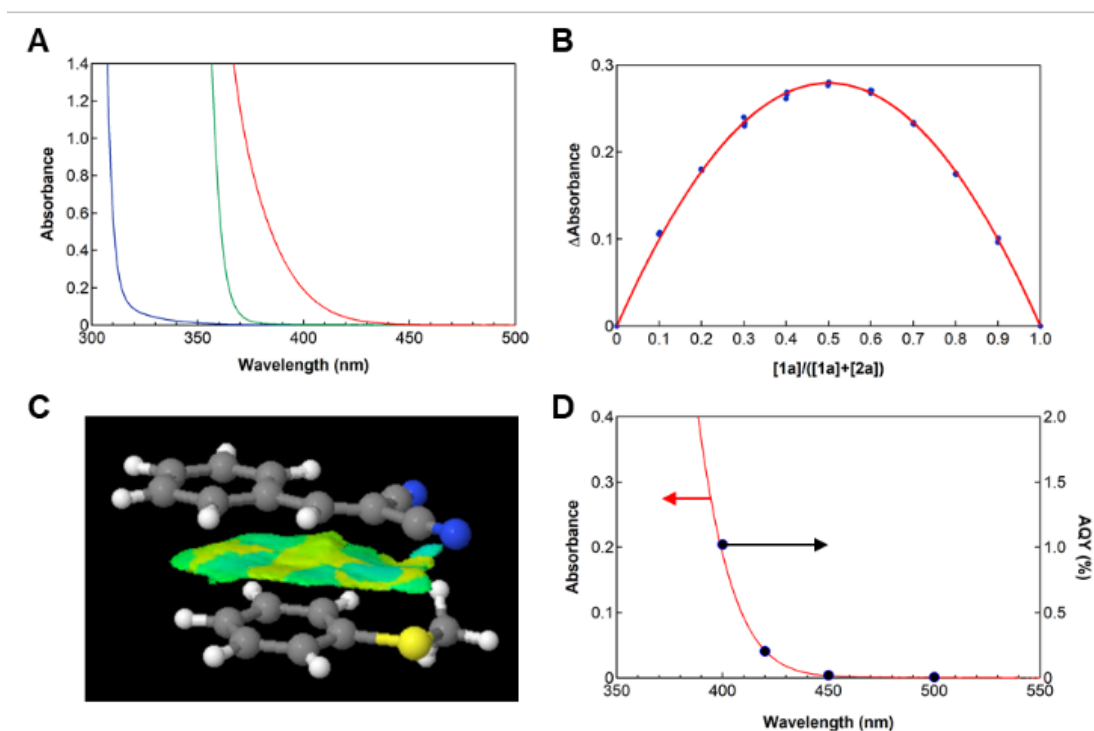


**Figure 2.** (A) Absorption spectra of **1a** (blue), **2a** (green), and the combined mixture of **1a** and **2a** (red) in acetonitrile. The concentration of **1a** is 250 mM, and **2a** is 50 mM. (B) Job's plot for **1a** with **2a**, where the total concentration is 1.0 M. The y-axis represents the averaged

absorption intensity from 410 nm to 500 nm, after deduction of the expected intensity presuming no interaction between **1a** and **2a**. Data from four experiments were utilized to carry out curve fitting using an equation based on 1:1 complexation. (C) Noncovalent interaction plots of the EDA complex between **1a** and **2a**. (D) The absorption spectrum (red line) of the combined mixture of **1a** and **2a** in acetonitrile and the action spectrum (black dots) of the formation reaction of **3a** from **1a** and **2a**. The right axis denotes the apparent quantum yield (AQY).



**Figure 3.** (I) Photographs of **1a**, **2a**, and EDA complex of **1a** and **2a**; and (II) Structure of **1a**, **2a**, and EDA complex of **1a** and **2a**.

Initially, a solution of **1a** and **2a** in acetonitrile with a 5:1 molar ratio was irradiated using blue LED lights in various solvents (Table 2). The best yield of **3a** (30%) was achieved when the reaction between **1a** and **2a** was conducted in acetonitrile (Table 2, entry 1). The yields of **3a** were observed to increase with the concentration of **1a** (Table 3, entries 1-4), a trend aligning with the small formation constant noted for the EDA complex between **1a** and **2a**. The yield of this reaction was less than 36%, even with the extended reaction time of 26 hours. It is thought that this may be due to the difficulty in forming the EDA complex as the reaction progresses, a situation likely arising from the decrease in both donor and acceptor concentrations.

No reaction was observed in the absence of light (Table 3, entry 5). Under atmospheric conditions, **3a** was not produced (Table 3, entry 6). Instead, methyl phenyl sulfoxide (76% based on **1a**) and methyl phenyl sulfone (14% based on **1a**) were produced, with **2a** remaining unreacted. These observations suggest that the reaction of the cation radical species (**1a**$^{•+}$) with dioxygen is more efficient than the reaction of **1a**$^{•+}$ with **2a**.

**Table 2.** Optimization of the solvent.[a]
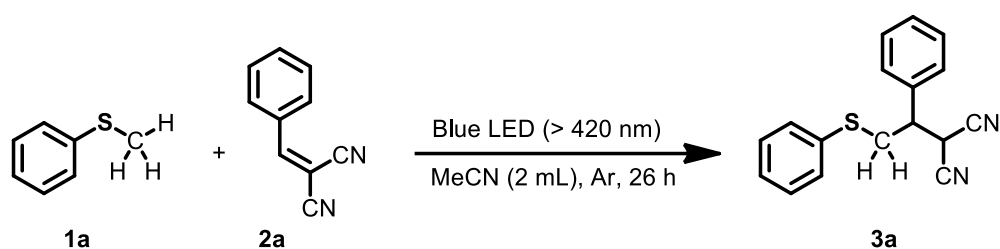


| Entry | Solvents | Yield **3a** (%)[b] |
|-------|----------|---------------------|
| **1** | **acetonitrile** | **30** |
| 2 | propionitrile | 5 |
| 3 | toluene | 0 |
| 4 | ethyl acetate | 0 |
| 5 | methanol | 0 |
| 6 | dichloromethane | 0 |

[a] Reaction conditions: **1a** (0.5 mmol), **2a** (0.1 mmol), solvent: 2.0 mL, Ar atmosphere under blue LED's (>420 nm) irradiation, reaction time: 26 h. [b] based on **2a**.

**Table 3.** Reaction of **1a** with **2a**.[a]
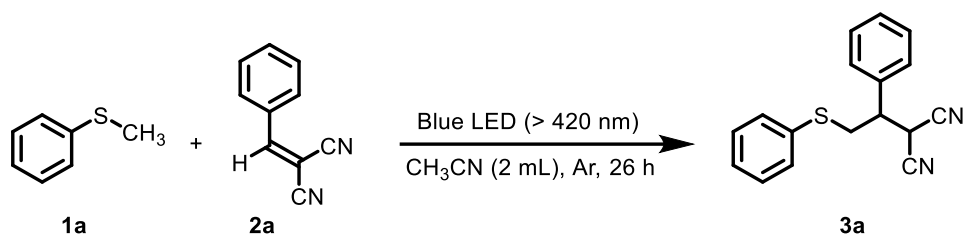


| entry | conditions | **3a** (%)[b] |
|-------|------------|---------------|
| 1 | **1a** (5 equiv.) | 30 |
| 2 | **1a** (1 equiv.) | 11 |
| 3 | **1a** (2.5 equiv.) | 19 |
| 4 | **1a** (10 equiv.) | 36 |
| 5 | no blue LEDs | 0 |
| 6 | under air | 0 |

[a] Reaction conditions: **2a** (0.1 mmol), acetonitrile: 2.0 mL, Ar atmosphere under blue LED's (> 420 nm) irradiation, reaction time: 26 h. [b] Yield based on **2a**.

The apparent quantum yield (AQY)[18] of the production of **3a** from precursors **1a** and **2a** was ascertained by exposing the system to monochromatic light irradiation at wavelengths of 400, 420, 450, and 500 nm, according to the reported procedure.[19] Notably, AQYs were recorded as 1.0% and 0.2% at 400 nm and 420 nm, respectively, as depicted in Figure 2D. The correlation between the absorption spectrum of the EDA complex encompassing **1a** and **2a** and the action spectrum conclusively affirms that the formation of **3a** is mediated by photo-irradiation to the EDA complex between **1a** and **2a**.

The highest occupied molecular orbital (HOMO) level of **1a** is anticipated to influence the absorption band wavelength of the EDA complex formed by **1a** and **2a**. A mixture of thioanisole derivatives featuring different substituents at the *para*-position (**1b–1e**) with **2a** in a 5:1 molar ratio yielded an absorption band above 400 nm, akin to what was observed with **1a**, with the longest wavelength appearing in the order R = CN < H < Br < Me < OMe (Figure 4). When these solutions were subjected to blue LED irradiation in an Ar atmosphere for 26 hours, carbon-carbon bond formation ensued in all instances, yielding the products **3b–3e**. The yield was found to be dependent on the substituents, and a Hammett plot revealed a volcano-shaped curve with the yield achieved with unsubstituted thioanisole **1a** at the apex (Figure 5, and Table 4). This result aligns with the proposed ET-PT mechanism for α-thiomethyl radical (**4**) formation, wherein the reaction proceeds via one-electron oxidation (ET) of thioanisole derivatives followed by deprotonation (PT) (Scheme 2). Thus, incorporating electron-donating substituents into thioanisole enhances one-electron oxidation (ET) but inhibits deprotonation (PT), which might partly elucidate the volcano-type Hammett plot.
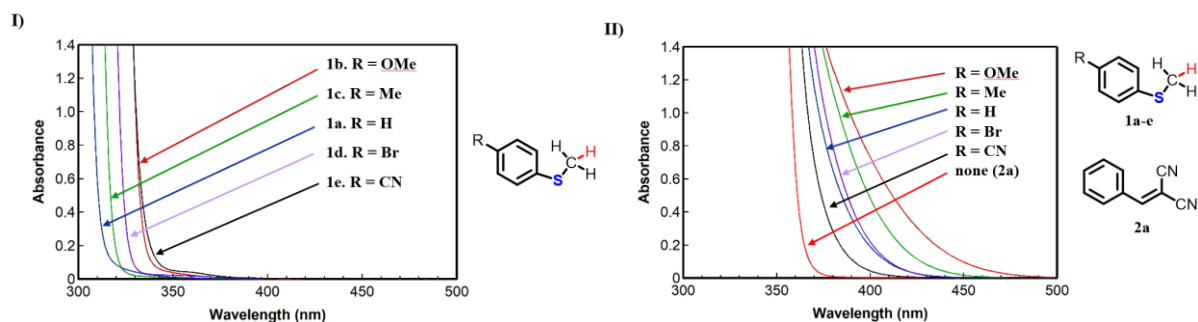


**Figure 4.** UV-Vis spectra of (I) 4-substituted thioanisole **1a-e** (250 mM) were dissolved in 2.2 mL acetonitrile, (II) 4-substituted thioanisole **1a-e** (250 mM) with **2a** (25 mM) were dissolved in 2.2 mL acetonitrile and formed their EDA complexes.
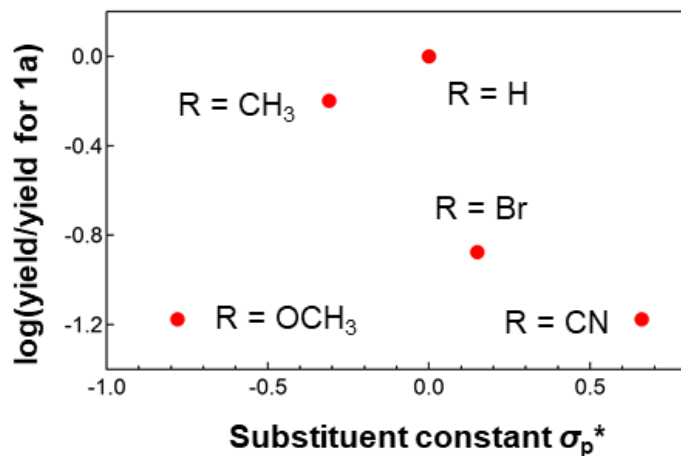
**Figure 5.** Hammett plot for the yield in the reaction of **1a-1e** with **2a**.

**Table 4.** Rection of **1a-1e** with **2a**.[a]
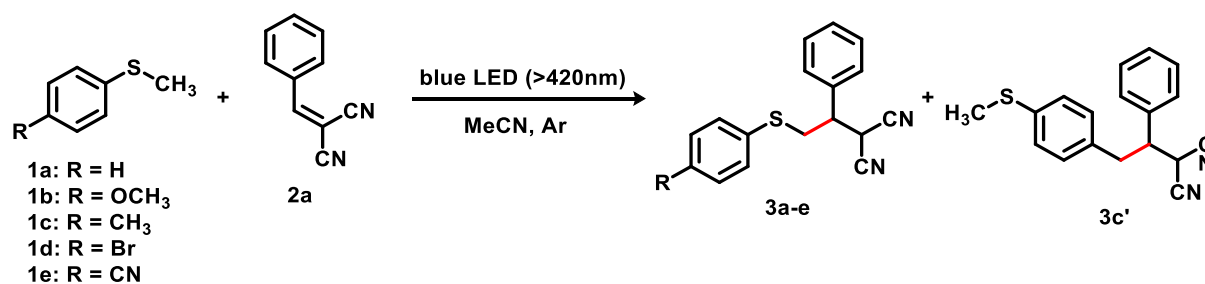


| Entry | R | Substituent constant $\sigma_p^+$ | Products yield **3a-e** (%)[b] | |
|:---:|:---:|:---:|:---:|:---:|
| | | | without base | With CF$_3$CO$_2$Na (0.05 mmol) |
| 1 | OCH$_3$ | -0.78 | 2 | 4 |
| 2 | CH$_3$ | -0.31 | 19 and **3c'** (7%) | 26 and **3c'** (1%) |
| 3 | H | 0 | 30 | 43 |
| 4 | Br | 0.15 | 4 | 12 |
| 5 | CN | 0.66 | 2 | 10 |

[a] Reaction conditions: **1a** (0.5 mmol), **2a** (0.1 mmol), acetonitrile: 2.0 mL, Ar atmosphere under blue LED's (>420 nm) irradiation, reaction time: 26 h. [b] based on **2a**.
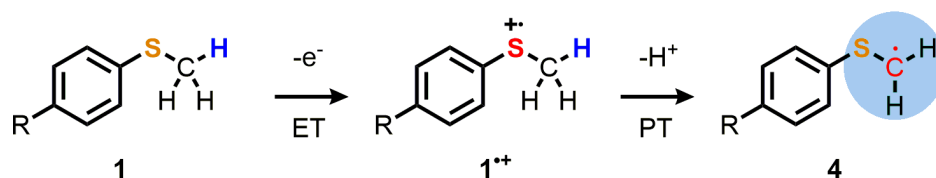


**Scheme 2.** Generation of α-Thiomethyl Radicals from Thioanisole derivatives.

25
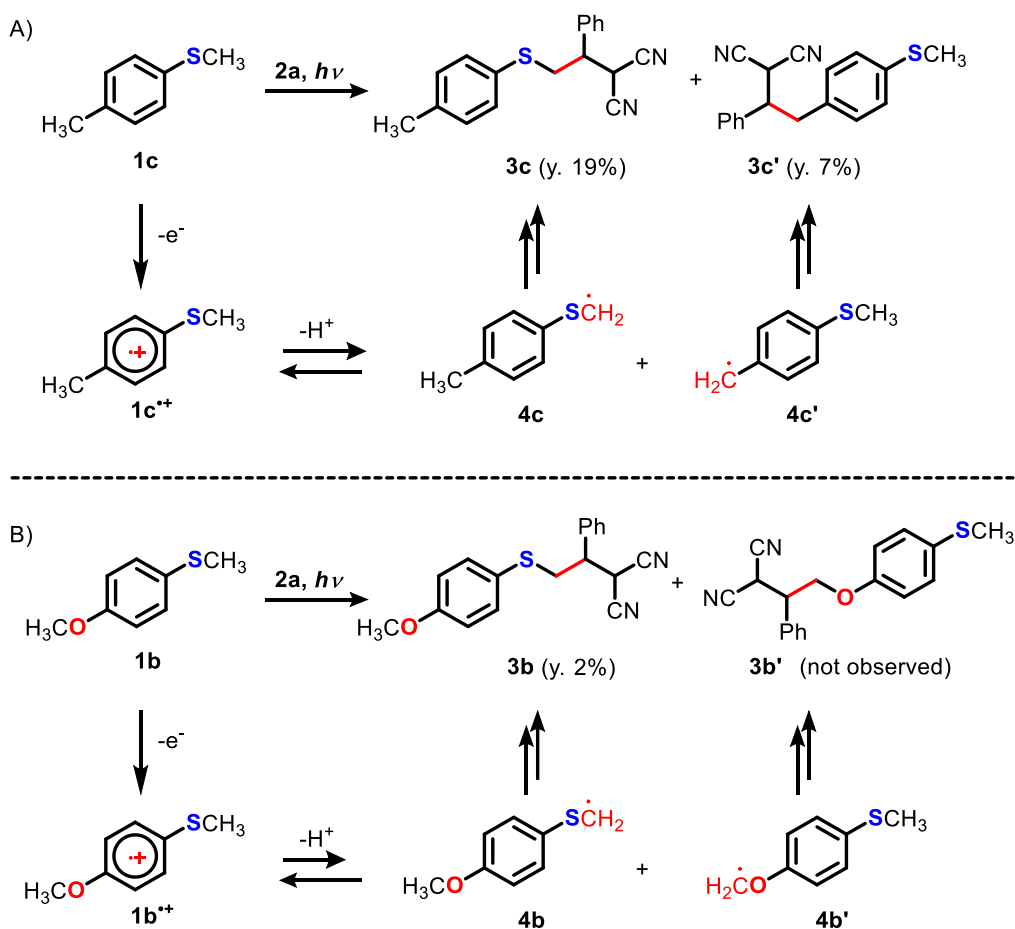
**Scheme 3.** Reactions potentially yielding two products.

In the reaction between **1c** and **2a**, two isomers, **3c** and **3c'**, were produced, as illustrated in Scheme 3. Presumably, **3c** originated from an α-thiomethyl radical (**4c**) generated via the deprotonation of the C–H bond at the α-position to sulfur in **1c·⁺**. Conversely, **3c'** likely emerged from a benzyl radical (**4c'**), formed by deprotonation from the benzyl position C–H bond in **1c·⁺**. Regarding intermediate radicals **4c** and **4c'**, DFT calculations suggest that **4c'** is more stable than **4c** by 0.22 eV (Table 5). Consequently, the tendency for deprotonation does not explain the favored formation of **3c** over **3c'**. Thus, the preferential formation of **3c** over **3c'** might stem from the higher nucleophilic character of **4c** compared to **4c'**. Indeed, the local nucleophilic index $N°_k$ [20] of **4c** surpasses that of **4c'** by 0.39 eV (Table 5). Conversely, only **3b** was detected from **1b**, despite the potential emergence of two products (**3b** and **3b'**). DFT calculations indicated that **4b** displays superior stability by 0.12 eV, but a lower $N°_k$ value by 0.89 eV than **4b'** (Table 5). Thus, the absence of **3b'** formation likely results from the more favorable formation of **4b** than **4b'**.
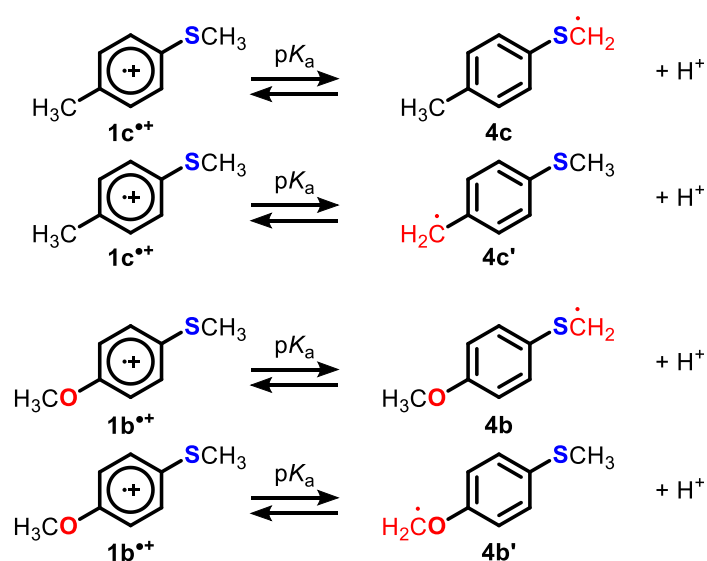
**Table 5.** Calculated energies and global and local nucleophilic indices.[a]

| molecule | $G/eV^b$ | $U/eV^c$ | $IP/eV^d$ | $N/eV^e$ | $ASD^f$ | $N^{\circ}_{k}/eV^g$ | $pK_a^h$ |
|---|---|---|---|---|---|---|---|
| **1c$^{•+}$** | -19284.82 | - | - | - | - | - | - |
| **4c** | -19273.03 | -19,271.84 | 2.63 | 2.50 | 0.85 | 2.11 | 8.5 |
| **4c'** | -19273.25 | -19,272.09 | 3.02 | 2.10 | 0.82 | 1.72 | 8.1 |
| **1b$^{•+}$** | -21331.68 | - | - | - | - | - | - |
| **4b** | -21319.70 | -21,318.46 | 2.57 | 2.55 | 0.87 | 2.22 | 11.8 |
| **4b'** | -21319.58 | -21,318.33 | 2.36 | 2.76 | 1.12 | 3.11 | 14.5 |
| Dicyanomethyl radical | -6109.64 | -6,108.76 | 5.12 | 0.00 | - | 0 | - |

[a] calculated at M062X(D3zero)/(ma-)def2-TZVP/CPCM(acetonitrile) using Orca. [b] Gibbs free energy [c] inner energy [d] ionization energy [e] local nucleophilicity index [f] Mulliken atomic spin density [g] local nucleophilicity index. [h] correspond to the above equations.

The divergence in product selectivity observed from **1c** and **1b** can be attributed to the variations in the $pK_a$ values of **1c$^{•+}$** and **1b$^{•+}$**. The corresponding $pK_a$ values associated with the generation of **4c** and **4c'** from **1c$^{•+}$** stand at 8.5 and 8.1, respectively (Table 5), enabling the simultaneous formation of both **4c** and **4c'**. Consequently, the disparity in nucleophilicity between **4c** and **4c'** dictates product selectivity. In contrast, deprotonation from **1b$^{•+}$** is less direct; the $pK_a$ values for forming **4b** and **4b'** from **1b$^{•+}$** are 11.8 and 14.5, respectively (Table 5). Thus, the deprotonation steps leading to **4b** and **4b'** from **1b$^{•+}$** are both unfavorable. As a

result, it is postulated that products primarily derive from **4b**, which undergoes deprotonation more readily than **4b'**. Thus, these results emphasize the critical role of the deprotonation step in the reaction depicted in Scheme 2.

Subsequently, I undertook photochemical reactions utilizing additional thioethers: ethyl phenyl sulfide **1f**, tetrahydrothiophene **1g**, and dodecyl methyl sulfide **1h** with **2a**. When **1f** was used, compound **3f** was isolated as a 9:10 diastereomer mixture, yielding 23% (Scheme 4). However, in the case of aliphatic thioethers (**1g** and **1h**), no reaction was evidenced, thereby highlighting the indispensable role of the thioanisole framework in enabling EDA-mediated photo-induced carbon-carbon bond formation.



**Scheme 4.** Reaction of **1f** with **2a**.

As outlined earlier, the deprotonation step significantly influences these reactions. Alfonzo and Hande have demonstrated that weak Brønsted bases effectively generate α-thioalkyl radicals by deprotonating C–H bonds in oxidized thioethers.[10] In light of this, I examined the impact of introducing a range of bases. In agreement with the findings reported by Alfonzo and Hande, we discovered that sodium trifluoroacetate yielded the most desirable outcome, specifically a 1.4-fold enhancement in yield. The yield decreased if the basicity of the introduced base deviated either above or below that of sodium trifluoroacetate. Sodium trifluoroacetate also boosted the yield of **3b**–**3e** (Table 4). Regarding **1b** where R = OCH$_3$, product selectivity (**3b** *vs.* **3b'**) is largely governed by their respective p$K_a$ values. While adding sodium trifluoroacetate increased the yield of **3b**, curiously, **3b'** remained undetected, reflecting conditions without sodium trifluoroacetate. This outcome could be ascribed to the insufficient formation of **4b'** even in the presence of sodium trifluoroacetate. Contrarily, when R = CH$_3$ in **1c**, the selectivity is enhanced (**3c** *vs.* **3c'**). This observation can be traced back to sodium trifluoroacetate fostering the formation of the more nucleophilically active species, **4c**, over **4c'**.

These results suggest that the base mediates deprotonation, and the consequent conjugate acid acts as a proton donor to form **3**. Considering these observations and the fact that the reactions proceeded exclusively in acetonitrile and propionitrile, I conjecture that acetonitrile may play a part in the requisite proton transfer in these reactions. Accordingly, I propose the probable mechanism in Scheme 5.
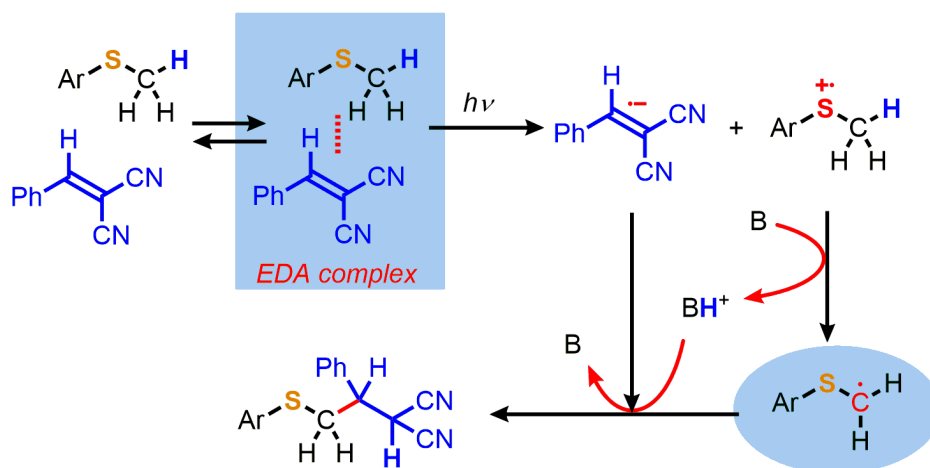


**Scheme 5.** Plausible mechanism.

## Experimental Section

### General Information

^{1}H and ^{13}C NMR spectra were obtained at ambient temperature on a JEOL JNM-ECA 500 MHz spectrometer where CDCl$_3$ (7.26 ppm and 77.13 ppm were reference signals for ^{1}H and ^{13}C respectively) used as a solvent. All chemical shifts *(δ)* are measured in ppm from TMS here chemical shift of TMS was 0.0 ppm, and spin-spin coupling constants (*J*) are mentioned in *Hz*. Unless otherwise specified, commercial reagents were used as received. Products were purified via chromatography using a Biotage Isolera One Flash Purification system. All organic solvents and reagents were purchased from TCI and Wako Pure Chemical Industries and used without further purification. Product analysis was conducted using gas chromatography (GC) with Shimadzu GC-2014 and GCMS-QP2020 instruments equipped with a GL-Science InertCap 1701 column (60 m). UV-Vis spectroscopy measurement for the Job's plot was carried out using an Agilent 8453 UV-visible spectrometer. DFT calculations were carried out at M062X/(ma-)def2-TZVP/CPCM(acetonitrile) with ORCA 5.0. All theoretical calculations were carried out using Orca 5.0 program.[21]

**Job's plot**

To estimate the binding constant of the thioanisole **1a** and **2a** complex, the absorbance of the EDA complex was measured at various molar ratios of **1a** and **2a**. In quartz cell, different ratios of **1a** and **2a** ([**1a**] + [**2a**] = 1.0 M) were mixed in 3.0 mL of MeCN. The maximum absorbance was obtained when the molar ratios of **1a** and **2a** were 1:1. This Job plot ($f$ = [**1a**]/([**1a**] + [**2a**])) supported 1:1 complex of **1a** and **2a** as EDA complex. The association constants were measured using the following method and followed by curve fitting using a program Igor Pro.

$$D + A \rightleftharpoons DA$$
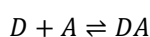
$$\Delta Abs_{obs} = \Delta epsiron \frac{1 + \frac{1}{K} - \sqrt{(1 + \frac{1}{K})^2 - 4f(1 - f)}}{2}$$

**General method of photocatalytic reactions**

Substrate **1** (0.5 mmol) and electron-deficient alkene **2a** (0.1 mmol) was added to a Hungate-type anaerobic tube with 2.0 mL acetonitrile solvent containing a small stirring bar. After argon gas was introduced through a butyl rubber stopper for 3 minutes, the light was irradiated from the side of reactors by two blue LED lamps (Kessil, A160WE Tuna Blue) fitted with a filter (> 420 nm, L420) (Figure 6, the reaction setup). After 26 hours of the reaction, a dimethyl sulfone solution in acetonitrile (0.1 M, 1.0 mL, 0.1 mmol) was added to the reaction mixture as a standard, followed by membrane filtration and GC-MS and NMR analyses. After that, the crude products were purified by chromatography using a Biotage Isolera One flash purification system (hexane: ethyl acetate = 98: 2 → 90: 10) to give **3**.
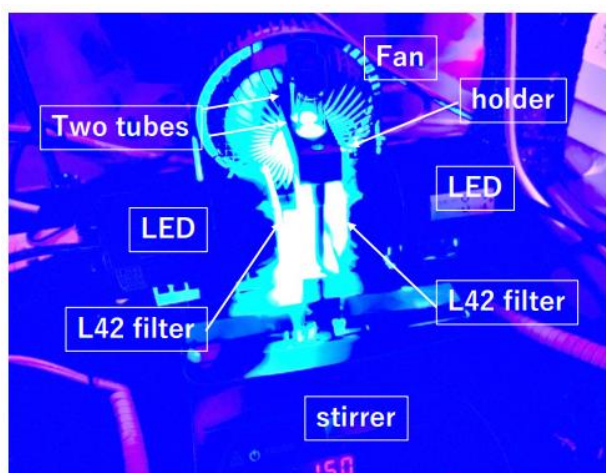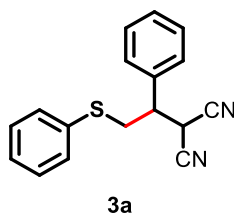


**Figure 6**. Experimental setup of the photoreaction system.

**NMR Data for New Compounds:**

**2-(1-phenyl-2-(phenylthio)ethyl)malononitrile: 3a**



**3a**

Colorless liquid. 12.0 mg (y. 43%). ^{1}H NMR (500 MHz, CDCl$_3$): δ 7.45-7.28 (m, 10H), 4.60 (d, $J$ = 4.6 Hz, 1H), 3.49 (dd, $J$ = 14.3, 5.7 Hz, 1H), 3.41 (dd, $J$ = 14.3, 9.7 Hz, 1H), 3.30 (ddd, $J$ = 9.7, 5.7, 4.6 Hz, 1H). ^{13}C NMR (126 MHz, CDCl$_3$): δ 135.46, 132.97, 130.80, 129.62, 129.46, 129.36, 127.94, 127.81, 111.87, 111.09, 45.61, 36.48, 27.91. HRMS (ESI): $m/z$ calcd for C$_{17}$H$_{14}$N$_2$S+Na$^+$: 301.0770 [$M$+Na]$^+$; found: 301.0782.

**2-(2-((4-methoxyphenyl)thio)-1-phenylethyl)malononitrile: 3b**



**3b**
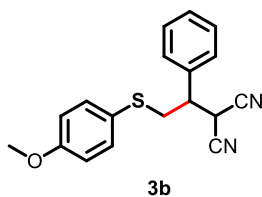
Colorless liquid. 1.2 mg (y. 4%). ^{1}H NMR (500 MHz, CDCl$_3$): δ 7.43 – 7.25 (m, 7H), 6.90–6.84 (d, $J$ = 8.6 Hz, 2H), 4.60 (d, $J$ = 5.1 Hz, 1H), 3.80 (s, 3H), 3.38 – 3.25 (m, 2H), 3.21 (dt, $J$ = 8.7, 5.5 Hz, 1H). ^{13}C NMR (126 MHz, CDCl$_3$): δ 160.09, 135.69, 134.42, 129.45, 129.39, 128.14, 123.22, 115.35, 112.15, 111.33, 55.54, 45.65, 38.32, 27.96. HRMS (ESI): $m/z$ calcd for C$_{18}$H$_{16}$N$_2$OS+Na$^+$: 331.0876 [$M$+Na]$^+$; found: 331.0880.

**2-(1-phenyl-2-(p-tolylthio)ethyl)malononitrile: 3c**



**3c**
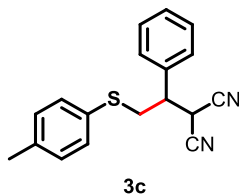
Colorless liquid. 7.6 mg (y. 26%). ^{1}H NMR (500 MHz, CDCl$_3$): δ 7.45 – 7.36 (m, 3H), 7.35 – 7.25 (m, 4H), 7.16 (d, $J$ = 7.9 Hz, 2H), 4.61 (d, $J$ = 4.7 Hz, 1H), 3.42 (dd, $J$ = 14.2, 5.6 Hz, 1H), 3.35 (dd, $J$ = 14.2, 9.6 Hz, 1H), 3.25 (ddd, $J$ = 9.6, 5.6, 4.7 Hz, 1H), 2.35 (s, 3H). ^{13}C NMR

(126 MHz, CDCl$_3$): δ 138.21, 135.53, 131.49, 130.39, 129.37, 129.29, 129.12, 127.96, 111.96, 111.13, 45.50, 37.03, 27.80, 21.11. HRMS (ESI): *m/z* calcd for C$_{18}$H$_{16}$N$_2$S+Na$^+$: 315.0926 [*M*+Na]$^+$; found: 315.0950.

**2-(2-(4-(methylthio)phenyl)-1-phenylethyl)malononitrile: 3c'**



**3c'**
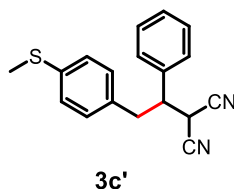
Colorless liquid. 2.1 mg (y. 7%). $^1$H NMR (500 MHz, CDCl$_3$): δ 7.46 – 7.35 (m, 5H), 7.25 – 7.13 (m, 2H), 7.13 – 7.07 (m, 2H), 3.86 (d, *J* = 5.2 Hz, 1H), 3.43 (ddd, *J* = 8.4, 7.3, 5.2 Hz, 1H), 3.29 – 3.16 (m, 2H), 2.47 (s, 3H). $^{13}$C NMR (126 MHz, CDCl$_3$): δ 137.98, 136.24, 133.17, 129.37, 129.24, 129.12, 128.02, 127.03, 111.99, 111.41, 48.30, 37.94, 28.53, 15.68. HRMS (ESI): *m/z* calcd for C$_{18}$H$_{16}$N$_2$S+Na$^+$: 315.0926 [*M*+Na]$^+$; found: 315.0931.

**2-(2-((4-bromophenyl)thio)-1-phenylethyl)malononitrile: 3d**



**3d**
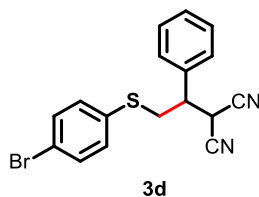
Colorless liquid. 4.3 mg (y. 12%). $^1$H NMR (500 MHz, CDCl$_3$): δ 7.47 – 7.44 (m, 2H), 7.43 – 7.39 (m, 3H), 7.33 – 7.27 (m, 2H), 7.23 – 7.20 (m, 2H), 4.48 (d, *J* = 5.0 Hz, 1H), 3.48 – 3.37 (m, 2H), 3.29 (ddd, *J* = 8.7, 6.5, 4.9 Hz, 1H). $^{13}$C NMR (126 MHz, CDCl$_3$): δ 135.19, 132.63, 132.28, 132.18, 129.51, 129.38, 127.86, 121.83, 111.67, 111.06, 45.54, 36.48, 28.09. HRMS (ESI): *m/z* calcd for C$_{17}$H$_{13}$BrN$_2$S+Na$^+$: 378.9875 [*M*+Na]$^+$; found: 378.9863.
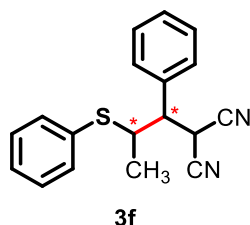
**2-(2-((4-cyanophenyl)thio)-1-phenylethyl)malononitrile: 3e**



**3e**
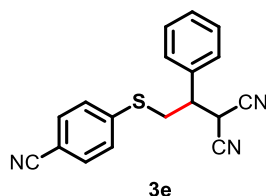
Colorless liquid. 3.0 mg (y. 10%). $^1$H NMR (500 MHz, CDCl$_3$): δ 7.61 – 7.55 (m, 2H), 7.48 – 7.40 (m, 3H), 7.34 (ddd, *J* = 8.0, 6.3, 2.1 Hz, 4H), 4.41 (d, *J* = 5.3 Hz, 1H), 3.62 – 3.50 (m,

2H), 3.42 (td, $J$ = 7.5, 5.2 Hz, 1H). $^{13}$C NMR (126 MHz, CDCl$_3$): δ 141.20, 135.02, 132.90, 129.86, 129.65, 128.48, 127.91, 118.48, 111.59, 111.20, 110.47, 45.64, 34.74, 28.60. HRMS (ESI): $m/z$ calcd for C$_{18}$H$_{13}$N$_3$S+Na$^+$: 326.0722 [$M$+Na]$^+$; found: 326.0724.

## 2-(1-phenyl-2-(phenylthio)propyl)malononitrile: 3f



**3f**

The diastereomeric ratio of A to B is 9:10.

**diastereomer A**



2-((1S,2R)-1-phenyl-2-(phenylthio)propyl)malononitrile

2-((1R,2S)-1-phenyl-2-(phenylthio)propyl)malononitrile
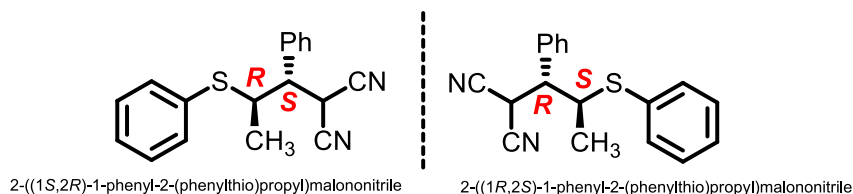
diastereomer A: White solid. 3.2 mg (y. 11%). $^1$H NMR (500 MHz, CDCl$_3$): δ 7.59 – 7.51 (m, 2H), 7.45 – 7.30 (m, 8H), 5.19 (d, $J$ = 4.5 Hz, 1H), 3.61 (dq, $J$ = 11.5, 6.7 Hz, 1H), 3.07 (dd, $J$ = 11.5, 4.5 Hz, 1H), 1.16 (d, $J$ = 6.7 Hz, 3H). $^{13}$C NMR (126 MHz, CDCl$_3$): δ 134.85, 134.40, 131.57, 129.65, 129.53, 129.44, 129.01, 128.48, 112.18, 111.62, 52.11, 46.36, 28.86, 20.71. HRMS (ESI): $m/z$ calcd for C$_{18}$H$_{16}$N$_2$S+Na$^+$: 315.0926 [$M$+Na]$^+$; found: 315.0943.

**diastereomer B**



2-((1R,2R)-1-phenyl-2-(phenylthio)propyl)malononitrile

2-((1S,2S)-1-phenyl-2-(phenylthio)propyl)malononitrile
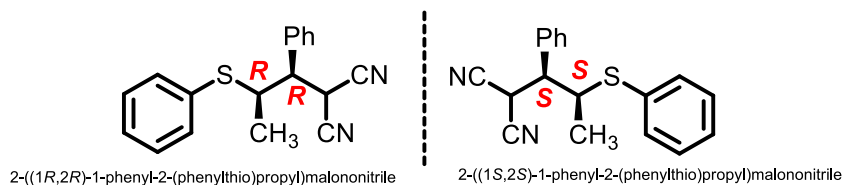
diastereomer B: White solid. 3.5 mg (y. 12%). $^1$H NMR (500 MHz, CDCl$_3$): δ 7.51 – 7.44 (m, 2H), 7.42 (dq, $J$ = 4.8, 1.6 Hz, 3H), 7.33 (tdq, $J$ = 5.3, 3.6, 1.6 Hz, 5H), 4.68 (d, $J$ = 10.0 Hz, 1H), 3.73 (dq, $J$ = 6.8, 5.2 Hz, 1H), 3.46 (dd, $J$ = 10.0, 5.2 Hz, 1H), 1.31 (d, $J$ = 6.8 Hz, 3H). $^{13}$C NMR (126 MHz, CDCl$_3$): δ 133.73, 133.57, 133.08, 129.55, 129.42, 129.23, 128.78, 128.50, 112.37, 112.02, 52.15, 47.81, 27.55, 21.07. HRMS (ESI): $m/z$ calcd for C$_{18}$H$_{16}$N$_2$S+Na$^+$: 315.0926 [$M$+Na]$^+$; found: 315.0942.

## Conclusion

The present study highlights the potential for the formation of α-thioalkyl radicals for carbon–carbon bond formation reactions by photoirradiation of EDA complexes. Significant findings highlight the importance of both one-electron oxidation and deprotonation processes for maximizing the reaction yield. The generation of α-thioalkyl radicals by such a mechanism is anticipated to lead to a more efficient synthesis. However, the present study also revealed the importance of the thioanisole backbone in EDA-mediated photo-induced C-C bond formation. Overall, the findings lay a solid foundation for further investigation and optimization of thioether chemistry, particularly the functionalization of thioanisole derivatives.

## References

(1)     R. Zhang, H. Ding, X. Pu, Z. Qian, Y. Xiao, *Catalysts* **2020**, *10*, 1339.

(2)     E. Hasegawa, M. A. Brumfield, P. S. Mariano, U. C. Yoon, *J. Org. Chem.* **1988**, *53*, 5435-5442.

(3)     M. Mella, M. Freccero, E. Fasani, A. Albini, *Chem. Soc. Rev.* **1998**, *27*, 81-89.

(4)     E. Baciocchi, T. Del Giacco, F. Elisei, A. Lapi, *J. Org. Chem.* **2006**, *71*, 853-860.

(5)     Y. Li, K. Miyazawa, T. Koike, M. Akita, *Org. Chem. Front.* **2015**, *2*, 319-323.

(6)     R. A. Garza-Sanchez, T. Patra, A. Tlahuext-Aca, F. Strieth-Kalthoff, F. Glorius, *Chem. Eur. J.* **2018**, *24*, 10064-10068.

(7)     C. Silva-Cuevas, E. Paleo, D. F. León-Rayo, J. A. Lujan-Montelongo, *RSC Adv.* **2018**, *8*, 24654-24659.

(8)     C. Le, Y. Liang, R. W. Evans, X. Li, D. W. C. MacMillan, *Nature* **2017**, *547*, 79-83.

(9)     J. Kim, B. X. Li, R. Y. C. Huang, J. X. Qiao, W. R. Ewing, D. W. C. MacMillan, *J. Am. Chem. Soc.* **2020**, *142*, 21260-21266.

(10)    E. Alfonzo, S. M. Hande, *ACS Catal.* **2020**, *10*, 12590-12595.

(11)    E. Alfonzo, S. M. Hande, *Org. Lett.* **2021**, *23*, 6115-6120.

(12)    Z. Tan, S. Zhu, Y. Liu, X. Feng, *Angew. Chem. Int. Ed.* **2022**, *61*, e202203374.

(13)    G. E. M. Crisenza, D. Mazzarella, P. Melchiorre, *J. Am. Chem. Soc.* **2020**, *142*, 5461-5476.

(14)    V. Abbu, V. Nampally, N. Baindla, P. Tigulla, *J. Solution. Chem.* **2019**, *48*, 61-81.

(15)    R. Zaini, A. C. Orcutt, B. R. Arnold, *Photochem. Photobiol.* **1999**, *69*, 443-447.

(16)    J. Contreras-García, E. R. Johnson, S. Keinan, R. Chaudret, J.-P. Piquemal, D. N. Beratan, W. Yang, *J. Chem. Theory Comput.* **2011**, *7*, 625-632.

(17)     B. Liu, C.-H. Lim, G. M. Miyake, *J. Am. Chem. Soc.* **2017**, *139*, 13616-13619.

(18)     H. Kisch, D. Bahnemann, *J. Phys. Chem. Lett.* **2015**, *6*, 1907-1910.

(19)     S. Okunaka, H. Tokudome, Y. Hitomi, *J. Catal.* **2020**, *391*, 480-484.

(20)     L. R. Domingo, P. Pérez, *Org. Biomol. Chem.* **2013**, *11*, 4350-4358.

(21)     F. Neese, *Wiley Interdiscip. Rev.: Comput. Mol. Sci.* **2022**, *12*, e1606.

<center>**Chapter 2**</center>

<center>**Blue Light-Promoted Synthesis of Thiochromenopyrroledione Derivatives via Titanium Dioxide-Catalyzed Dual Carbon–Carbon Bond Formation with Thioanisole and Maleimide Derivatives**</center>

## Abstract

Under anaerobic conditions, thioanisole derivatives bearing a thiomethyl group participated in dual carbon-carbon bond-forming reactions with maleimide derivatives in the presence of titanium dioxide. Blue light irradiation facilitated these reactions, producing thiochromenopyrroledione derivatives and nearly equimolar quantities of succinimide derivatives. Specifically, a thiochromenopyrroledione derivative formed from thioanisole and $N$-benzylmaleimide was achieved with a 43% yield after 12 hours of blue light exposure (>420 nm), approaching its theoretical maximum yield of 50%. Without titanium dioxide, the reaction remained dormant. My investigations with five varieties of 4-substituted thioanisoles and four $N$-substituted maleimides as precursors resulted in the synthesis of 20 distinct thiochromenopyrroledione derivatives with moderate to high yields. From observed substituent effects, I postulate that this reaction proceeds through a charge transfer from thioanisole to the conduction band of titanium dioxide during blue light irradiation, initiating the one-electron oxidation of thioanisole and subsequent generation of α-thioalkyl radicals *via* deprotonation.

## Introduction

Heterocyclic compounds have been highly sought for their potential physiological activity and use as precursors to functional materials, stimulating the search for novel and efficient chemical conversion methodologies for constructing these complex cyclic

structures.[1,2] The aza-Diels-Alder reaction represents a robust method for building heterocyclic compounds such as tetrahydropyridine,[3] but radical addition/cyclization presents another promising approach. For instance, in 2004, Hoffmann and his team synthesized tetrahydroquinoline derivatives (**A1** in Scheme 1a) from *N,N*-dimethylaniline and electron-deficient alkenes, (5*R*)-menthyloxy-2[5*H*]furanone, *via* a radical addition/cyclization pathway, harnessing semiconductor photocatalysts like titanium dioxide (TiO$_2$).[4] In 2012, employing a ruthenium complex as a photoredox catalyst, Yu and Bian achieved the synthesis of tetrahydroquinoline (**A2** in Scheme 1b) through an analogous radical addition/cyclization pathway, using *N,N*-dimethylaniline, and maleimides.[5] As such, several research groups have reported on annulation reactions using aniline derivatives.[6-11] On the other hand, annulation involving anisole or thioanisole derivatives *via* a radical addition/cyclization pathway has been reported only by Walton et al. (**A3** and **A4** in Scheme 1c and 1d, respectively).[12,13] These reactions leverage the single electron oxidation and decarboxylation of aryl acetate to generate α-oxygen methyl radicals or α-thiomethyl radicals. This insight affords a fresh paradigm for the conversion of heteroatom-enriched substrates using TiO$_2$ as a visible-light photocatalyst.
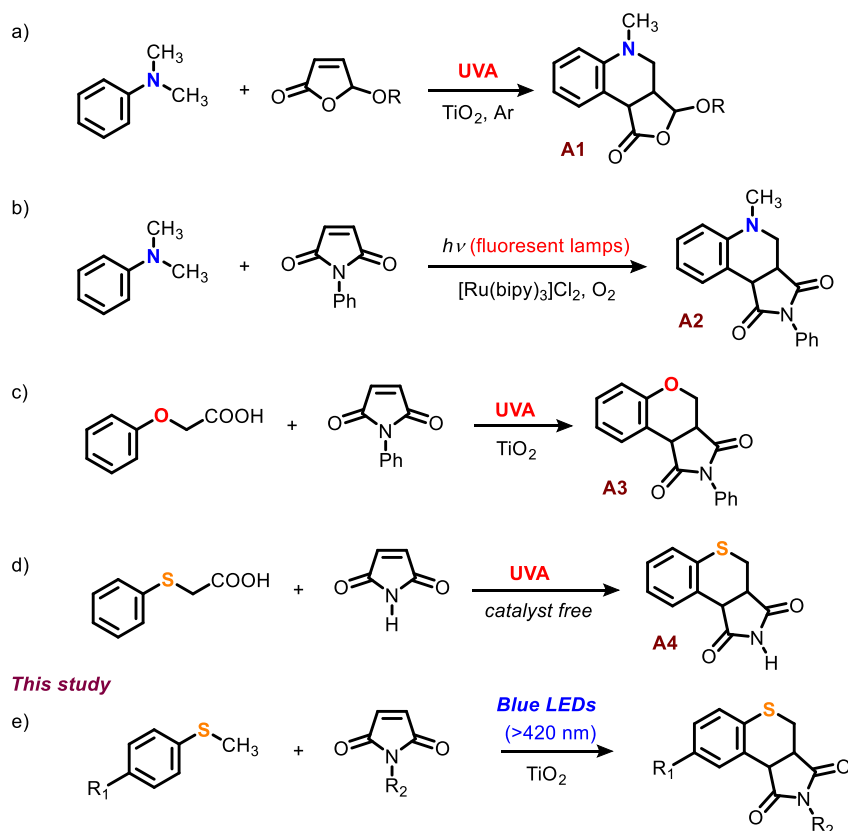


**Scheme 1.** Photocatalytic radical addition/cyclization for annulation with maleimide derivatives.
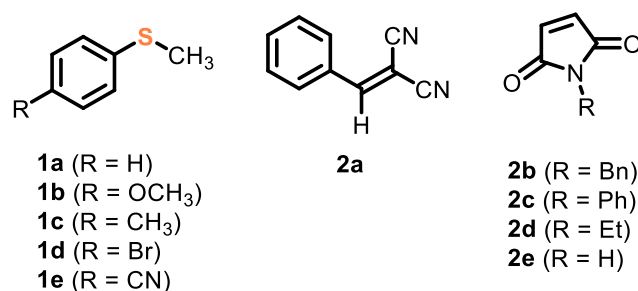
**Figure 1.** Structures of thioanisole derivatives (**1a-e**) and electron-deficient alkenes (**2a-e**) employed in this study.

Previously, I reported the formation of an electron-donor-acceptor (EDA) complex between a thioanisole derivative (Figure 1, **1a-e**) and benzylidenemalononitrile (BMN, Figure 1, **2a**), an electron-deficient alkene.[14] I revealed that an α-thiomethyl radical is produced upon blue light irradiation through the single electron oxidation and deprotonation of thioanisole. The strategy of C–C bond formation through C–H bond cleavage using EDA complex formation is notable, as the reactions proceed without any photocatalyst. However, these reactions are restricted to specific donor and acceptor molecules capable of forming EDA complexes. Additionally, unreacted substrates persist even with extended reaction times, capping the yield at 43%. This limitation arises because the EDA complex's concentration decreases as the reactants are consumed.

The use of TiO$_2$ as a photocatalyst in organic synthesis has been vigorously researched in recent years.[15-19] Herein, I discerned that in the presence of TiO$_2$, C–C bond formation can be achieved without forming an EDA complex. When maleimides were employed, an annulation reaction with thioanisole derivatives under blue light irradiation yielded thiochromenopyrrolediones (Scheme 1e) with moderate to high yields.

## Results and discussion

As I previously reported,[14] thioanisole (**1a**) and BMN (**2a**) form an EDA complex that exhibits an absorption band in the visible light region (>420 nm). Upon exposure to this absorption band, a carbon-carbon bond formation reaction proceeds to afford carbon-carbon bond forming product **3a** with a yield of 30% (Scheme 2). Additionally, I reported that adding an appropriate base improves the reaction efficiency by up to 43%. Subsequently, I discovered that adding TiO$_2$ dramatically enhanced the reaction efficiency up to 98% of yield (Scheme 2).

The time course of the reactions in the absence and presence of TiO₂ shows that TiO₂ accelerated the reaction (Figure 2). For other thioanisole derivatives, the yield also improved in the presence of TiO₂ (Scheme 2). These findings demonstrate that for reactant pairs forming an EDA complex and exhibiting a charge transfer (CT) absorption band in the visible region (>420 nm), the addition of TiO₂ enhances the yield. Additionally, even though the combination of tetrahydrothiophene and BMN does not exhibit a CT absorption band attributable to the EDA complex in the visible region (>420 nm), it facilitates C–C bond formation, resulting in the generation of **3g** under blue light irradiation in the presence of TiO₂.
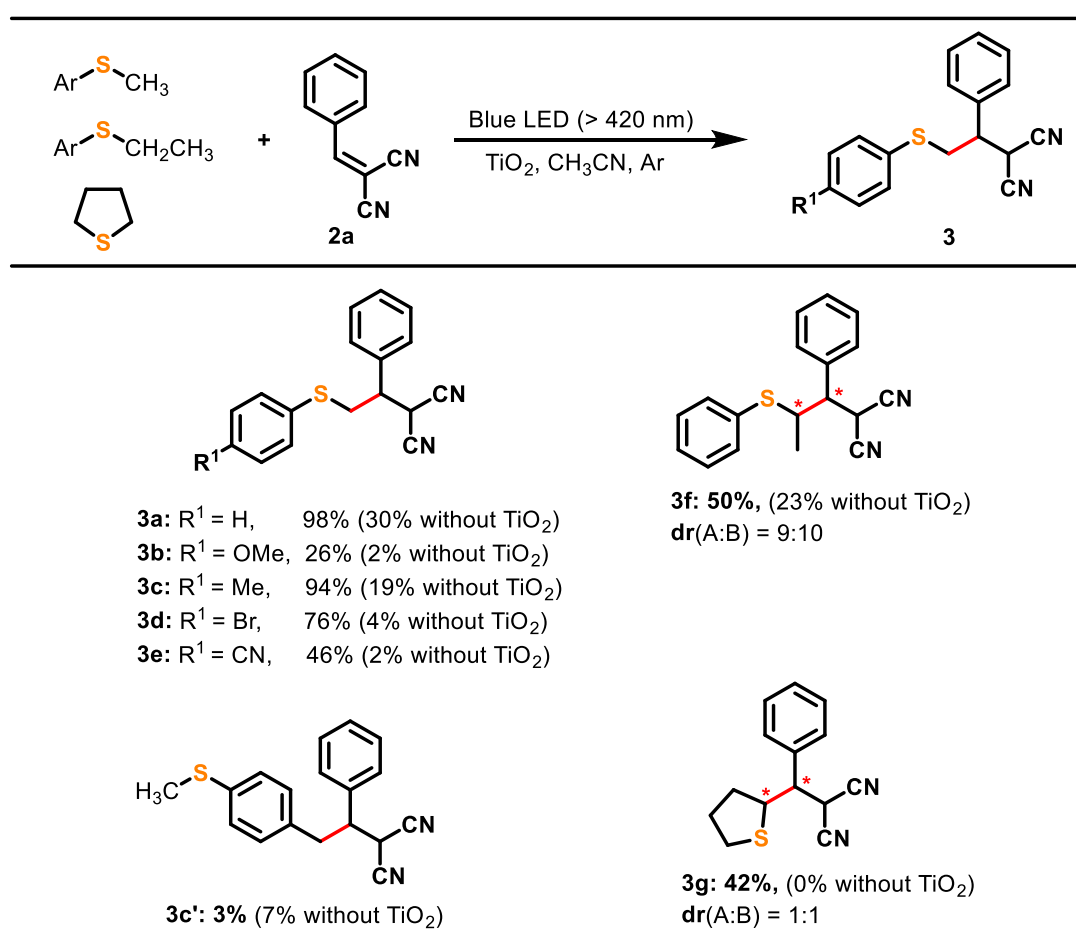


**Scheme 2.** Effect of TiO₂ on the reaction of thioanisole derivatives and tetrahydrothiophene with BMN **2a**. Reaction conditions: TiO₂ (5 mg), thioether (0.3 mmol), **2a** (0.1 mmol) in CH₃CN (2 mL), under an Ar atmosphere for 26 h. Yield based on **2a**.
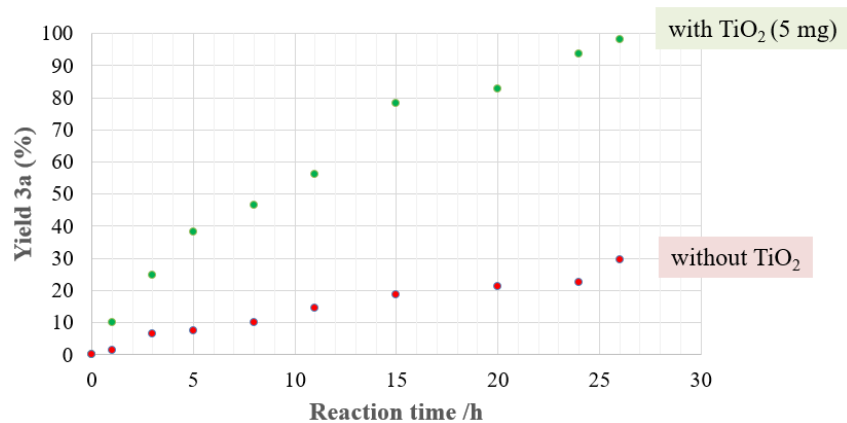
**Figure 2.** Yield of product **3a** as a function of reaction time in the presence (green) and absence (red) of TiO₂.
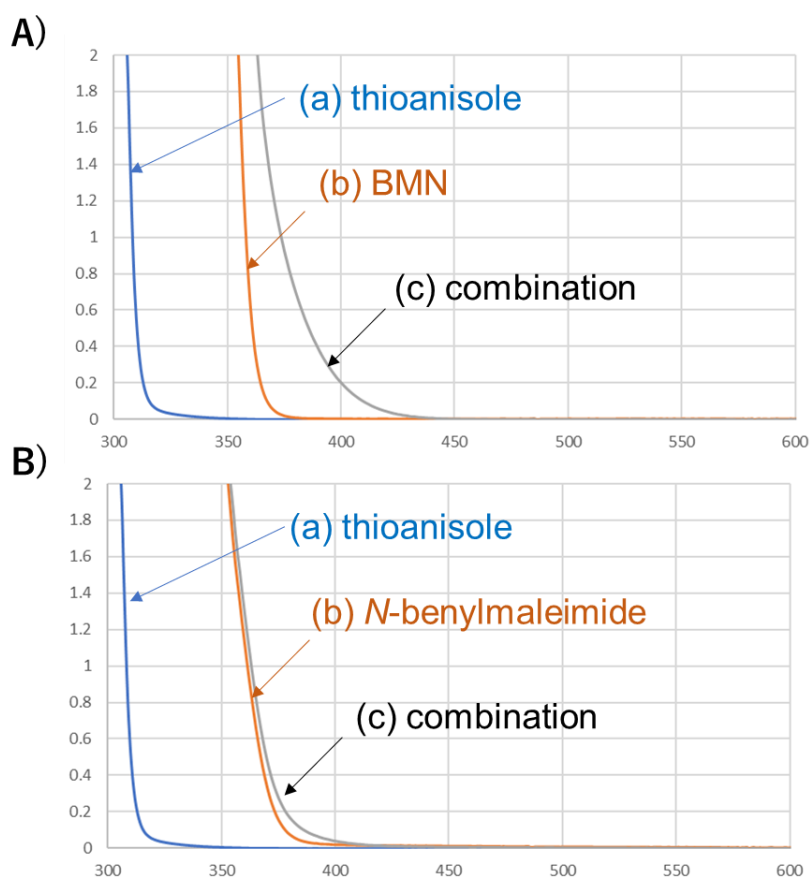


**Figure 3.** (A) Absorption spectra of thioanisole (**1a**) and BMN (**2a**), and the combination of **1a** and **2a** in MeCN. [**1a**] = 250 mM, and [**2a**] = 50 mM. (B) Absorption spectra of thioanisole (**1a**) and *N*-benzyl maleimide (**2b**), and the combination of **1a** and **2b** in MeCN. [**1a**] = 250 mM, and [**2b**] = 50 mM.

**Table 1.** The reaction of **1a** and **2b** under various conditions.[a]



| entry | conditions | **4b**[b] | **5b**[b] | Ratio of **5b/4b** |
|-------|------------|-----------|-----------|--------------------|
| 1 | standard | 43 | 57 | 1.3 |
| 2 | SiO$_2$ instead of TiO$_2$ | 0 | 0 | - |
| 3 | Al$_2$O$_3$ instead of TiO$_2$ | 0 | 0 | - |
| 4 | no blue LEDs | 0 | 0 | - |
| 5 | under air | 0 | 0 | - |
| 6 | under O$_2$ | 0 | 0 | - |
| 7 | CD$_3$CN | 44 | 47 | 1.1 |
| 8 | CH$_3$OH | 0.4 | 18 | 45 |
| 9 | ethyl acetate | 21 | 29 | 1.4 |
| 10 | CH$_3$NO$_2$ | 14 | 1 | 0.1 |

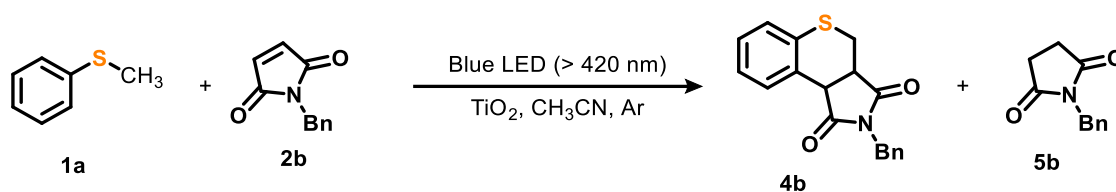[a] Reaction conditions: TiO$_2$ (5 mg), **1a** (0.3 mmol), **2b** (0.1 mmol) in CH$_3$CN (2 mL), under an Ar atmosphere and blue LED irradiation (> 420 nm) for 12 h. [b] Yield (%) based on **2b**.

Unlike BMN, the combination of thioanisole and *N*-benzylmaleimide displays no absorption band at >420 nm (Figure 3), and in agreement with this observation, no reaction proceeded upon irradiation with blue light. However, with the introduction of TiO$_2$, I observed the formation of an annulation product **4b**, alongside *N*-benzylsuccinimide **5b** (Table 1). The ratio of the yields for **4b** and **5b** will be addressed in the following sections. No product was obtained when Al$_2$O$_3$ or SiO$_2$ was added instead of TiO$_2$ (Table 1, entries 2 and 3). Hence, these findings suggest that the reaction progresses upon light exposure not because of EDA complex formation but because TiO$_2$ acts as a photocatalyst. While TiO$_2$ is typically driven by UV light, it has been reported that visible light-induced electron transfer from molecules on the surface of TiO$_2$ to its conduction band is possible.[20] For instance, I reported that when blue light was irradiated onto a suspension of toluene in TiO$_2$, the toluene oxidation progresses to yield benzaldehyde under aerobic conditions.[21]

The apparent quantum yield (AQY) of the production of **4b** from precursors **1a** and **2b** was determined using monochromatic light irradiation at wavelengths of 400, 420, 450, and 500 nm, according to the reported procedure (Table 2).[14] The AQY value is 0.3% for forming **4b** under 420 nm light irradiation. Thus, the reaction proceeded even upon >400 nm light irradiation. Additionally, the diffuse reflectance spectrum of $TiO_2$ dispersed in thioanisole revealed an absorption band at a lower energy than pure $TiO_2$ (Figure 4). Moreover, thioanisole does not absorb light at wavelengths greater than 400 nm (Figure 3). These observations suggest a potential electron transfer from thioanisole to the $TiO_2$ conduction band, forming a thioanisole cation radical.

**Table 2.** AQYs for the formation of **4b** from **1a** and **2b**.[a]

| Wave length/nm | Yield **4b**[b] (%) | AQY (%) |
| --- | --- | --- |
| 400 | 6.6 | 1.3 |
| 420 | 4.7 | 0.3 |
| 450 | 1.9 | 0.1 |
| 500 | ~0 | n.d. |

[a] Reaction conditions: $TiO_2$ (5 mg), **1a** (0.3 mmol), **2b** (0.1 mmol) in acetonitrile (2 mL), under an Ar atmosphere for 12 h.  [b] Yield based on **2b**.
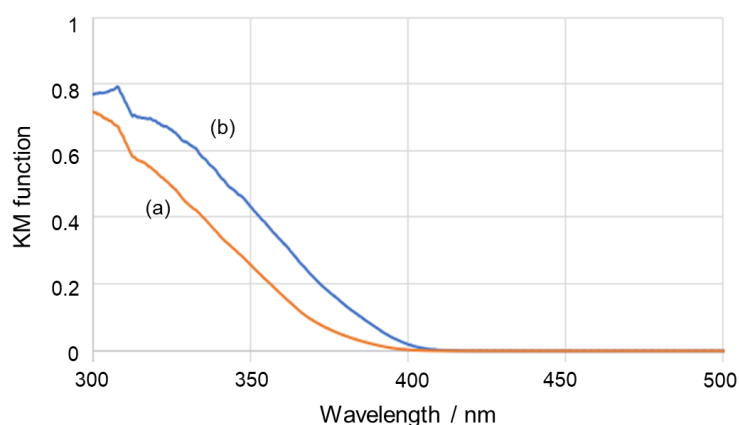


**Figure 4.** Diffuse reflectance spectra of (a) $TiO_2$ and (b) $TiO_2$ dispersed in thioanisole.

In the reaction between **1a** and **2b**, the yield of the annulation product **4b**, based on **2b**, was 43%. Reactant **2b** was completely consumed, yielding **5b**, a reduced form of **2b**, at 57%

(Table 1, entry 1). The expected stoichiometric outcome would be an equimolar formation of **4b** and **5b**. Nevertheless, there was a slight deviation from this expectation: the observed ratio of **5b** over **4b** with a 1.3:1 ratio. Switching the solvent to $CD_3CN$ from $CH_3CN$ lowered this ratio to 1.1:1 (Table 1, entry 7). In addition, using methanol, a more readily oxidizable solvent than $CH_3CN$, escalated the ratio to 45:1 (Table 1, entry 8). This inclination towards **5b** production suggests the solvent oxidation, which leads to the formation of electrons and protons that facilitate **5b** reduction. Additional investigations revealed the reaction's sensitivity to light and its inhibition in the presence of oxygen (Table 1, entries 4 to 6). Among the tested solvents, $CH_3CN$ proved to be the optimal choice (Table 1, entries 8 to 10).



**Figure 5.** Stereochemistry of the products.
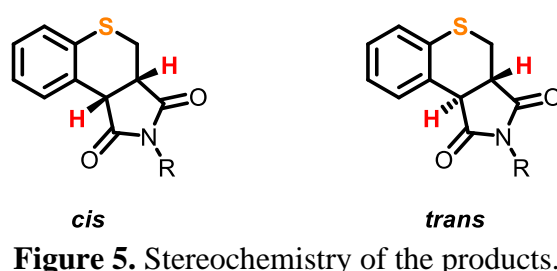
Annulation product **4b** possesses two chiral carbons, thereby permitting the potential existence of both *cis-* and *trans*-isomers (Figure 5). Nevertheless, the NMR spectrum of the reaction mixture indicated the existence of a single isomer of **4b**. DFT calculations revealed a stability differential of ca. 5.6 kcal/mol in favor of the *cis*-isomer over the *trans*-isomer (Figure 6). Furthermore, through theoretical calculation, the dihedral angles derived from the vicinal proton-proton $^3J_{HH}$ coupling constants of annulation product **4b** were compared with the dihedral angles of the computationally optimized *cis-* and *trans*-isomers of **4b** (Table 3). This analysis corroborated the identification of annulation product **4b** as the *cis*-isomer.
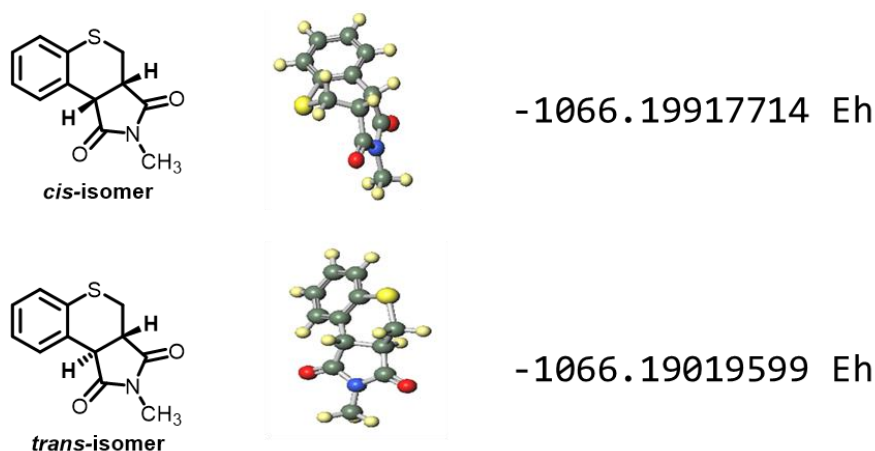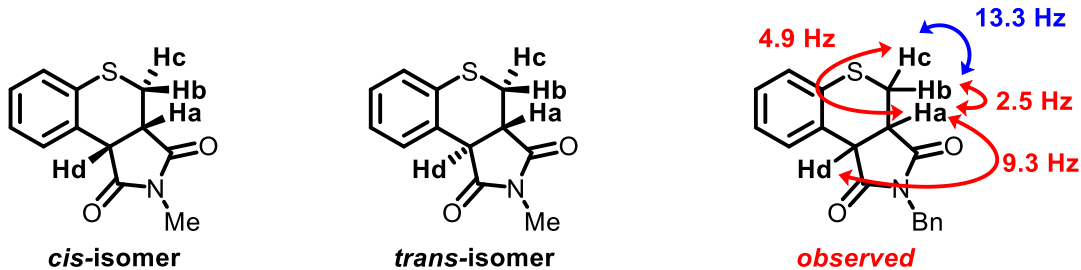


**Figure 6.** Computationally optimized structures of *cis-* and *trans*-isomers.

43

**Table 3.** Proton-proton $^3J_{HH}$ coupling constants of annulation product.



| $J_{HH}$ | observed $J$ coupling/Hz | *calculated J* coupling constant of cis configuration/Hz | *calculated J* coupling constant of trans configuration/Hz |
|---|---|---|---|
| a_b | 2.5 | 2.057 | 4.585 |
| a_c | 4.9 | 5.065 | 13.584 |
| a_d | 9.3 | 8.544 | 9.629 |
| b_c | 13.3 | 14.235 | 12.494 |

NMR *J* coupling constants were calculated using the Orca computational chemistry software package. Calculations were performed at the B3LYP/PCSEG-2 level of theory with the Conductor-like Polarizable Continuum Model (CPCM) solvent model for chloroform. The auxiliary basis sets were automatically assigned.
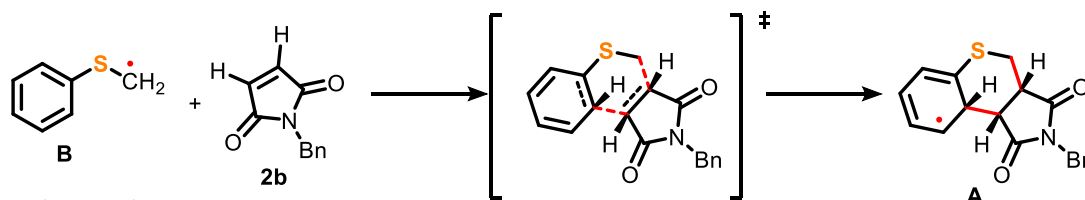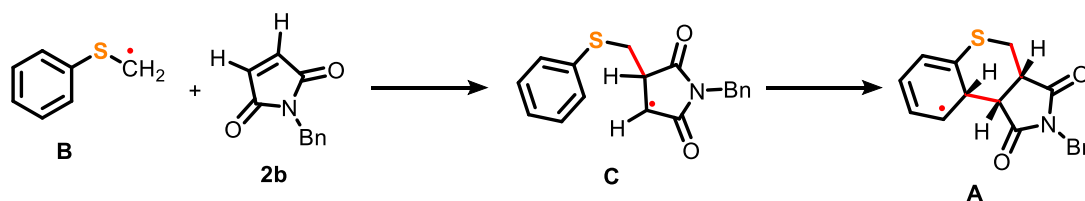


**Scheme 3.** Possible mechanisms for the annulation step.

Annulation product **4b** is assumed to originate from radical species **A** (Scheme 3). Employing the Nudged Elastic Band (NEB) method, the potential for the formation of radical species by the reaction of the radical derived from thioanisole (**B**) and *N*-benyzlmaleimide **2b** was examined, and further confirmed by DFT calculations (Figure 7). The results revealed a stepwise, rather than concerted (Scheme 3a), reaction pathway *via* radical species **C** (Scheme 3b).

**Figure 7.** (a) Minimum energy path determined by NEB method. (b) Calculated energy for intermediates and transition states for the reaction of α-thiomethyl radical of thioanisole and *N*-methylmaleimide.
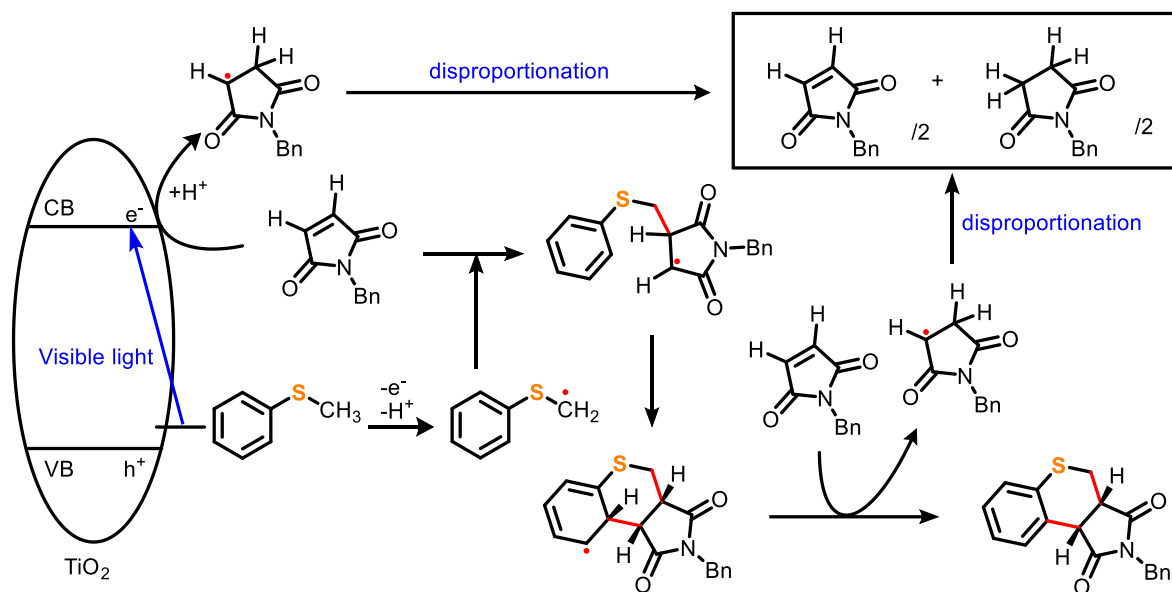
**Scheme 4.** Proposed mechanism.

The putative reaction mechanism is delineated in Scheme 4. The one-electron-reduced maleimide is likely to undergo rapid disproportionation to yield maleimide and succinimide. The disproportionation constant was estimated to be $\log K \sim 33$, as determined by DFT calculations (Figure 8).



**BH (0 2)**
-359.98179454 Eh

**BH2 (0 1)**
-360.62511973 Eh

**B (0 1)**
-359.41222316 Eh

$$\Delta G = -46.28 \text{ kcal/mol} = -RT\ln(K)$$

$$K = \exp(46.28 \times 10^3/RT) = \exp(46.28 \times 10^3/(1.9872 \times 298.15)) = 8.4 \times 10^{33}$$
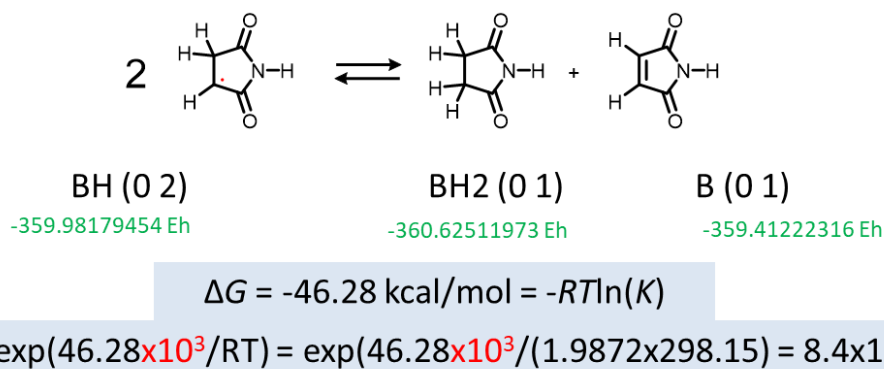
**Figure 8.** Calculation of disproportionation constant.
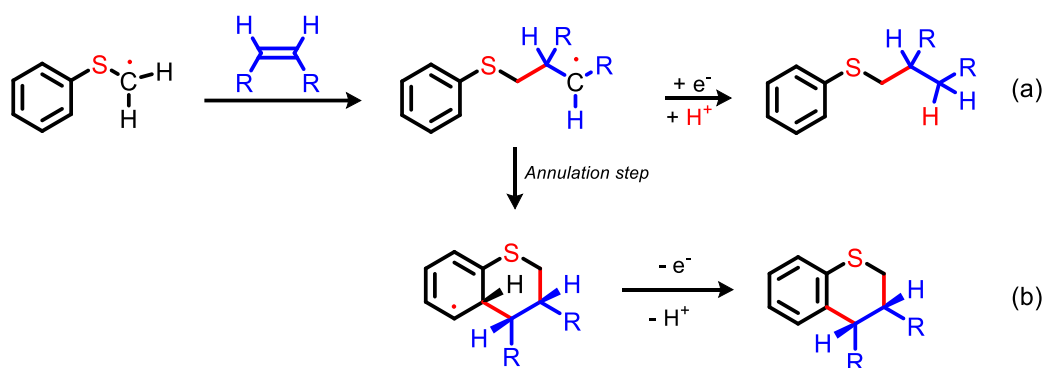
**Scheme 5.** Possible competition between single C–C bond forming reaction (a) and annulation reaction (b).

My theoretical calculations determined that the reaction proceeds stepwise rather than concurrently. I posit that this singular C–C bond formation competes with a reduction of the radical intermediate, as illustrated in Scheme 5. If the annulation step is unfavorable, solely the single bond formation transpires. Utilizing *N*-substituted maleimides results exclusively in annulation. In contrast, with BMN **2a**, only a reaction leading to a single C-C bond was observed. My computations in Scheme 6 suggest that employing BMN makes the annulation step energetically demanding, with *ΔG* of 69 kcal/mol. Conversely, using maleimide facilitates the annulation, necessitating a reduced energy of *ΔG* of -2.1 kcal/mol (Scheme 6).
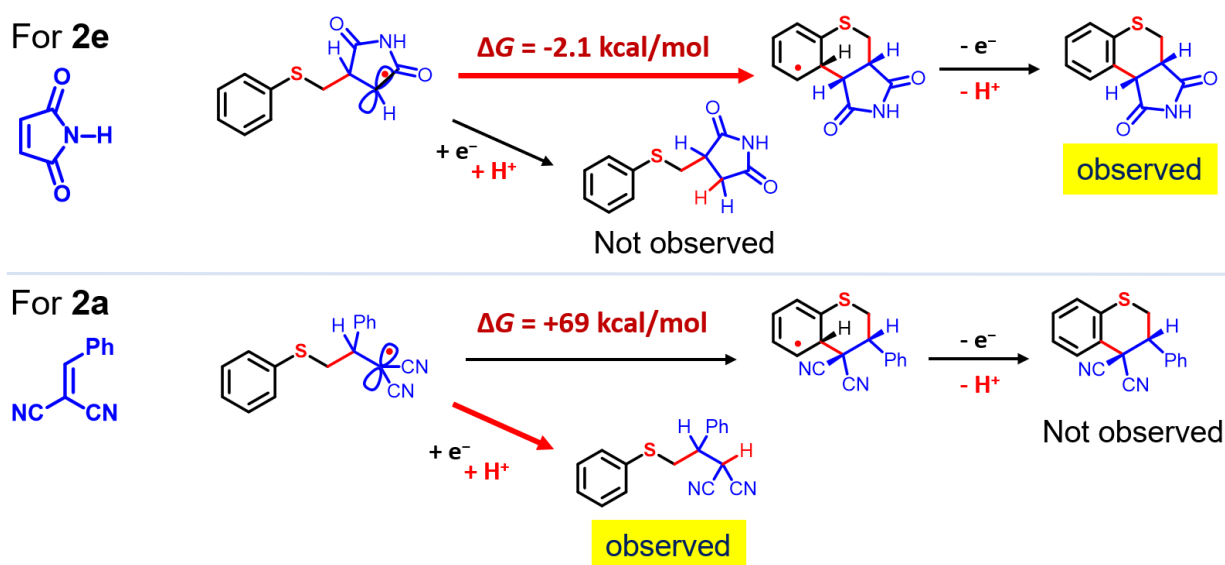


**Scheme 6.** ΔG for the formation of annulation and single C-C bond adduct products. ΔG was calculated at M062X/(ma-)def2-TZVP/CPCM(acetonitrile) using Orca 5.0.

**Table 4.** Reaction of **1a-e** with maleimide **2b-e**.[a]
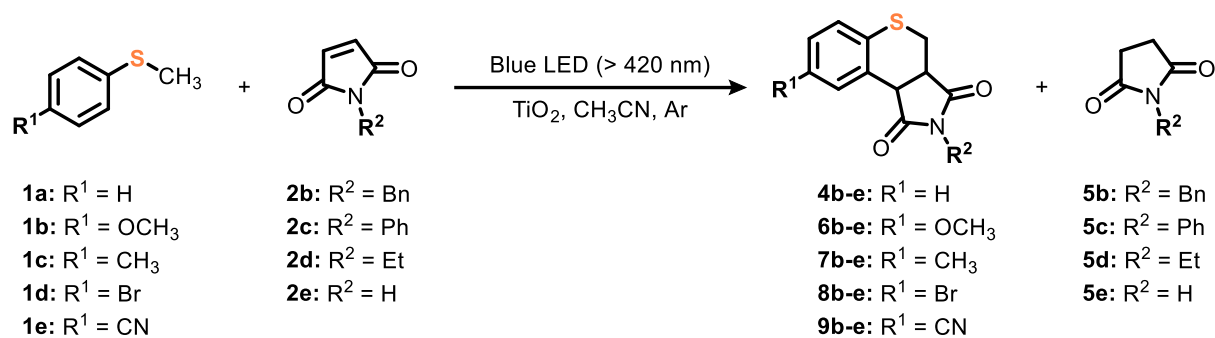


| 1a: R$^1$ = H | 2b: R$^2$ = Bn | | 4b-e: R$^1$ = H | 5b: R$^2$ = Bn |
| 1b: R$^1$ = OCH$_3$ | 2c: R$^2$ = Ph | | 6b-e: R$^1$ = OCH$_3$ | 5c: R$^2$ = Ph |
| 1c: R$^1$ = CH$_3$ | 2d: R$^2$ = Et | | 7b-e: R$^1$ = CH$_3$ | 5d: R$^2$ = Et |
| 1d: R$^1$ = Br | 2e: R$^2$ = H | | 8b-e: R$^1$ = Br | 5e: R$^2$ = H |
| 1e: R$^1$ = CN | | | 9b-e: R$^1$ = CN | |

| thioanisole | maleimide | Yield of **4** and **6-9** (%)[b] | Yield of **5** (%)[b] |
| --- | --- | --- | --- |
| **1a** | **2b** | 43 (**4b**) | 57 (**5b**) |
| **1a** | **2c** | 33 (**4c**) | 35 (**5c**) |
| **1a** | **2d** | 41 (**4d**) | 45 (**5d**) |
| **1a** | **2e** | 26 (**4e**) | 28 (**5e**) |
| **1b** | **2b** | 4 (**6b**) | 4 (**5b**) |
| **1b** | **2c** | 2 (**6c**) | 2 (**5c**) |
| **1b** | **2d** | 6 (**6d**) | 7 (**5d**) |
| **1b** | **2e** | 2 (**6e**) | 3 (**5e**) |
| **1c** | **2b** | 44 (**7b**) | 52 (**5b**) |
| **1c** | **2c** | 37 (**7c**) | 47 (**5c**) |
| **1c** | **2d** | 43 (**7d**) | 57 (**5d**) |
| **1c** | **2e** | 27 (**7e**) | 30 (**5e**) |
| **1d** | **2b** | 29 (**8b**) | 31 (**5b**) |
| **1d** | **2c** | 25 (**8c**) | 27 (**5c**) |
| **1d** | **2d** | 30 (**8d**) | 33 (**5d**) |
| **1d** | **2e** | 19 (**8e**) | 20 (**5e**) |
| **1e** | **2b** | 11 (**9b**) | 11 (**5b**) |
| **1e** | **2c** | 11 (**9c**) | 13 (**5c**) |
| **1e** | **2d** | 20 (**9d**) | 25 (**5d**) |
| **1e** | **2e** | 10 (**9e**) | 10 (**5e**) |

[a] Reaction conditions: TiO$_2$ (5 mg), **1a-e** (0.3 mmol), **2b-e** (0.1 mmol) in acetonitrile (2 mL), under an Ar atmosphere for 12 h.  [b] Yield based on **2b-e**.

Next, I carried out reactions using three additional maleimides (**2c-e**). Similar to **2b**, my findings revealed the concurrent formation of annulation products (**4b-e**) and corresponding succinimide (**5b-e**), as shown in Table 4. However, I identified that the reaction efficiency of the unsubstituted maleimide was low (**2e** in Table 4). I believe that the observed differences in yield reflect variations in reactivity towards the nucleophilic radical of the maleimides.

**Table 5**. Reaction of **1a-e** with **2b**.[a]



**1a**. R = H
**1b**. R = OCH$_3$
**1c**. R = CH$_3$
**1d**. R = Br
**1e**. R = CN

**2b**

**4b**. R = H
**6b**. R = OCH$_3$
**7b**. R = CH$_3$
**8b**. R = Br
**9b**. R = CN

**5b**
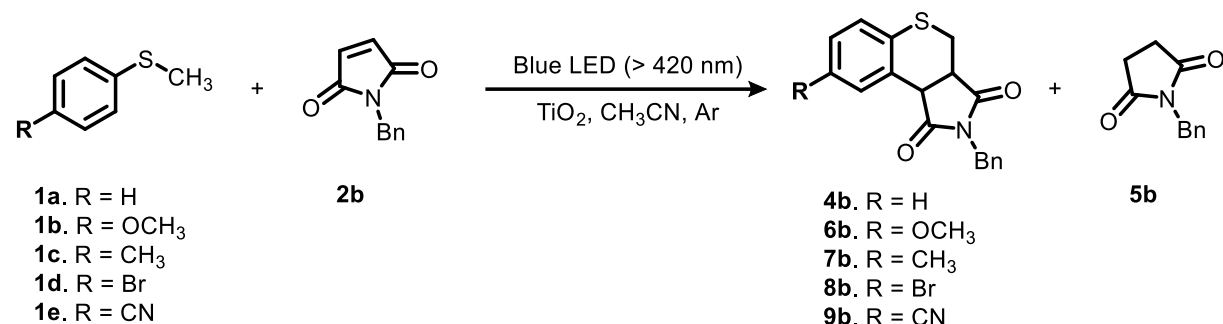
| Entry | R | Substituent constant $\sigma_p^+$ | **4b**[b] | **5b**[b] |
|-------|------|-------|-------|-------|
| 1 | OCH$_3$ | -0.78 | 1 | 1 |
| 2 | CH$_3$ | -0.31 | 22 | 23 |
| 3 | H | 0 | 15 | 17 |
| 4 | Br | 0.15 | 12 | 13 |
| 5 | CN | 0.66 | 4 | 5 |

[a] Reaction conditions: TiO$_2$ (5 mg), **1a-e** (0.3 mmol), **2b** (0.1 mmol), acetonitrile: 2.0 mL, Ar atmosphere under blue LED's (> 420 nm) irradiation, reaction time: 2 h. [b] Yield (%) based on **2b**.

In the presence of TiO$_2$, I conducted the photoreaction between 4-substituted thioanisole derivatives **1a-e** and *N*-benzylmaleimide **2b** for two hours, as detailed in Table 5. The Hammett plot illustrated in Figure 9, except compound **1b** (R = OCH$_3$), displays a negative slope ($\rho$ = -0.78), indicating a correlation between the substrate's ease of oxidation and yield. For substrates excluding compound **1b** (R = OCH$_3$), this trend suggests that the rate-determining step is the generation of cation radical species via one-electron oxidation of **1a** and **1c-e**, as depicted in Table 6. The deviation of compound **1b** (R = OCH$_3$) from this trend can be attributed to the challenging deprotonation of its cation radical oxidized species. The trend of increasing ease of oxidation in the order of R = CN, Br, H, CH$_3$, and OCH$_3$, along with

the concomitant rise in the $pK_a$ of the cation radical species, has been corroborated by DFT calculations, as presented in Table 6. The DFT theoretical calculations suggest that although the compound **1b** (R = OCH$_3$) is the most readily oxidized in the series, deprotonation from its cation radical species is notably less favorable than the others.
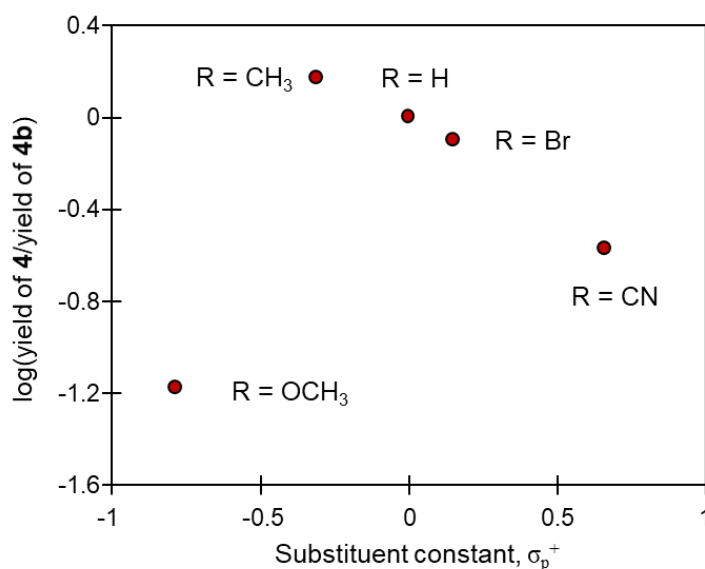


**Figure 9.** Hammett plot for the yields of reactions between 4-substituted thioanisoles **1a-e** and **2b**.

**Table 6.** Calculated oxidation potential of thioanisole (**1a-e**) and acidity of cation radical (**1⁺·**) in acetonitrile.[a]
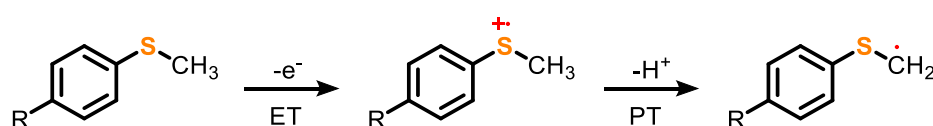


| thioanisole | V vs. Cp$_2$Fe$^{+/0}$ | $pK_a$ | BDFE (kcal/mol) |
|---|---|---|---|
| **1b** (R = OCH$_3$) | 0.62 | 11.8 | 85.5 |
| **1c** (R = CH$_3$) | 0.85 | 8.5 | 86.2 |
| **1a** (R = H) | 1.01 | 6.4 | 86.8 |
| **1d** (R = Br) | 1.05 | 5.5 | 86.7 |
| **1e** (R = CN) | 1.32 | 1.3 | 87.3 |

[a] calculated at M062X(D3zero)/(ma-)def2-TZVP/CPCM(acetonitrile) using Orca.

I synthesized 20 annulation compounds using five 4-substituted thioanisoles and four *N*-substituted maleimides. The yields of the reactions are tabulated in Table 4, and the yields of the annulation products are graphically represented in Figure 10. These results show that the 4-substituted thioanisole with $R^1$ = OMe is less prone to generate radicals compared to other thioanisole derivatives. Additionally, it was observed that the maleimide with $R^2$ = H exhibited lower reactivity than other maleimide derivatives.
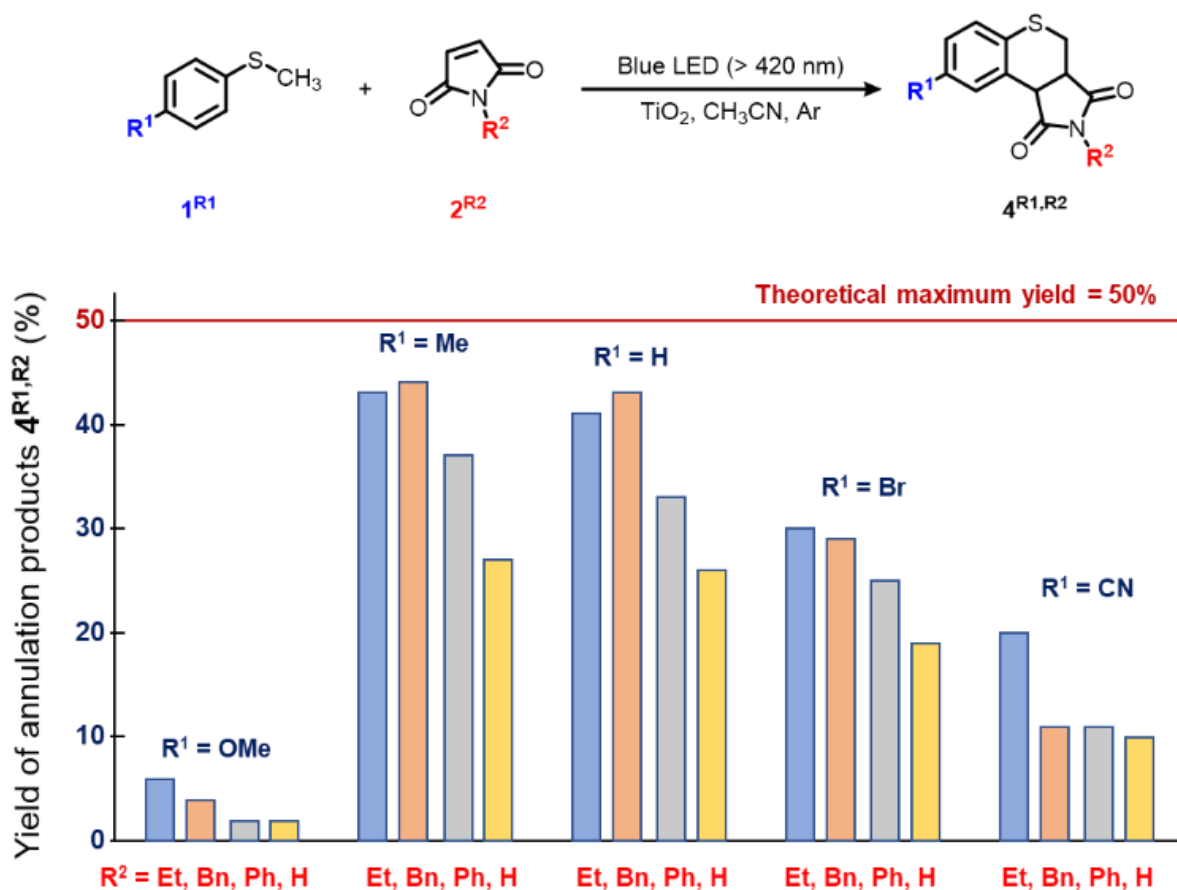


**Figure 10.** Yield of 20 annulation compounds using five 4-substituted thioanisole derivatives and four *N*-substituted maleimide derivatives.

## Experimental Section

### Materials

TiO₂ powder (JRC-TIO-17, average diameter: 21 nm, equivalent to Degussa P25) was supplied from the Catalysis Society of Japan. All reagents and organic solvents were purchased from Tokyo Chemical Industry or Wako Pure Chemical Industry, and used without further purification.

## Physical measurements

$^1$H and $^{13}$C NMR spectra were recorded at ambient temperature on a JEOL JNM-ECA 500 MHz spectrometer, where CDCl3 or DMSO-d$_6$ was used as a solvent. All chemical shifts ($\delta$) are measured in ppm from TMS, and spin-spin coupling constants ($J$) are mentioned in Hz. Reactions were monitored by analytical thin-layer chromatography using silica gel 60 F254 as a stationary phase. Products were purified via chromatography using a Biotage Isolera One Flash Purification system. Product analysis was also conducted using a GCMS-QP2020 instrument equipped with a GL-Science InertCap 1701 column (60 m). The diffuse reflectance spectra of TiO$_2$ and the mixture of TiO$_2$ and thioanisole were measured using a Shimadzu SolidSpec 3700 UV-Vis-NIR spectrophotometer. DFT calculations were carried out at M062X/(ma-)def2-TZVP/CPCM(acetonitrile) with ORCA 5.0.[22] ESI-MS (electrospray ionization mass spectra) measurements were performed on a JEOL JMS-T100CS spectrometer.

## Computational Details

All calculations were performed using the ORCA quantum chemistry package, version 5.0. The M06-2X functional, which includes a range-separated hybrid meta-GGA, was selected due to its robust performance for main-group thermochemistry, noncovalent interactions, and barrier heights. The def2-TZVP basis set was used for all atoms, as it provides a good compromise between computational cost and accuracy for geometry optimizations and frequency calculations.

Prior to energy evaluations, geometry optimizations were conducted for all molecular structures without imposing any symmetry constraints. Vibrational frequency calculations followed to confirm that the optimized structures were at local minima (zero imaginary frequencies) and to determine zero-point vibrational energy (ZPVE) corrections.

The solvent effects of acetonitrile were approximated using the Conductor-like Polarizable Continuum Model (CPCM) with a dielectric constant of 35.688, which is appropriate for acetonitrile at 298 K. The default non-equilibrium solvation model in ORCA was used for geometry optimizations, frequency calculations, and single-point energy evaluations.

Single-point energies were computed on the optimized geometries to confirm the relative stability of the species investigated. Transition states were identified by the presence

of one imaginary frequency and were characterized further by intrinsic reaction coordinate (IRC) calculations to confirm the correct association with the reactants and products.

**Photocatalytic reaction**

TiO$_2$ (5 mg), substrate **1a-e** (0.3 mmol), electron-deficient alkene **2b-e** (0.1 mmol), and CH$_3$CN (2 mL) were added to a glass tube containing a small stirring bar. Argon gas was then introduced through a rubber stopper for 3 minutes. The reactors were irradiated with light from two blue LED lamps (Kessil, A160WE Tuna Blue) fitted with a filter (> 420 nm) on the side. The resulting mixture was subjected to membrane filtration. After that, the crude products were purified by chromatography using a Biotage Isolera One Flash Purification system (hexane: ethyl acetate = 85: 15 → 70: 30) to analyze using GC-MS and NMR and determine the isolated yields of the products. A dimethyl sulfone solution in CH$_3$CN (0.1 M, 1 mL, 0.1 mmol) was added to the reaction mixture as a standard to construct the Hammett plot.

**Compound Data:**

**2-(1-phenyl-2-(phenylthio)ethyl)malononitrile: 3a**



**3a**
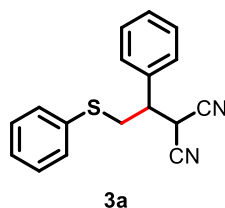
Colorless liquid. 25.9 mg (y. 93%). $^1$H NMR (500 MHz, CDCl$_3$): δ 7.45-7.28 (m, 10H), 4.60 (d, $J$ = 4.6 Hz, 1H), 3.49 (dd, $J$ = 14.3, 5.7 Hz, 1H), 3.41 (dd, $J$ = 14.3, 9.7 Hz, 1H), 3.30 (ddd, $J$ = 9.7, 5.7, 4.6 Hz, 1H). $^{13}$C NMR (126 MHz, CDCl$_3$): δ 135.46, 132.97, 130.80, 129.62, 129.46, 129.36, 127.94, 127.81, 111.87, 111.09, 45.61, 36.48, 27.91. HRMS (ESI): $m/z$ calcd for C$_{17}$H$_{14}$N$_2$S+Na$^+$: 301.0770 [$M$+Na]$^+$; found: 301.0782.

**2-(2-((4-methoxyphenyl)thio)-1-phenylethyl)malononitrile: 3b**



**3b**
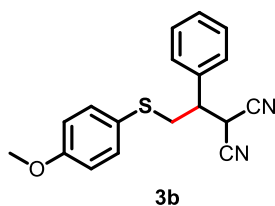
Colorless liquid. 8.0 mg (y. 26%). $^1$H NMR (500 MHz, CDCl$_3$): δ 7.43 – 7.25 (m, 7H), 6.90– 6.84 (d, $J$ = 8.6 Hz, 2H), 4.60 (d, $J$ = 5.1 Hz, 1H), 3.80 (s, 3H), 3.38 – 3.25 (m, 2H), 3.21 (dt,

$J$ = 8.7, 5.5 Hz, 1H). $^{13}$C NMR (126 MHz, CDCl$_3$): δ 160.09, 135.69, 134.42, 129.45, 129.39, 128.14, 123.22, 115.35, 112.15, 111.33, 55.54, 45.65, 38.32, 27.96. HRMS (ESI): $m/z$ calcd for C$_{18}$H$_{16}$N$_2$OS+Na$^+$: 331.0876 [$M$+Na]$^+$; found: 331.0880.

**2-(1-phenyl-2-(p-tolylthio)ethyl)malononitrile: 3c**



**3c**
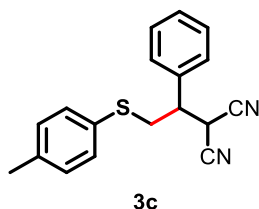
Colorless liquid. 27.5 mg (y. 94%). $^1$H NMR (500 MHz, CDCl$_3$): δ 7.45 – 7.36 (m, 3H), 7.35 – 7.25 (m, 4H), 7.16 (d, $J$ = 7.9 Hz, 2H), 4.61 (d, $J$ = 4.7 Hz, 1H), 3.42 (dd, $J$ = 14.2, 5.6 Hz, 1H), 3.35 (dd, $J$ = 14.2, 9.6 Hz, 1H), 3.25 (ddd, $J$ = 9.6, 5.6, 4.7 Hz, 1H), 2.35 (s, 3H). $^{13}$C NMR (126 MHz, CDCl$_3$): δ 138.21, 135.53, 131.49, 130.39, 129.37, 129.29, 129.12, 127.96, 111.96, 111.13, 45.50, 37.03, 27.80, 21.11. HRMS (ESI): $m/z$ calcd for C$_{18}$H$_{16}$N$_2$S+Na$^+$: 315.0926 [$M$+Na]$^+$; found: 315.0950.

**2-(2-(4-(methylthio)phenyl)-1-phenylethyl)malononitrile: 3c'**



**3c'**
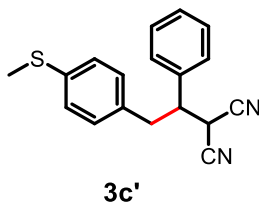
Colorless liquid. 0.9 mg (y. 3%). $^1$H NMR (500 MHz, CDCl$_3$): δ 7.46 – 7.35 (m, 5H), 7.25 – 7.13 (m, 2H), 7.13 – 7.07 (m, 2H), 3.86 (d, $J$ = 5.2 Hz, 1H), 3.43 (ddd, $J$ = 8.4, 7.3, 5.2 Hz, 1H), 3.29 – 3.16 (m, 2H), 2.47 (s, 3H). $^{13}$C NMR (126 MHz, CDCl$_3$): δ 137.98, 136.24, 133.17, 129.37, 129.24, 129.12, 128.02, 127.03, 111.99, 111.41, 48.30, 37.94, 28.53, 15.68. HRMS (ESI): $m/z$ calcd for C$_{18}$H$_{16}$N$_2$S+Na$^+$: 315.0926 [$M$+Na]$^+$; found: 315.0931.

**2-(2-((4-bromophenyl)thio)-1-phenylethyl)malononitrile: 3d**



**3d**
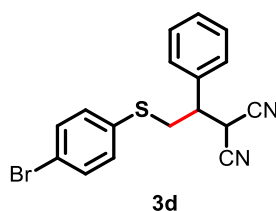
Colorless liquid. 27.1 mg (y. 76%). $^1$H NMR (500 MHz, CDCl$_3$): δ 7.47 – 7.44 (m, 2H), 7.43 – 7.39 (m, 3H), 7.33 – 7.27 (m, 2H), 7.23 – 7.20 (m, 2H), 4.48 (d, $J$ = 5.0 Hz, 1H), 3.48 – 3.37 (m, 2H), 3.29 (ddd, $J$ = 8.7, 6.5, 4.9 Hz, 1H). $^{13}$C NMR (126 MHz, CDCl$_3$): δ 135.19, 132.63, 132.28, 132.18, 129.51, 129.38, 127.86, 121.83, 111.67, 111.06, 45.54, 36.48, 28.09. HRMS (ESI): $m/z$ calcd for C$_{17}$H$_{13}$BrN$_2$S+Na$^+$: 378.9875 [$M$+Na]$^+$; found: 378.9863.
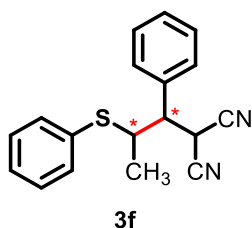
## 2-(2-((4-cyanophenyl)thio)-1-phenylethyl)malononitrile: 3e



**3e**
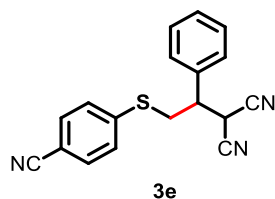
Colorless liquid. 13.9 mg (y. 46%). $^1$H NMR (500 MHz, CDCl$_3$): δ 7.61 – 7.55 (m, 2H), 7.48 – 7.40 (m, 3H), 7.34 (ddd, $J$ = 8.0, 6.3, 2.1 Hz, 4H), 4.41 (d, $J$ = 5.3 Hz, 1H), 3.62 – 3.50 (m, 2H), 3.42 (td, $J$ = 7.5, 5.2 Hz, 1H). $^{13}$C NMR (126 MHz, CDCl$_3$): δ 141.20, 135.02, 132.90, 129.86, 129.65, 128.48, 127.91, 118.48, 111.59, 111.20, 110.47, 45.64, 34.74, 28.60. HRMS (ESI): $m/z$ calcd for C$_{18}$H$_{13}$N$_3$S+Na$^+$: 326.0722 [$M$+Na]$^+$; found: 326.0724.

## 2-(1-phenyl-2-(phenylthio)propyl)malononitrile: 3f



**3f**

The diastereomeric ratio of A to B is 9:10.

**diastereomer A**



2-((1S,2R)-1-phenyl-2-(phenylthio)propyl)malononitrile          2-((1R,2S)-1-phenyl-2-(phenylthio)propyl)malononitrile
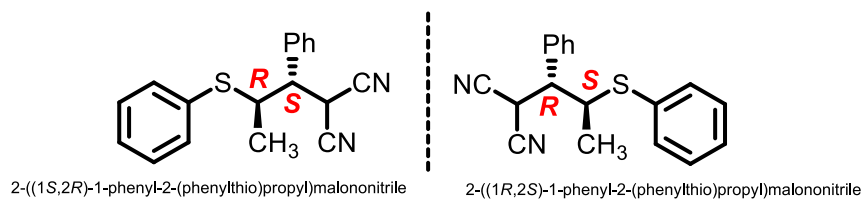
diastereomer A: White solid. 7.0 mg (y. 24%). $^1$H NMR (500 MHz, CDCl$_3$): δ 7.59 – 7.51 (m, 2H), 7.45 – 7.30 (m, 8H), 5.19 (d, $J$ = 4.5 Hz, 1H), 3.61 (dq, $J$ = 11.5, 6.7 Hz, 1H), 3.07 (dd, $J$ = 11.5, 4.5 Hz, 1H), 1.16 (d, $J$ = 6.7 Hz, 3H). $^{13}$C NMR (126 MHz, CDCl$_3$): δ 134.85, 134.40,

131.57, 129.65, 129.53, 129.44, 129.01, 128.48, 112.18, 111.62, 52.11, 46.36, 28.86, 20.71. HRMS (ESI): $m/z$ calcd for $C_{18}H_{16}N_2S+Na^+$: 315.0926 $[M+Na]^+$; found: 315.0943.

**diastereomer B**



2-((1R,2R)-1-phenyl-2-(phenylthio)propyl)malononitrile     2-((1S,2S)-1-phenyl-2-(phenylthio)propyl)malononitrile
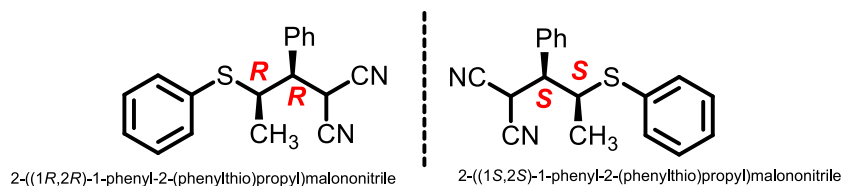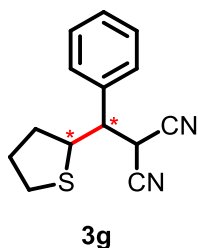
diastereomer B: White solid. 7.6 mg (y. 26%). $^1$H NMR (500 MHz, CDCl₃): δ 7.51 – 7.44 (m, 2H), 7.42 (dq, $J$ = 4.8, 1.6 Hz, 3H), 7.33 (tdq, $J$ = 5.3, 3.6, 1.6 Hz, 5H), 4.68 (d, $J$ = 10.0 Hz, 1H), 3.73 (dq, $J$ = 6.8, 5.2 Hz, 1H), 3.46 (dd, $J$ = 10.0, 5.2 Hz, 1H), 1.31 (d, $J$ = 6.8 Hz, 3H). $^{13}$C NMR (126 MHz, CDCl₃): δ 133.73, 133.57, 133.08, 129.55, 129.42, 129.23, 128.78, 128.50, 112.37, 112.02, 52.15, 47.81, 27.55, 21.07. HRMS (ESI): $m/z$ calcd for $C_{18}H_{16}N_2S+Na^+$: 315.0926 $[M+Na]^+$; found: 315.0942.

**2-(phenyl(tetrahydrothiophen-2-yl)methyl)malononitrile: 3g**



**3g**

**diastereomer A**: White solid. 5.1 mg (y. 21%). $^1$H NMR (500 MHz, CDCl₃): δ 7.42 (m, 5H), 4.64 – 4.57 (m, 1H), 3.97 (dq, $J$ = 11.1, 5.4 Hz, 1H), 3.00 (dddd, $J$ = 19.5, 12.1, 9.8, 5.5 Hz, 3H), 2.09 – 1.85 (m, 3H), 1.64 – 1.55 (m, 1H). $^{13}$C NMR (126 MHz, CDCl₃): δ 135.74, 129.43, 129.37, 128.45, 112.18, 111.57, 53.90, 50.03, 35.81, 33.27, 29.76, 29.74. HRMS (ESI): $m/z$ calcd for $C_{14}H_{14}N_2S+Na^+$: 265.0770 $[M+Na]^+$; found: 265.0782.

**diastereomer B**: White solid. 5.1 mg (y. 21%). $^1$H NMR (500 MHz, CDCl₃): δ 7.46 – 7.37 (m, 5H), 4.17 (d, $J$ = 6.2 Hz, 1H), 4.11 (td, $J$ = 8.7, 6.2 Hz, 1H), 3.33 (dd, $J$ = 9.0, 6.1 Hz, 1H), 2.87 – 2.72 (m, 2H), 2.41 – 2.32 (m, 1H), 2.07 – 1.89 (m, 2H), 1.68 (dddd, $J$ = 12.3, 10.2, 8.3, 5.7 Hz, 1H). $^{13}$C NMR (126 MHz, CDCl₃): δ 136.28, 129.41, 129.24, 128.42, 111.71, 111.62, 52.03, 50.33, 35.62, 32.54, 31.23, 28.78. HRMS (ESI): $m/z$ calcd for $C_{14}H_{14}N_2S+Na^+$: 265.0770 $[M+Na]^+$; found: 265.0783.

**2-benzyl-3a,4-dihydrothiochromeno[3,4-c]pyrrole-1,3(2H,9bH)-dione: 4b**



**4b**
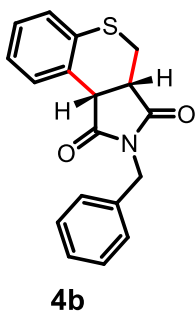
Colorless liquid. 13.3 mg (y. 43%). $^1$H NMR (500 MHz, CDCl$_3$): δ 7.43 (dd, $J$ = 7.4, 1.7 Hz, 1H), 7.38 – 7.32 (m, 2H), 7.32 – 7.18 (m, 6H), 4.76 – 4.65 (m, 2H), 4.09 (d, $J$ = 9.3 Hz, 1H), 3.66 (ddd, $J$ = 9.3, 4.9, 2.5 Hz, 1H), 3.34 (dd, $J$ = 13.3, 2.5 Hz, 1H), 2.88 (dd, $J$ = 13.3, 4.9 Hz, 1H). $^{13}$C NMR (126 MHz, CDCl$_3$): δ 177.63, 175.62, 135.36, 134.58, 131.86, 130.30, 129.65, 128.61, 128.56, 128.00, 127.92, 126.92, 45.38, 44.54, 43.11, 29.86. HRMS (ESI): $m/z$ calcd for C$_{18}$H$_{15}$NO$_2$S+Na$^+$: 332.0716 [$M$+Na]$^+$; found: 332.0691.
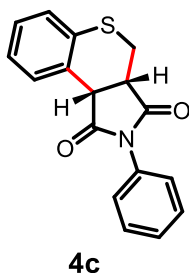
**2-phenyl-3a,4-dihydrothiochromeno[3,4-c]pyrrole-1,3(2H,9bH)-dione: 4c**



**4c**

White solid. 9.7 mg (y. 33%). $^1$H NMR (500 MHz, CDCl$_3$): δ 7.49 (dd, $J$ = 7.2, 1.9 Hz, 1H), 7.48 – 7.42 (m, 2H), 7.42 – 7.36 (m, 1H), 7.33 (dd, $J$ = 7.2, 1.9 Hz, 1H), 7.32 – 7.20 (m, 4H), 4.28 (d, $J$ = 9.4 Hz, 1H), 3.84 (ddd, $J$ = 9.4, 4.8, 2.4 Hz, 1H), 3.45 (dd, $J$ = 13.3, 2.5 Hz, 1H), 2.96 (dd, $J$ = 13.3, 4.8 Hz, 1H). $^{13}$C NMR (126 MHz, CDCl$_3$): δ 177.29, 175.09, 134.88, 132.12, 132.02, 130.62, 129.85, 129.26, 128.93, 128.21, 127.14, 126.61, 45.73, 44.78, 30.53. HRMS (ESI): $m/z$ calcd for C$_{17}$H$_{13}$NO$_2$S+Na$^+$: 318.0559 [$M$+Na]$^+$; found: 318.0538.

**2-ethyl-3a,4-dihydrothiochromeno[3,4-c]pyrrole-1,3(2H,9bH)-dione: 4d**



**4d**
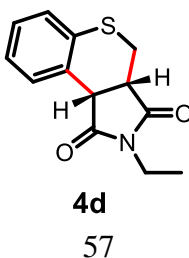
Colorless liquid. 10.1 mg (y. 41%). $^1$H NMR (500 MHz, CDCl$_3$): δ 7.48 – 7.42 (m, 1H), 7.32 – 7.19 (m, 3H), 4.08 (d, $J$ = 9.3 Hz, 1H), 3.66 (ddd, $J$ = 9.3, 4.9, 2.4 Hz, 1H), 3.61 (q, $J$ = 7.2 Hz, 2H), 3.35 (dd, $J$ = 13.3, 2.4 Hz, 1H), 2.89 (dd, $J$ = 13.3, 4.9 Hz, 1H), 1.18 (t, $J$ = 7.2 Hz, 3H). $^{13}$C NMR (126 MHz, CDCl$_3$): δ 177.88, 175.77, 134.77, 131.97, 130.62, 129.75, 128.04, 127.01, 45.52, 44.57, 34.66, 30.10, 13.10. HRMS (ESI): $m/z$ calcd for C$_{13}$H$_{13}$NO$_2$S+Na$^+$: 270.0559 [$M$+Na]$^+$; found: 270.0586.

**3a,4-dihydrothiochromeno[3,4-c]pyrrole-1,3(2H,9bH)-dione: 4e**



**4e**
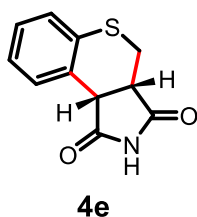
White solid. 5.7 mg (y. 26%). $^1$H NMR (500 MHz, CDCl$_3$): δ 8.52 (br-s, 1H), 7.45 – 7.38 (m, 1H), 7.31 (dd, $J$ = 7.2, 1.8 Hz, 1H), 7.31 – 7.20 (m, 2H), 4.17 (d, $J$ = 9.2 Hz, 1H), 3.73 (ddd, $J$ = 9.4, 4.9, 2.5 Hz, 1H), 3.32 (dd, $J$ = 13.4, 2.5 Hz, 1H), 2.88 (dd, $J$ = 13.4, 4.9 Hz, 1H). $^{13}$C NMR (126 MHz, CDCl$_3$): δ 177.87, 175.96, 134.79, 131.83, 129.98, 129.81, 128.23, 127.09, 46.60, 45.83, 29.65. HRMS (ESI): $m/z$ calcd for C$_{11}$H$_9$NO$_2$S+Na$^+$: 242.0246 [$M$+Na]$^+$; found: 242.0243.

**2-benzyl-8-methoxy-3a,4-dihydrothiochromeno[3,4-c]pyrrole-1,3(2H,9bH)-dione: 6b**



**6b**
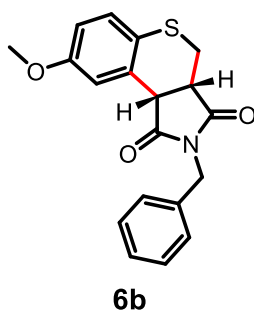
Colorless liquid. 1.3 mg (y. 4%). $^1$H NMR (500 MHz, CDCl$_3$): δ 7.39 – 7.33 (m, 2H), 7.33 – 7.23 (m, 3H), 7.19 (d, $J$ = 8.5 Hz, 1H), 7.00 (d, $J$ = 2.7 Hz, 1H), 6.80 (dd, $J$ = 8.5, 2.8 Hz, 1H), 4.78 – 4.67 (m, 2H), 4.06 (d, $J$ = 9.2 Hz, 1H), 3.82 (s, 3H), 3.65 (ddd, $J$ = 9.3, 4.9, 2.4 Hz, 1H), 3.33 (dd, $J$ = 13.3, 2.4 Hz, 1H), 2.85 (dd, $J$ = 13.3, 4.9 Hz, 1H). $^{13}$C NMR (126 MHz, CDCl$_3$): δ 177.68, 175.53, 158.59, 135.36, 131.53, 130.56, 128.60, 128.55, 127.91, 125.32, 117.34, 114.09, 55.46, 45.76, 44.41, 43.11, 30.41. HRMS (ESI): $m/z$ calcd for C$_{19}$H$_{17}$NO$_3$S+Na$^+$: 362.0821 [$M$+Na]$^+$; found: 362.0806.

**8-methoxy-2-phenyl-3a,4-dihydrothiochromeno[3,4-c]pyrrole-1,3(2H,9bH)-dione: 6c**



**6c**
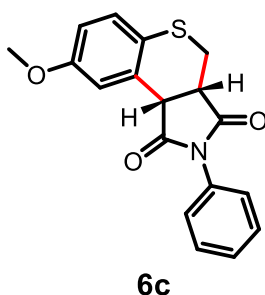
White solid. 0.6 mg (y. 2%). $^1$H NMR (500 MHz, CDCl$_3$): δ 7.52 – 7.43 (m, 2H), 7.43 – 7.35 (m, 1H), 7.33 – 7.21 (m, 3H), 7.06 (d, $J$ = 2.8 Hz, 1H), 6.85 – 6.79 (m, 1H), 4.22 (d, $J$ = 9.4 Hz, 1H), 3.85 – 3.77 (m, 4H), 3.43 (dd, $J$ = 13.4, 2.4 Hz, 1H), 2.94 (dd, $J$ = 13.4, 4.7 Hz, 1H). $^{13}$C NMR (126 MHz, CDCl$_3$): δ 177.24, 174.92, 158.67, 131.94, 131.77, 130.65, 129.16, 128.83, 126.53, 125.53, 117.58, 114.11, 55.50, 46.01, 44.55, 30.99. HRMS (ESI): $m/z$ calcd for C$_{18}$H$_{15}$NO$_3$S+Na$^+$: 348.0665 [$M$+Na]$^+$; found: 348.0668.

**2-ethyl-8-methoxy-3a,4-dihydrothiochromeno[3,4-c]pyrrole-1,3(2H,9bH)-dione: 6d**



**6d**
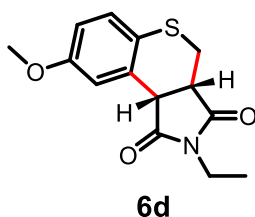
Colorless liquid. 1.7 mg (y. 6%). $^1$H NMR (500 MHz, CDCl$_3$): δ 7.20 (d, $J$ = 8.5 Hz, 1H), 7.01 (d, $J$ = 2.7 Hz, 1H), 6.80 (dd, $J$ = 8.6, 2.7 Hz, 1H), 4.03 (d, $J$ = 9.2 Hz, 1H), 3.83 (s, 3H), 3.66 – 3.58 (m, 3H), 3.32 (dd, $J$ = 13.2, 2.4 Hz, 1H), 2.84 (dd, $J$ = 13.2, 4.9 Hz, 1H), 1.18 (t, $J$ = 7.2 Hz, 3H). $^{13}$C NMR (126 MHz, CDCl$_3$): δ 177.83, 175.59, 158.59, 131.78, 130.57, 125.44, 117.45, 113.97, 55.47, 45.82, 44.36, 34.57, 30.58, 13.00. HRMS (ESI): $m/z$ calcd for C$_{14}$H$_{15}$NO$_3$S+Na$^+$: 300.0665 [$M$+Na]$^+$; found: 300.0691.

**8-methoxy-3a,4-dihydrothiochromeno[3,4-c]pyrrole-1,3(2H,9bH)-dione: 6e**



**6e**
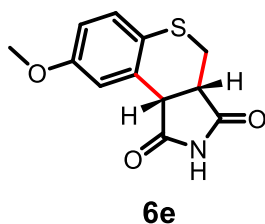
White solid. 0.5 mg (y. 2%). $^1$H NMR (500 MHz, CDCl$_3$): δ 8.23 (s, 1H), 7.22 (d, $J$ = 8.5 Hz, 1H), 6.99 (d, $J$ = 2.8 Hz, 1H), 6.81 (dd, $J$ = 8.6, 2.8 Hz, 1H), 4.12 (d, $J$ = 9.4 Hz, 1H), 3.83 (s, 3H), 3.70 (ddd, $J$ = 9.3, 5.0, 2.4 Hz, 1H), 3.30 (dd, $J$ = 13.3, 2.4 Hz, 1H), 2.84 (dd, $J$ = 13.3, 5.0 Hz, 1H). $^{13}$C NMR (126 MHz, CDCl$_3$): δ 177.41, 175.46, 158.66, 131.34, 130.65, 125.48, 117.35, 114.13, 55.49, 46.93, 45.66, 30.19. HRMS (ESI): $m/z$ calcd for C$_{12}$H$_{11}$NO$_3$S+Na$^+$: 272.0352 [$M$+Na]$^+$; found: 272.0339.

**2-benzyl-8-methyl-3a,4-dihydrothiochromeno[3,4-c]pyrrole-1,3(2H,9bH)-dione: 7b**
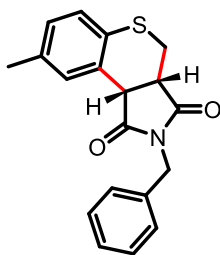


**7b**

Colorless liquid. 14.2 mg (y. 44%). $^1$H NMR (500 MHz, CDCl$_3$): δ 7.39 – 7.33 (m, 2H), 7.32 – 7.26 (m, 2H), 7.29 – 7.22 (m, 2H), 7.17 (d, $J$ = 7.8 Hz, 1H), 7.06 – 7.00 (m, 1H), 4.77 – 4.65 (m, 2H), 4.04 (d, $J$ = 9.3 Hz, 1H), 3.64 (ddd, $J$ = 9.2, 4.9, 2.4 Hz, 1H), 3.33 (dd, $J$ = 13.2, 2.4 Hz, 1H), 2.85 (dd, $J$ = 13.3, 4.9 Hz, 1H), 2.35 (s, 3H). $^{13}$C NMR (126 MHz, CDCl$_3$): δ 177.72, 175.78, 136.87, 135.39, 132.50, 131.07, 130.09, 129.49, 128.88, 128.60, 128.58, 127.91, 45.45, 44.54, 43.10, 30.11, 21.07. HRMS (ESI): $m/z$ calcd for C$_{19}$H$_{17}$NO$_2$S+Na$^+$: 346.0872 [$M$+Na]$^+$; found: 346.0864.

**8-methyl-2-phenyl-3a,4-dihydrothiochromeno[3,4-c]pyrrole-1,3(2H,9bH)-dione: 7c**
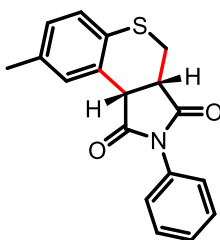


**7c**

White solid. 11.4 mg (y. 37%). $^1$H NMR (500 MHz, CDCl$_3$): δ 7.49 – 7.40 (m, 2H), 7.42 – 7.35 (m, 1H), 7.33 – 7.24 (m, 3H), 7.22 (d, $J$ = 7.9 Hz, 1H), 7.06 (dd, $J$ = 7.9, 1.9 Hz, 1H), 4.22 (d, $J$ = 9.4 Hz, 1H), 3.82 (ddd, $J$ = 9.4, 4.9, 2.4 Hz, 1H), 3.43 (dd, $J$ = 13.3, 2.4 Hz, 1H), 2.92 (dd, $J$ = 13.3, 4.9 Hz, 1H), 2.37 (s, 3H). $^{13}$C NMR (126 MHz, CDCl$_3$): δ 177.29, 175.14, 136.98,

132.64, 131.94, 131.25, 130.31, 129.58, 129.14, 128.97, 128.79, 126.51, 45.69, 44.67, 30.67, 21.10. HRMS (ESI): $m/z$ calcd for $C_{18}H_{15}NO_2S+Na^+$: 332.0716 $[M+Na]^+$; found: 332.0732.

**2-ethyl-8-methyl-3a,4-dihydrothiochromeno[3,4-c]pyrrole-1,3(2H,9bH)-dione: 7d**



**7d**
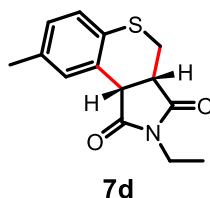
Colorless liquid. 11.2 mg (y. 43%). ^{1}H NMR (500 MHz, CDCl$_3$): δ 7.26 (s, 1H), 7.17 (d, $J$ = 7.9 Hz, 1H), 7.04 (ddd, $J$ = 7.9, 2.0, 0.8 Hz, 1H), 4.03 (d, $J$ = 9.2 Hz, 1H), 3.66 – 3.56 (m, 3H), 3.33 (dd, $J$ = 13.3, 2.4 Hz, 1H), 2.84 (dd, $J$ = 13.3, 4.9 Hz, 1H), 2.36 (s, 3H), 1.17 (t, $J$ = 7.2 Hz, 3H). ^{13}C NMR (126 MHz, CDCl$_3$): δ 177.89, 175.82, 136.84, 132.52, 131.16, 130.33, 129.50, 128.83, 45.49, 44.47, 34.54, 30.27, 21.09, 12.99. HRMS (ESI): $m/z$ calcd for $C_{14}H_{15}NO_2S+Na^+$: 284.0716 $[M+Na]^+$; found: 284.0705.

**8-methyl-3a,4-dihydrothiochromeno[3,4-c]pyrrole-1,3(2H,9bH)-dione: 7e**



**7e**
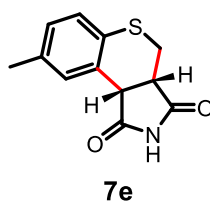
White solid. 6.3 mg (y. 27%). ^{1}H NMR (500 MHz, CDCl$_3$): δ 8.22 (s, 1H), 7.25 – 7.22 (m, 1H), 7.20 (d, $J$ = 7.9 Hz, 1H), 7.06 (dd, $J$ = 7.8, 1.9 Hz, 1H), 4.12 (d, $J$ = 9.3 Hz, 1H), 3.71 (ddd, $J$ = 9.3, 4.9, 2.4 Hz, 1H), 3.31 (dd, $J$ = 13.3, 2.4 Hz, 1H), 2.84 (dd, $J$ = 13.3, 4.9 Hz, 1H), 2.36 (s, 3H). ^{13}C NMR (126 MHz, CDCl$_3$): δ 177.61, 175.74, 136.98, 132.37, 131.21, 129.72, 129.58, 129.04, 46.62, 45.78, 29.88, 21.10. HRMS (ESI): $m/z$ calcd for $C_{12}H_{11}NO_2S+Na^+$: 256.0403 $[M+Na]^+$; found: 256.0422.

**2-benzyl-8-bromo-3a,4-dihydrothiochromeno[3,4-c]pyrrole-1,3(2H,9bH)-dione: 8b**



**8b**
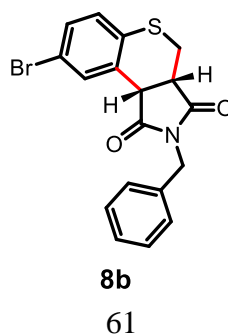
Colorless liquid. 11.2 mg (y. 29%). $^1$H NMR (500 MHz, CDCl$_3$): δ 7.59 (d, $J$ = 2.1 Hz, 1H), 7.37 – 7.22 (m, 6H), 7.15 (dd, $J$ = 8.3, 0.9 Hz, 1H), 4.76 – 4.65 (m, 2H), 4.03 (d, $J$ = 9.3 Hz, 1H), 3.65 (ddd, $J$ = 9.2, 4.8, 2.5 Hz, 1H), 3.33 (ddd, $J$ = 13.3, 2.6, 0.8 Hz, 1H), 2.86 (ddd, $J$ = 13.3, 4.9, 0.9 Hz, 1H). $^{13}$C NMR (126 MHz, CDCl$_3$): δ 177.18, 174.93, 135.20, 134.50, 133.73, 132.16, 131.03, 130.90, 128.65, 128.58, 128.01, 120.20, 45.01, 44.22, 43.22, 29.75. HRMS (ESI): $m/z$ calcd for C$_{18}$H$_{14}$BrNO$_2$S+Na$^+$: 409.9821 [$M$+Na]$^+$; found: 409.9814.

**8-bromo-2-phenyl-3a,4-dihydrothiochromeno[3,4-c]pyrrole-1,3(2H,9bH)-dione: 8c**



**8c**
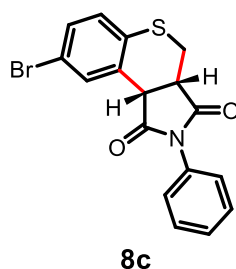
White solid. 9.3 mg (y. 25%). $^1$H NMR (500 MHz, CDCl$_3$): δ 7.64 (d, $J$ = 2.1 Hz, 1H), 7.50 – 7.42 (m, 2H), 7.45 – 7.34 (m, 2H), 7.31 – 7.24 (m, 2H), 7.20 (d, $J$ = 8.3 Hz, 1H), 4.21 (d, $J$ = 9.5 Hz, 1H), 3.82 (ddd, $J$ = 9.4, 4.9, 2.5 Hz, 1H), 3.44 (dd, $J$ = 13.3, 2.5 Hz, 1H), 2.93 (dd, $J$ = 13.4, 4.8 Hz, 1H). $^{13}$C NMR (126 MHz, CDCl$_3$): δ 176.73, 174.31, 134.64, 133.93, 132.38, 131.76, 131.14, 131.00, 129.20, 128.93, 126.43, 120.32, 45.26, 44.37, 30.29. HRMS (ESI): $m/z$ calcd for C$_{17}$H$_{12}$BrNO$_2$S+Na$^+$: 395.9664 [$M$+Na]$^+$; found: 395.9661.

**8-bromo-2-ethyl-3a,4-dihydrothiochromeno[3,4-c]pyrrole-1,3(2H,9bH)-dione: 8d**



**8d**
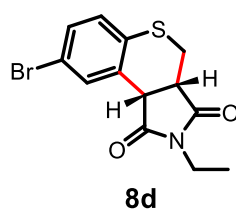
Colorless liquid. 9.8 mg (y. 30%). $^1$H NMR (500 MHz, CDCl$_3$): δ 7.62 – 7.58 (m, 1H), 7.35 (dd, $J$ = 8.3, 2.2 Hz, 1H), 7.16 (d, $J$ = 8.3 Hz, 1H), 4.03 (d, $J$ = 9.2 Hz, 1H), 3.68 – 3.60 (m, 3H), 3.35 (dd, $J$ = 13.3, 2.5 Hz, 1H), 2.86 (dd, $J$ = 13.3, 4.8 Hz, 1H), 1.17 (t, $J$ = 7.2 Hz, 3H). $^{13}$C NMR (126 MHz, CDCl$_3$): δ 177.33, 174.96, 134.51, 133.84, 132.41, 130.98, 130.92, 120.19, 45.07, 44.18, 34.69, 29.91, 12.98. HRMS (ESI): $m/z$ calcd for C$_{13}$H$_{12}$BrNO$_2$S+Na$^+$: 347.9664 [$M$+Na]$^+$; found: 347.9673.

**8-bromo-3a,4-dihydrothiochromeno[3,4-c]pyrrole-1,3(2H,9bH)-dione: 8e**



**8e**
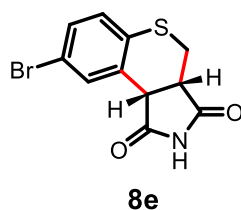
White solid. 5.7 mg (y. 19%). $^1$H NMR (500 MHz, CDCl$_3$): δ 8.63 (s, 1H), 7.60 – 7.56 (m, 1H), 7.36 (dd, $J$ = 8.3, 2.2 Hz, 1H), 7.18 (d, $J$ = 8.3 Hz, 1H), 4.12 (d, $J$ = 9.4 Hz, 1H), 3.72 (ddd, $J$ = 9.4, 4.9, 2.6 Hz, 1H), 3.32 (dd, $J$ = 13.4, 2.6 Hz, 1H), 2.86 (dd, $J$ = 13.4, 4.9 Hz, 1H). $^{13}$C NMR (126 MHz, CDCl$_3$): δ 177.41, 175.16, 134.39, 133.85, 131.74, 131.18, 130.97, 120.28, 46.14, 45.44, 29.47. HRMS (ESI): $m/z$ calcd for C$_{11}$H$_8$BrNO$_2$S+Na$^+$: 319.9351 [$M$+Na]$^+$; found: 319.9335.

**2-benzyl-1,3-dioxo-1,2,3,3a,4,9b-hexahydrothiochromeno[3,4-c]pyrrole-8-carbonitrile: 9b**



**9b**
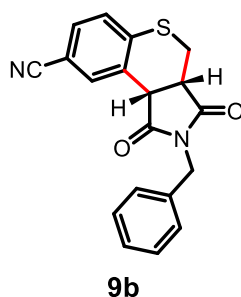
White solid. 3.7 mg (y. 11%). $^1$H NMR (500 MHz, CDCl$_3$): δ 7.74 (d, $J$ = 1.8 Hz, 1H), 7.47 (dd, $J$ = 8.1, 1.8 Hz, 1H), 7.41 – 7.21 (m, 6H), 4.78 – 4.64 (m, 2H), 4.12 (d, $J$ = 9.4 Hz, 1H), 3.71 (ddd, $J$ = 9.4, 4.8, 2.9 Hz, 1H), 3.38 (dd, $J$ = 13.4, 2.9 Hz, 1H), 2.94 (dd, $J$ = 13.4, 4.8 Hz, 1H). $^{13}$C NMR (126 MHz, CDCl$_3$): δ 176.69, 174.40, 141.34, 135.06, 135.03, 131.26, 131.02, 130.12, 128.70, 128.58, 128.12, 118.19, 110.32, 44.65, 43.99, 43.35, 29.10. HRMS (ESI): $m/z$ calcd for C$_{19}$H$_{14}$N$_2$O$_2$S+Na$^+$: 357.0668 [$M$+Na]$^+$; found: 357.0647.

**1,3-dioxo-2-phenyl-1,2,3,3a,4,9b-hexahydrothiochromeno[3,4-c]pyrrole-8-carbonitrile: 9c**



9c

White solid. 3.5 mg (y. 11%). $^1$H NMR (500 MHz, CDCl$_3$): δ 7.79 (d, $J$ = 1.7 Hz, 1H), 7.52 – 7.23 (m, 7H), 4.30 (d, $J$ = 9.5 Hz, 1H), 3.88 (ddd, $J$ = 9.5, 4.7, 2.7 Hz, 1H), 3.49 (dd, $J$ = 13.4, 2.8 Hz, 1H), 3.00 (dd, $J$ = 13.4, 4.7 Hz, 1H). $^{13}$C NMR (126 MHz, CDCl$_3$): δ 173.82, 141.51, 135.17, 131.60, 131.47, 131.15, 130.23, 129.27, 129.08, 126.36, 118.19, 110.44, 44.89, 44.12, 29.57. HRMS (ESI): $m/z$ calcd for C$_{18}$H$_{12}$N$_2$O$_2$S+Na$^+$: 343.0512 [$M$+Na]$^+$; found: 343.0515.

**2-ethyl-1,3-dioxo-1,2,3,3a,4,9b-hexahydrothiochromeno[3,4-c]pyrrole-8-carbonitrile: 9d**



9d
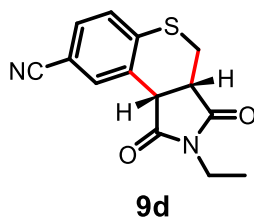
White solid. 5.4 mg (y. 20%). $^1$H NMR (500 MHz, CDCl$_3$): δ 7.76 (d, $J$ = 1.8 Hz, 1H), 7.49 (dd, $J$ = 8.1, 1.8 Hz, 1H), 7.39 (d, $J$ = 8.1 Hz, 1H), 4.11 (d, $J$ = 9.3 Hz, 1H), 3.71 (ddd, $J$ = 9.3, 4.7, 2.8 Hz, 1H), 3.62 (qd, $J$ = 7.2, 1.1 Hz, 2H), 3.39 (dd, $J$ = 13.4, 2.8 Hz, 1H), 2.94 (dd, $J$ = 13.4, 4.8 Hz, 1H), 1.18 (t, $J$ = 7.2 Hz, 3H). $^{13}$C NMR (126 MHz, CDCl$_3$): δ 176.82, 174.43, 141.44, 135.04, 131.50, 130.99, 130.14, 118.23, 110.34, 44.72, 43.96, 34.84, 29.23, 12.98. HRMS (ESI): $m/z$ calcd for C$_{14}$H$_{12}$N$_2$O$_2$S+Na$^+$: 295.0512 [$M$+Na]$^+$; found: 295.0485.
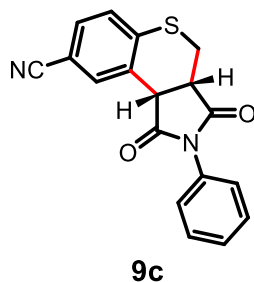
**1,3-dioxo-1,2,3,3a,4,9b-hexahydrothiochromeno[3,4-c]pyrrole-8-carbonitrile: 9e**



9e
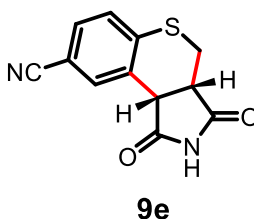
White solid. 2.4 mg (y. 10%). $^1$H NMR (500 MHz, DMSO-$d_6$): δ 11.65 (s, 1H), 7.84 (d, $J$ = 1.8 Hz, 1H), 7.63 (dd, $J$ = 8.1, 1.9 Hz, 1H), 7.46 (d, $J$ = 8.1 Hz, 1H), 4.35 (d, $J$ = 9.4 Hz, 1H), 3.77 (ddd, $J$ = 9.4, 4.8, 2.8 Hz, 1H), 3.20 (dd, $J$ = 13.4, 2.8 Hz, 1H), 2.90 (dd, $J$ = 13.4, 4.9 Hz, 1H). $^{13}$C NMR (126 MHz, DMSO-$d_6$): δ 179.63, 177.32, 141.90, 135.60, 133.20, 131.10, 130.33, 119.07, 108.98, 45.85, 45.16, 28.94. HRMS (ESI): $m/z$ calcd for $C_{12}H_8N_2O_2S+Na^+$: 267.0199 [$M$+Na]$^+$; found: 267.0224.

**1-benzylpyrrolidine-2,5-dione: 5b**



**5b**
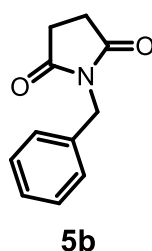
White solid. 10.8 mg (y. 57%). $^1$H NMR (500 MHz, CDCl$_3$): δ 7.42 – 7.35 (m, 2H), 7.34 – 7.24 (m, 3H), 4.66 (s, 2H), 2.70 (s, 4H). $^{13}$C NMR (126 MHz, CDCl$_3$): δ 176.98, 135.88, 129.02, 128.74, 128.08, 42.50, 28.30. HRMS (ESI): $m/z$ calcd for $C_{11}H_{11}NO_2+Na^+$: 212.0682 [$M$+Na]$^+$; found: 212.0661.

**1-phenylpyrrolidine-2,5-dione: 5c**



**5c**
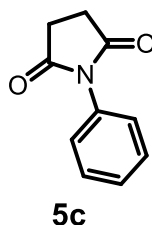
White solid. 6.1 mg (y. 35%). $^1$H NMR (500 MHz, CDCl$_3$): δ 7.54 – 7.43 (m, 2H), 7.47 – 7.37 (m, 1H), 7.32 – 7.23 (m, 2H), 2.91 (s, 4H). $^{13}$C NMR (126 MHz, CDCl$_3$): δ 176.23, 131.87, 129.24, 128.70, 126.48, 28.43. HRMS (ESI): $m/z$ calcd for $C_{10}H_9NO_2+Na^+$: 198.0526 [$M$+Na]$^+$; found: 198.0529.

**1-ethylpyrrolidine-2,5-dione: 5d**



**5d**
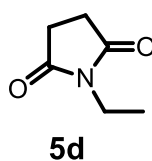
White solid. 5.7 mg (y. 45%). $^1$H NMR (500 MHz, CDCl$_3$): δ 3.56 (q, $J$ = 7.2 Hz, 2H), 2.70 (s, 4H), 1.16 (t, $J$ = 7.2 Hz, 3H). $^{13}$C NMR (126 MHz, CDCl$_3$): δ 177.28, 33.73, 28.24, 13.03. HRMS (ESI): $m/z$ calcd for C$_6$H$_9$NO$_2$+Na$^+$: 150.0526 [$M$+Na]$^+$; found: 150.0499.

**Pyrrolidine-2,5-dione: 5e**



**5e**
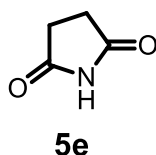
White solid. 2.8 mg (y. 28%). $^1$H NMR (500 MHz, CDCl$_3$): δ 8.96 (s, 1H), 2.77 (s, 4H). $^{13}$C NMR (126 MHz, CDCl$_3$): δ 178.19, 29.66. HRMS (ESI): $m/z$ calcd for C$_4$H$_5$NO$_2$+Na$^+$: 122.0213 [$M$+Na]$^+$; found: 122.0238.

## Conclusion

In this investigation, I elucidate the critical role of TiO$_2$ in mediating carbon-carbon bond formation between thiomethyl-bearing thioanisole derivatives and maleimide derivatives in anaerobic environments. Blue light irradiation (>420 nm) effectively catalyzed this reaction, yielding thiochromenopyrroledione derivatives. Specifically, the synthesis of a thiochromenopyrroledione derivative from thioanisole and $N$-benzylmaleimide reached a significant yield of 43% within 12 hours, approaching its theoretical optimum of 50%. The reaction remained inert without TiO$_2$, highlighting its essential role. Broadening our scope to various thioanisole and maleimide derivatives, I synthesized 20 distinct thiochromenopyrroledione derivatives, achieving yields from moderate to high. From a mechanistic standpoint, substituent effects hint at a charge transfer from thioanisole to the conduction band of TiO$_2$ upon blue light irradiation. This instigates the one-electron oxidation of thioanisole, leading to the generation of α-thioalkyl radicals following deprotonation. These insights advance heterocyclic compound synthesis and offer a refined methodology for employing TiO$_2$ in visible-light photocatalysis.

## References

(1)    E. Kabir, M. Uzzaman, *Results Chem.* **2022**, *4*, 100606.

(2)    A. Borissov, Y. K. Maurya, L. Moshniaha, W.-S. Wong, M. Żyła-Karwowska, M. Stepien, *Chem. Rev.* **2022**, *122*, 565-788.

(3)     M.-H. Cao, N. J. Green, S.-Z. Xu, *Org. Biomol. Chem.* **2017**, *15*, 3105-3129.

(4)     S. Marinković, N. Hoffmann, *Eur. J. Org. Chem.* **2004**, *2004*, 3102-3107.

(5)     X. Ju, D. Li, W.Li, W. Yu, F. Bian, *Adv. Synth. Catal.* **2012**, *354*, 3561-3567.

(6)     J. Li, W. Bao, Y. Zhang, Y. Rao, *Org. Biomol. Chem.* **2019**, *17*, 8958-8962.

(7)     X.-L. Yang, J.-D. Guo, T. Lei, B. Chen, C.-H. Tung, L.-Z. Wu, *Org. Lett.* **2018**, *20*, 2916-2920.

(8)     A. K. Yadav, L. D. S. Yadav, *Tetrahedron Lett.* **2017**, *58*, 552-555.

(9)     J. Tang, G. Grampp, Y. Liu, B.-X. Wang, F.-F. Tao, L.-J. Wang, X.-Z. Liang, H.-Q. Xiao, Y.-M. Shen, *J. Org. Chem.* **2015**, *80*, 2724-2732.

(10)    Z. Liang, S. Xu, W. Tian, R. Zhang, *Beilstein J. Org. Chem.* **2015**, *11*, 425-430.

(11)    A. Runemark, H. Sundén, *J. Org. Chem.* **2023**, *88*, 462-474.

(12)    D. W. Manley, R. T. McBurney, P. Miller, R. F. Howe, S. Rhydderch, J. C. Walton, *J. Am. Chem. Soc.* **2012**, *134*, 13580-13583.

(13)    D. W. Manley, A. Mills, C. O'Rourke, A. M. Z. Slawin, J. C. Walton, *Chem. Eur. J.* **2014**, *20*, 5492-5500.

(14)    P. K. Roy, Y. Hitomi, *Asian J. Org. Chem.* **2023**, e202300378.

(15)    D. Ma, Y. Yan, H. Ji, C. Chen, J. Zhao, *Chem. Commun.* **2015**, *51*, 17451-17454.

(16)    D. Ma, A. Liu, C. Lu, C. Chen, *ACS Omega* **2017**, *2*, 4161-4172.

(17)    X. Qiao, Y. Lin, J. Li, W. Ma, J. Zhao, *Sci. China Chem.* **2021**, *64*, 770-777.

(18)    X. Qiao, Y. Lin, D. Huang, H. Ji, C. Chen, W. Ma, J. Zhao, *J. Org. Chem.* **2022**, *87*, 13627-13642.

(19)    L. E. Oi, M.-Y. Choo, H. V. Lee, H. C. Ong, S. B. A. Hamid, J. C. Juan, *RSC Advances* **2016**. *6*, 108741-108754.

(20)    A. Yamamoto, T. Ohara, H. Yoshida, *Catal. Sci. Technol.* **2018**, *8*, 2046-2050.

(21)    K. Aitsuki, D. Fukushima, H. Nakahara, K. Yo, M. Kodera, S. Okunaka, H. Tokudome, T. Koitaya, Y. Hitomi, *New. J. Chem.* **2022**, *46*, 9010-9016.

(22)    F. Neese, F. Wennmohs, U. Becker, C. Riplinger, *J. Chem. Phys.* **2020**, *152*, 224108.

# Chapter 3

## Solvent-Dependent Photocatalytic Synthesis of Sulfoxides: Trifluoroethanol-Enhanced Conversion of Thioethers and Application in Ricobendazole Production

## Abstract

Sulfoxide compounds hold a pivotal role in medicinal chemistry. The synthesis of sulfoxides from thioether precursors has been extensively investigated, yielding a diverse array of methodologies to date. Notably, photocatalytic processes utilizing molecular oxygen as the oxygen atom donor have emerged as environmentally benign and indispensable techniques. This study meticulously examines the influence of various solvents on the photocatalytic conversion of thioanisole to its sulfoxide counterpart, employing ultraviolet light irradiation at 370 nm. The findings reveal that nonpolar solvents, such as toluene, predominantly lead to the formation of methyl phenyl sulfone. In contrast, employing alcoholic solvents markedly improves the selectivity toward sulfoxide formation. Trifluoroethanol, in particular, exhibits outstanding selectivity in transforming thioanisole into methyl phenyl sulfoxide. Furthermore, the study demonstrates the high efficacy of trifluoroethanol as a solvent for the selective synthesis of the anthelmintic agent ricobendazole, also known as albendazole sulfoxide, from albendazole.

## Introduction

Sulfoxide compounds are pivotal in organic synthesis, particularly in medicinal chemistry.[1] Traditional methods of oxidizing sulfides to sulfoxides employ oxidants such as *m*-CPBA,[2] often necessitating an excessive amount of these oxidants and producing undesirable by-products. To mitigate these issues, researchers have focused on developing environmentally friendly methodologies. Hydrogen peroxide is a sustainable alternative, with

68

water being its only by-product,[3] however, oxygen emerges as an even superior green oxidant.[4] Numerous approaches have been devised for the selective oxidation of thioethers, utilizing oxygen as the principal oxidant. Schenck first revealed the potential of light-mediated thioether oxidation in 1962.[5] Since then, the mechanisms underlying the photochemical aerobic oxidation of thioethers have been the focus of intense research. Foote and his colleague demonstrated that the oxidation of thioethers with singlet oxygen, generated using photosensitizers, predominantly yields a persulfoxide intermediate (**1**) in protic solvents caused by hydrogen-bonding-induced stabilization. In contrast, cyclic sulfurane (**2**) is the primary product in aprotic solvents.[6] The persulfoxide intermediate (**1**) can produce two molecules of sulfoxide (**3**) through a disproportionation reaction with the thioether, and it has also been shown that the persulfoxide intermediate (**2**) can directly convert into a sulfone (**4**).

**1) Foote's mechasnim**
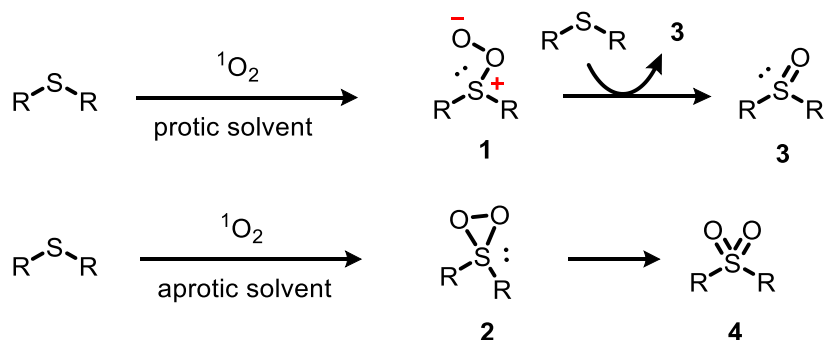


**2) Direct irradiation of thioanisoles**
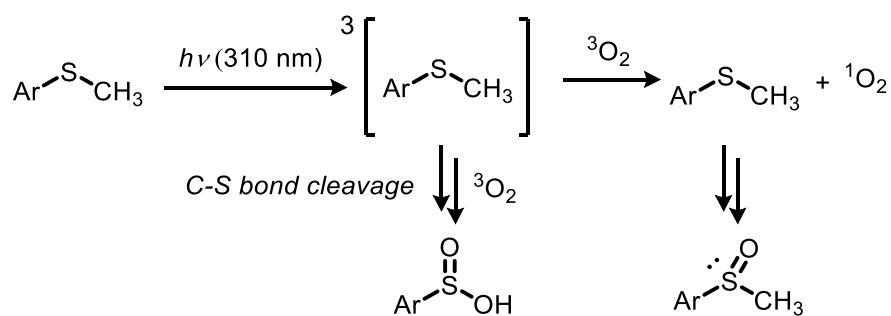


**Scheme 1.** Routes for selective oxidation of sulfides.

Many reactions involving photosensitizers have been reported in the study of aerobic photo-oxidation of thioethers, but those that do not require photosensitizers have also drawn interest.[7] Notably, the UV-photooxidation of aryl sulfides without a catalyst, as explored and reported by Bonesi et al. in 2017, warrants special attention.[8] Exposure to light with a wavelength of 310 nm induces the oxidation of *para*-substituted thioanisoles to sulfinic acids

and sulfoxides. In 2022, Kokotos and associates examined the effect of irradiation wavelength on the photochemical aerobic oxidation of thioanisole in acetonitrile, reporting that the selectivity of sulfone (**3**) over sulfoxide (**4**) was dependent on the wavelength employed for irradiation.[9] In my previous work, methyl phenyl sulfoxide **6a** and methyl phenyl sulfone **7a** were formed from the oxidation of thioanisole **5a** in acetonitrile solvent under atmospheric conditions.[10] In this study, I report the investigation of the solvent effect on the aerobic oxidation of thioanisole derivatives under irradiation by a 370 nm wavelength ultraviolet LED lamp. In this method, I did not use any metal or metal complex catalyst compared to other reported methods.[11-17]

## Results and discussion

In my investigation of aerobic oxidation, I exposed **5a** to 370 nm LED light irradiation using various solvents, including acetonitrile, acetone, dichloromethane, ethanol, methanol, 2,2,2-trifluoroethanol (TFE), trifluorotoluene and toluene. Analysis of the products revealed exclusive formation of sulfoxide **6a** when employing TFE, ethanol, or methanol as solvents (Table 1, entries 1, 3, 4, 10, and 12). Conversely, acetonitrile, acetone, dichloromethane, and trifluorotoluene yielded both sulfoxide **6a** and sulofone **7a** (Table 1, entries 2, 5, 6, and 7), with sulfoxide selectivities of 68%, 92%, 96%, and 91%, respectively. These results are consistent with Foote's findings,[6] supporting the stability of persulfoxide intermediates (**1**) in protic solvents, leading to sulfoxides and the formation of cyclic sulfuranes (**2**) in aprotic solvents, resulting in sulfones. Notably, I observed the formation of sulfoxide **6a** with 100% yield and selectivity in TFE and ethanol (Table 1, entries 1 and 4) and selective production of **6a** in ethanol within 3 hours (Table 1, entry 10). This suggests hydrogen bond formation between sulfoxide **6a** and polar solvents like TFE and ethanol. In less polar or nonpolar solvents such as acetonitrile and toluene, sulfoxide **6a** and sulfone **7a** were formed (Table 1, entries 9 and 11). No reaction occurred under blue LED (>420 nm) irradiation or in an argon atmosphere (Table 1, entries 13 and 14), indicating that the reaction proceeds exclusively in the presence of oxygen and under UV light (370 nm) irradiation. Figure 1 reveals the absorption bands of thioanisole derivatives below 390 nm, with the longest wavelength absorption occurring in the order R = H < $CH_3$ < Br < $OCH_3$ < CN, barring 4-nitrothioanisole, which is yellow and absorbs blue light (450-485 nm). These observations imply that selective oxidation of thioanisole derivatives is feasible under UV LED irradiation at 370 nm, encompassing wavelengths between 350 and 390 nm.

**Table 1.** Effects of solvents on the aerobic photooxidation of **5a.**[a)]
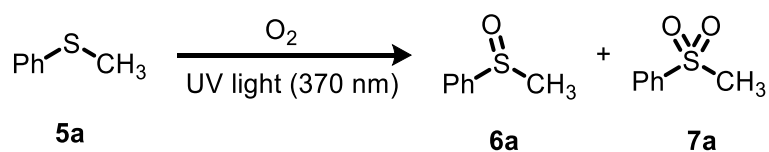


| Entry | Solvent | Time (h) | 5a (%) | 6a (%) | 7a (%) | 6a/(6a+7a) (%) |
|-------|---------|----------|--------|--------|--------|-----------------|
| 1 | TFE | 9 | **0** | **100** | **0** | **100** |
| 2 | CH₃CN | 9 | 1 | 67 | 32 | 68 |
| 3 | CH₃OH | 9 | 4 | 96 | 0 | 100 |
| 4 | CH₃CH₂OH | 9 | 1 | 99 | 0 | 100 |
| 5 | acetone | 9 | 1 | 91 | 8 | 92 |
| 6 | CH₂Cl₂ | 9 | 1 | 95 | 4 | 96 |
| 7 | PhCF₃ | 9 | 6 | 86 | 8 | 91 |
| 8 | toluene | 9 | 0 | 85 | 15 | 85 |
| 9 | CH₃CN | 3 | 57 | 42 | 1 | 98 |
| 10 | CH₃CH₂OH | 3 | 66 | 34 | 0 | 100 |
| 11 | toluene | 3 | 78 | 21 | 1 | 95 |
| 12 | CH₃CH₂OH[b)] | 9 | 37 | 63 | 0 | 100 |
| 13 | CH₃CH₂OH[c)] | 9 | 100 | 0 | 0 | - |
| 14 | CH₃CH₂OH[d)] | 9 | 100 | 0 | 0 | - |

[a)] Reaction conditions: **5a** (0.6 mmol), solvent (2.0 mL), O₂ balloon, UV light (370 nm) irradiation, yield (%) based on **5a**. [b)] Under air, [c)] Blue LED (>420 nm), [d)] Under Ar atmosphere.
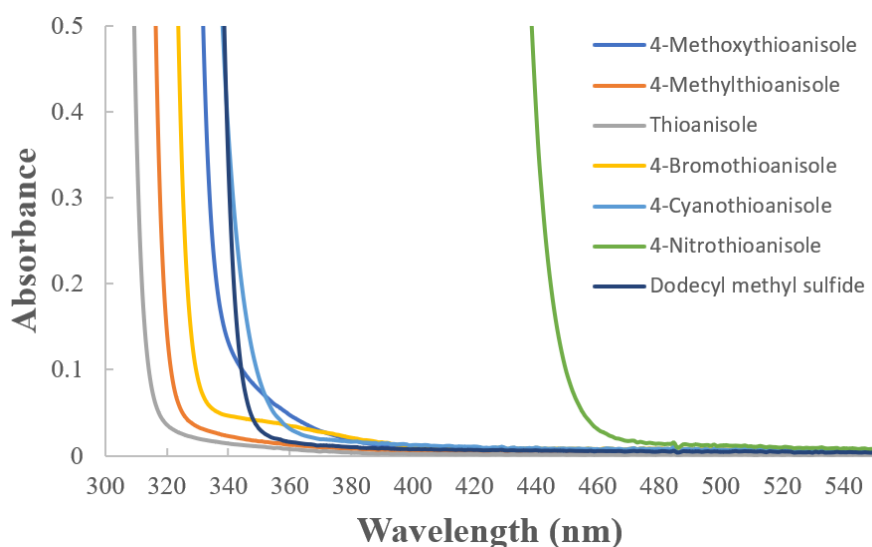


**Figure 1.** Absorption spectra of thioanisole derivatives (0.6 mmol) in 2.0 mL ethanol.

**Table 2.** Selective oxidation of sulfides with $O_2$ under UV-light irradiation.[a]



**5a:** R = H
**5b:** R = OCH$_3$
**5c:** R = CH$_3$
**5d:** R = Br
**5e:** R = CN
**5f:** R = NO$_2$
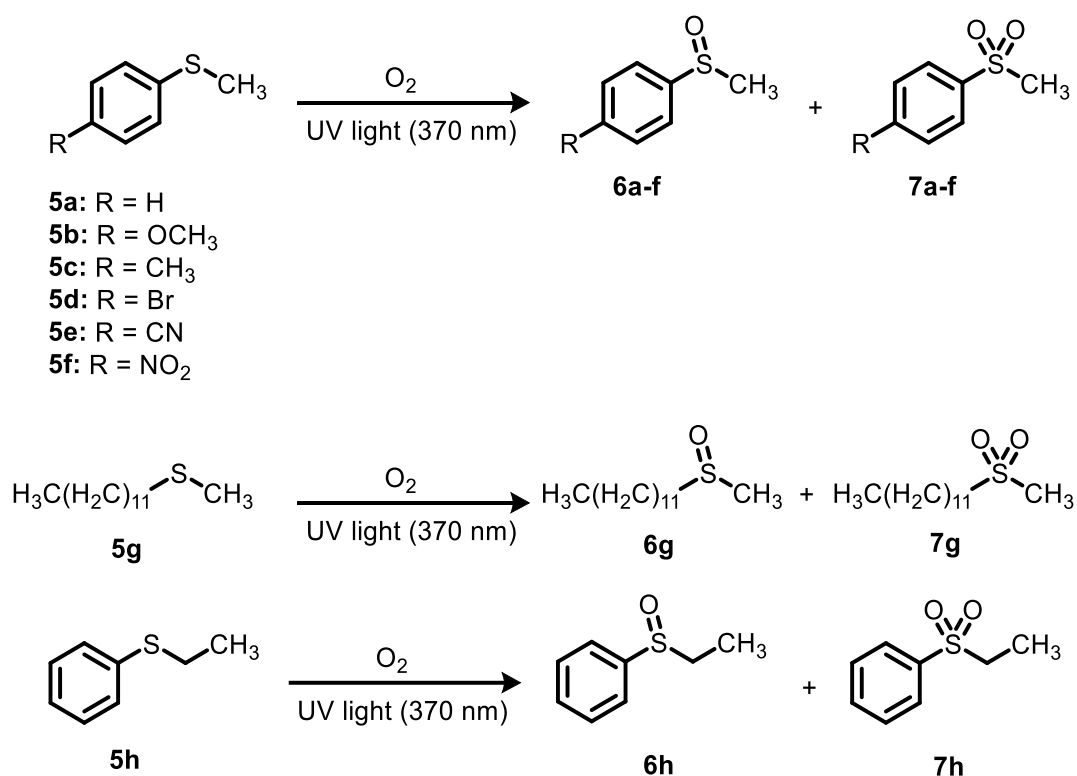




| Entry | Substrate | 5 (%) | 6 (%) | 7 (%) |
|-------|-----------|-------|-------|-------|
| 1 | **5a** | 1 | 99 | 0 |
| 2[b] | **5a** | 0 | 100 | 0 |
| 3 | **5b** | 0 | 90 | 10 |
| 4[b] | **5b** | 0 | 100 | 0 |
| 5 | **5c** | 0 | 96 | 4 |
| 6[b] | **5c** | 0 | 100 | 0 |
| 7 | **5d** | 0 | 88 | 12 |
| 8[b] | **5d** | 0 | 100 | 0 |
| 9 | **5e** | 74 | 26 | 0 |
| 10 | **5f** | 83 | 17 | 0 |
| 11 | **5g** | 13 | 87 | 0 |
| 12[b] | **5h** | 0 | 100 | 0 |

[a] Reaction conditions: **5** (0.6 mmol), ethanol (2.0 mL), $O_2$ balloon, UV light (370 nm) irradiation, time (9 h), yield (%) based on **5**. [b] Under CF$_3$CH$_2$OH instead of ethanol.

A comprehensive array of *para*-substituted thioanisoles (**5a-f**) was evaluted in ethanol, yielding the corresponding sulfoxides (**6a-f**) with good to excellent efficiency (Table 2). Notably, when employing dodecyl methyl sulfide **5g** and ethyl phenyl sulfide **5h** as substrates,

the resulting dodecyl methyl sulfoxide **6g** and ethyl phenyl sulfoxide **6h** were produced in high yields, without the formation of their sulfone counterparts (**7g** and **7h**, respectively) (Table 2, entries 11 and 12). This demonstrates the protocol's applicability in converting aliphatic sulfides to sulfoxides. Furthermore, under identical conditions in ethanol, oxidation of thioanisole **5a** and its derivatives 4-methoxythioanisole **5b**, 4-methylthioanisole **5c**, 4-bromothioanisole **5d**, 4-cyanothioanisole **5e**, 4-nitrothioanisole **5f**, alongside dodecyl methyl sulfide **5g**, consistently yielded sulfoxides **6a-g** with high selectivity—100%, 90%, 96%, 88%, 100%, 100%, and 100%, respectively (Table 2, entries 1, 3, 5, 7, 9, 10, and 11). This high selectivity is attributed to the suppression of overoxidation to sulfones **7a-g**, likely due to hydrogen bond formation between sulfoxides **6a-g** and ethanol. However, in the cases of 4-methoxythioanisole **5b**, 4-methylthioanisole **5c**, and 4-bromothioanisole **5d** in ethanol, overoxidation to sulfones **7b-d** was observed within a 9-hour reaction period (Table 1, entries 3, 5, and 7). A shift to TFE solvent, owing to its superior donor properties compared to ethanol, resulted in a more selective formation of sulfoxides **6b**, **6c**, and **6d** (Table 2, entries 4, 6, and 8).

To demonstrate the scalability of the synthetic approach, a gram-scale reaction was conducted, yielding the isolated product **6a** with a 100% yield. This was achieved solely through solvent evaporation, without any purification steps, as illustrated in Scheme 2. Additionally, the practical applicability of this selective oxidation strategy was evidenced by converting the drug albendazole **8** into albendazole sulfoxide **9**. A reaction with 10 mg of albendazole **8** resulted in the desired product, albendazole sulfoxide **9**, with a 100% yield, as depicted in Scheme 3.
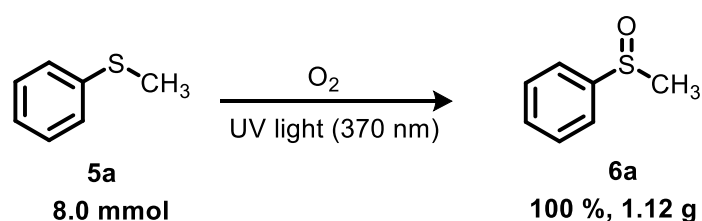


**Scheme 2.** Gram-scale synthesis of methyl phenyl sulfoxide **6a**. Reaction conditions: **5a** (8.0 mmol), TFE (3.0 mL), $O_2$ balloon, UV light (370 nm) irradiation, time (15 h).
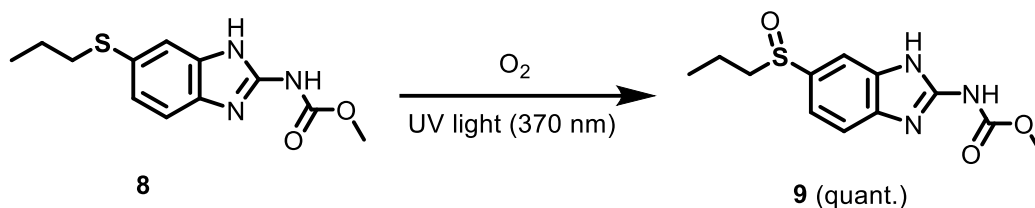
**Scheme 3.** Selective synthesis of albendazole **8** to albendazole sulfoxide **9**. Reaction conditions: **8** (10.0 mg), TFE (3.0 mL), O$_2$ balloon, UV light (370 nm) irradiation, time (9 h).

The aerobic photooxidation of 4-substituted thioanisoles (**5a-f**) was executed in ethanol solvent over two hours, selectively yielding sulfoxides **6a-f**, as delineated in Table 3. An increase in reaction efficiency was noted with the addition of various 4-substituents, transitioning from electron-withdrawing (NO$_2$) to electron-donating (OCH$_3$) groups. However, an anomaly was observed in the case of the Br substitution (see Table 3, entry 4), leading to an almost linear enhancement in the Hammett plot, with the notable exception of **5d** (R = Br), as illustrated in Figure 2.

**Table 3.** Aerobic photooxidation of thioanisole derivatives for 2 h.[a]



**5a:** R = H
**5b:** R = OCH$_3$
**5c:** R = CH$_3$
**5d:** R = Br
**5e:** R = CN
**5f:** R = NO$_2$
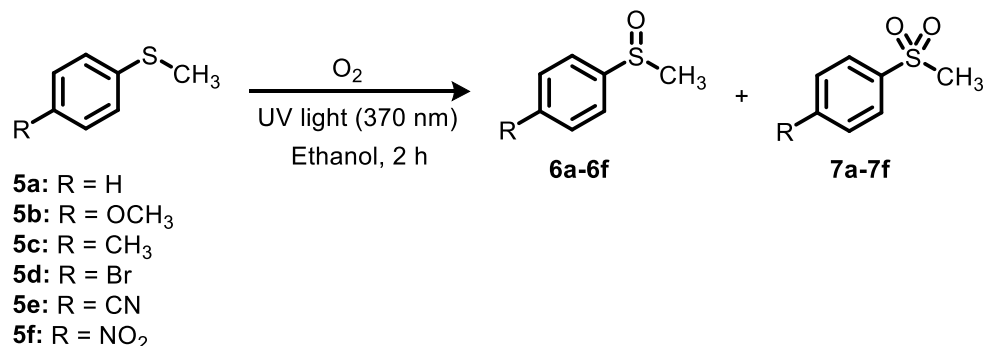
| entry | thioanisole | substituent constant $\sigma_p^+$ | 6 (%) | 7 (%) |
|-------|-------------|-----------------------------------|-------|-------|
| 1 | **5b** (R = OCH$_3$) | -0.78 | 69 | 0 |
| 2 | **5c** (R = CH$_3$) | -0.31 | 50 | 0 |
| 3 | **5a** (R = H) | 0 | 47 | 0 |
| 4 | **5d** (R = Br) | 0.15 | 98 | 0 |
| 5 | **5e** (R = CN) | 0.66 | 7 | 0 |
| 6 | **5f** (R = NO$_2$) | 0.79 | 5 | 0 |
| 7 | **5a + 5d** | | 97 (**6a**), 80 (**6d**) | 0 |
| 8 | **5e + 5d** | | 24 (**5e**), 82 (**6d**) | 0 |

[a] Reaction conditions: **5** (0.6 mmol), ethanol (2.0 mL), O$_2$ balloon, UV light (370 nm) irradiation, time (2 h), yield (%) based on **5**.

It is postulated that **5d** (R = Br) might enhance the formation of singlet oxygen, potentially due to the heavy atom effect. When **5d** (R = Br) was present, a marked increase in the yield of **6a** from 47% to 97% was observed upon oxidizing **5a**, and a similar enhancement in the yield of **6e** from 7% to 24% was noted upon oxidizing **5e**, as indicated in Table 3, entries 7 and 8.
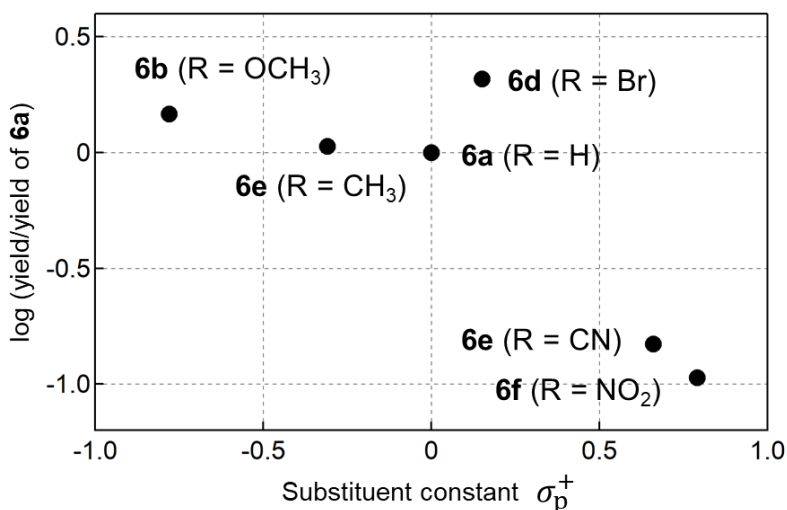


**Figure 2.** Hammett plot for the yields of sulfoxides **6a-f**.

Scheme 4 illustrates a proposed reaction mechanism. When thioanisole is irradiated with UV light (370 nm), the triplet excited state of thioanisole, $^3$[**5a**], produces singlet oxygen $^1O_2$ via an energy transfer mechanism. This singlet oxygen $^1O_2$ subsequently reacts with thioanisole in its ground state, **5a**, forming the persulfoxide intermediate (**1**). This intermediate is then consumed by another molecule of thioanisole **5a**, forming two molecules of methyl phenyl sulfoxide **6a**. Overoxidation of sulfoxide **6a**, through a similar process, yields methyl phenyl sulfone **7a**. Alternatively, the persulfoxide intermediate (**1**) may form cyclic sulfurane (**2**), producing methyl phenyl sulfone **7a**.
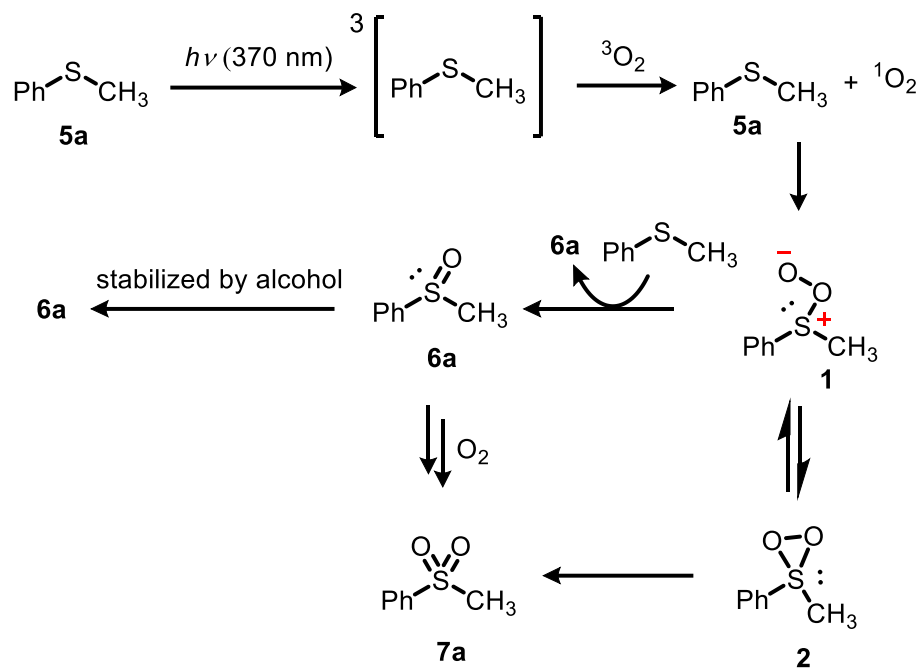
**Scheme 4.** Plausible mechanism.

## Experimental Section

### General Information

$^1$H and $^{13}$C NMR spectra were recorded on a 500 MHz JEOL spectrometer, where CDCl$_3$ and DMSO-$d_6$ were used as solvents. All chemical shifts ($\delta$) are measured in ppm from TMS. Here, the chemical shift of TMS was 0.0 ppm, and spin-spin coupling constants ($J$) are mentioned in Hz. All reagents and organic solvents were purchased from TCI and Wako Pure Chemical Industries and used without further purification, except for toluene. A distillation process purified toluene. Reactions were monitored by analytical thin-layer chromatography using silica gel 60 F254 as a stationary phase. Column chromatography was executed on Biotage SNAP Cartridge using Isolera.

### General procedure for the photochemical reaction

Substrate **5a**-**h** (0.6 mmol) was dissoloved in 2.0 mL of solvent in a galss tube with a small stirring bar. An oxygen balloon was introduced at atmospheric pressure through a rubber stopper. The reaction vessel was laterally irradiated using a UV LED lamp (Kessil PR160-370 nm) (Figure 3, the reaction setup). Following a 9-hour reaction period, the mixture was

subjected to membrance filtration. The crude products underwent purification through chromatography on a Biotage Isolera One Flash Purification system, empoying a gradient of hexane : ethyl acetate (85: 15 to 65: 35), yielding the compounds.
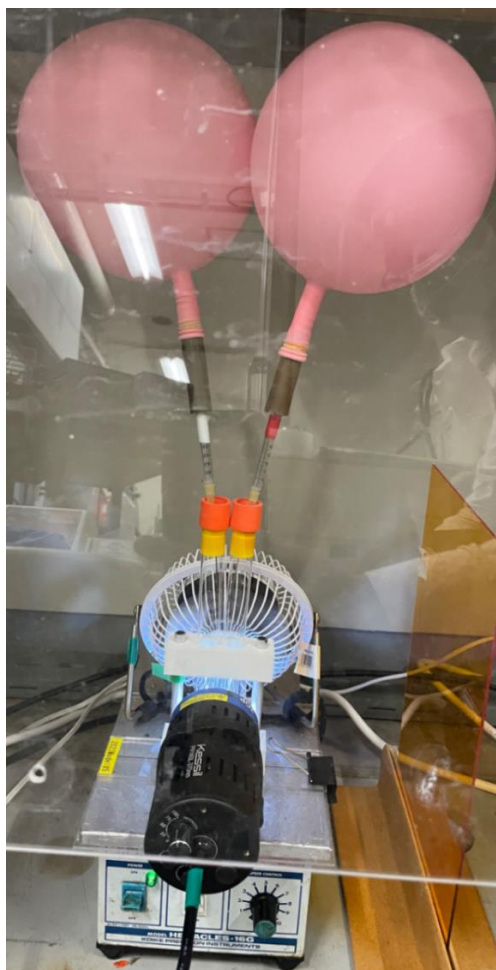


**Figure 3.** Experimental setup of the photochemical reaction.

**NMR data for compounds:**

**Methyl phenyl sulfoxide**: **6a**
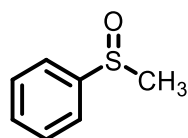


**6a**

Liquid. $^{1}$H NMR (500 MHz, CDCl$_3$): δ 7.70 – 7.62 (m, 2H), 7.58 – 7.46 (m, 3H), 2.73 (s, 3H). $^{13}$C NMR (126 MHz, CDCl$_3$): δ 145.71, 131.12, 129.43, 123.55, 44.00.

**4-Methoxyphenyl methyl sulfoxide**: **6b**
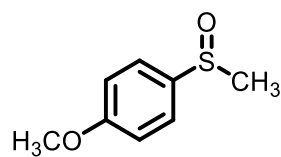


**6b**

Solid. $^1$H NMR (500 MHz, CDCl$_3$): δ 7.63 – 7.56 (m, 2H), 7.06 – 7.00 (m, 2H), 3.85 (s, 3H), 2.70 (s, 3H). $^{13}$C NMR (126 MHz, CDCl$_3$): δ 161.99, 136.52, 125.50, 114.89, 55.56, 43.98.

**Methyl *p*-tolyl sulfoxide**: **6c**
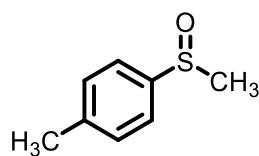


**6c**

Solid. $^1$H NMR (500 MHz, CDCl$_3$): δ 7.56 – 7.50 (m, 2H), 7.30 (d, *J* = 8.6 Hz, 2H), 2.67 (s, 3H), 2.37 (s, 3H). $^{13}$C NMR (126 MHz, CDCl$_3$): δ 142.49, 141.15, 129.85, 123.37, 43.79, 21.21.

**4-Bromophenyl methyl sulfoxide**: **6d**
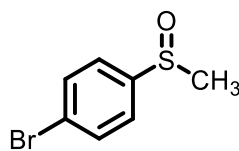


**6d**

Solid. $^1$H NMR (500 MHz, CDCl$_3$): δ 7.76 – 7.63 (m, 2H), 7.57 – 7.49 (m, 2H), 2.74 (s, 3H). $^{13}$C NMR (126 MHz, CDCl$_3$): δ 144.62, 132.64, 125.57, 125.30, 43.88.

**4-(Methylsulfinyl)benzonitrile**: **6e**
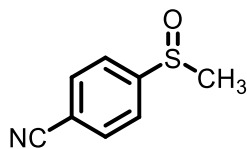


**6e**

Solid. $^1$H NMR (500 MHz, CDCl$_3$): δ 7.90 – 7.84 (m, 2H), 7.84 – 7.75 (m, 2H), 2.82 (s, 3H). $^{13}$C NMR (126 MHz, CDCl$_3$): δ 151.20, 133.11, 124.48, 117.85, 114.78, 43.71.

**1-(Methylsulfinyl)-4-nitrobenzene: 6f**



**6f**
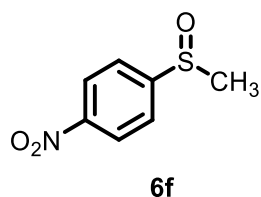
Solid. $^1$H NMR (500 MHz, CDCl$_3$): δ 8.44 – 8.37 (m, 2H), 7.90 – 7.83 (m, 2H), 2.82 (s, 3H). $^{13}$C NMR (126 MHz, CDCl$_3$): δ 153.24, 149.56, 124.79, 124.58, 43.90.

**Dodecyl methyl sulfoxide: 6g**



**6g**
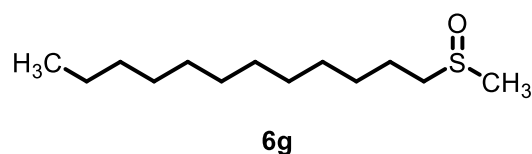
Solid. $^1$H NMR (500 MHz, CDCl$_3$): δ 2.80 – 2.72 (m, 1H), 2.71 – 2.62 (m, 1H), 2.58 (s, 3H), 1.84 – 1.68 (m, 2H), 1.54 – 1.38 (m, 2H), 1.36-1.20 (m, 16H), 0.88 (t, $J$ = 6.8 Hz, 3H). $^{13}$C NMR (126 MHz, CDCl$_3$): δ 54.66, 38.46, 31.93, 29.63, 29.56, 29.37, 29.23, 28.80, 22.71, 22.58, 14.16.

**Ethyl phenyl sulfoxide: 6h**



**6h**
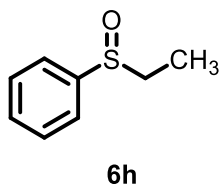
Solid. $^1$H NMR (500 MHz, CDCl$_3$): δ 7.61 (dd, $J$ = 7.5, 1.8 Hz, 2H), 7.57 – 7.46 (m, 3H), 2.91 (dq, $J$ = 12.7, 7.5 Hz, 1H), 2.82 – 2.72 (m, 1H), 1.19 (t, $J$ = 7.4 Hz, 3H). $^{13}$C NMR (126 MHz, CDCl$_3$): δ 143.20, 131.00, 129.20, 124.19, 50.26, 5.99.

**Methyl phenyl sulfone: 7a**



**7a**
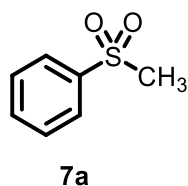
Solid. $^1$H NMR (500 MHz, CDCl$_3$): δ 8.00 – 7.91 (m, 2H), 7.70 – 7.63 (m, 1H), 7.63 – 7.51 (m, 2H), 3.06 (s, 3H). $^{13}$C NMR (126 MHz, CDCl$_3$): δ 140.59, 133.73, 129.40, 127.36, 44.50.

**Methyl *p*-tolyl sulfone**: **7c**



**7c**
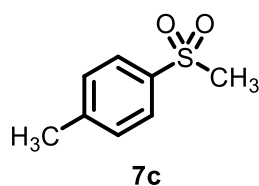
Solid. $^1$H NMR (500 MHz, CDCl$_3$): δ 7.86 – 7.80 (m, 2H), 7.40 – 7.34 (m, 2H), 3.04 (s, 3H), 2.45 (s, 3H). $^{13}$C NMR (126 MHz, CDCl$_3$): δ 144.79, 137.78, 130.06, 127.45, 44.69, 21.70.

**4-Bromophenyl methyl sulfone**: **7d**



**7d**
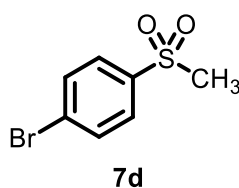
Solid. $^1$H NMR (500 MHz, CDCl$_3$): δ 7.85 – 7.79 (m, 2H), 7.82 – 7.70 (m, 2H), 3.06 (s, 3H). $^{13}$C NMR (126 MHz, CDCl$_3$): δ 139.55, 132.74, 129.06, 129.01, 44.54.

**4-(Methylsulfonyl)benzonitrile**: **7e**



**7e**
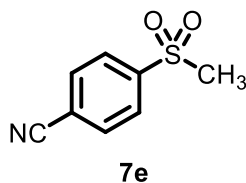
Solid. $^1$H NMR (500 MHz, CDCl$_3$): δ 8.12 – 8.02 (m, 2H), 7.94 – 7.86 (m, 2H), 3.10 (s, 3H). $^{13}$C NMR (126 MHz, CDCl$_3$): δ 144.57, 133.32, 128.33, 117.74, 117.14, 44.35.

**1-(Methylsulfonyl)-4-nitrobenzene**: **7f**



**7f**
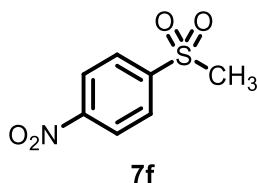
Solid. $^1$H NMR (500 MHz, CDCl$_3$): δ 8.47 – 8.41 (m, 2H), 8.20 – 8.14 (m, 2H), 3.12 (s, 3H). $^{13}$C NMR (126 MHz, CDCl$_3$): δ 150.87, 145.91, 128.94, 124.78, 44.32.

**Albendazole sulfoxide**: **9**



**9**
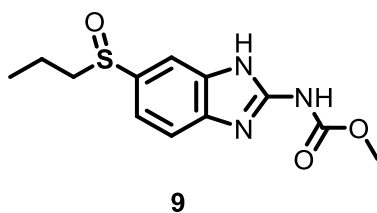
Solid. $^{1}$H NMR (500 MHz, DMSO-d$_6$): δ 7.72 (d, $J$ = 1.7 Hz, 1H), 7.57 (d, $J$ = 8.3 Hz, 1H), 7.34 (dd, $J$ = 8.3, 1.7 Hz, 1H), 3.79 (s, 3H), 2.84 (ddd, $J$ = 13.1, 9.1, 6.5 Hz, 1H), 2.76 (ddd, $J$ = 13.1, 9.0, 5.4 Hz, 1H), 1.61 (dddd, $J$ = 13.9, 9.2, 7.7, 6.6 Hz, 1H), 1.55 – 1.41 (m, 1H), 0.95 (t, $J$ = 7.4 Hz, 3H). $^{13}$C NMR (126 MHz, DMSO-d$_6$): 154.69, 149.07, 137.26, 136.77, 136.68, 117.35, 114.65, 110.51, 58.68, 53.18, 15.92, 13.46.

## Conclusion

In this investigation into the aerobic photooxidation of 4-substituted thioanisoles, I gained valuable insights into the mechanics of selective oxidation. Throughout my experiments, various solvents were subjected to UV light irradiation. I observed that protic solvents, namely TFE, ethanol, and methanol, predominantly facilitated the formation of a single product, sulfoxide **6a**. Conversely, aprotic solvents resulted in the generation of two distinct products, sulfoxide **6a** and sulfone **7a**. This distinction underscores the significant role of solvent properties in influencing oxidation outcomes, reinforcing previous research on the stability of intermediates within different solvent contexts. Remarkably, TFE and ethanol achieved an exceptional 100% yield and selectivity for sulfoxide **6a**, indicative of potential hydrogen bonding interactions with these solvents. Additionally, I extended this methodology to encompass a broader range of thioanisoles and aliphatic sulfides, attaining high selectivity in ethanol. This high selectivity is attributed to the prevention of overoxidation of sulfoxide to sulfones. However, some substrates demonstrated overoxidation in ethanol, a limitation successfully mitigated by switching to a TFE solvent.

The significance of this study resides in its contribution to advancing selective oxidation techniques, underscoring the pivotal role of solvent selection in steering product formation and specificity. This research enhances the understanding of oxidation mechanisms and offers a practical and scalable approach for synthesizing sulfoxides. It includes efficiently converting the pharmaceutical agent albendazole into its sulfoxide derivative, imparting

valuable insights for academic research and prospective industrial applications in chemical synthesis.

## References

(1) A. S. Surur, L. Schulig, A. Link, A., *Arch. der Pharm.* **2019**, *352*, 1800248.

(2) G. V. Kaiser, R. D. G. Cooper, R. E. Koehler, C. F. Murphy, J. A. Webber, I. G. Wright, E. M. Van Heyningen, *J. Org. Chem.* **1970**, *35*, 2430-2433.

(3) I. Triandafillidi, D. I. Tzaras, C. G. Kokotos, *ChemCatChem* **2018**, *10*, 2521-2538.

(4) K.-J. Liu, J.-H. Deng, J. Yang, S.-F. Gong, Y.-W. Lin, J.-Y. He, Z. Cao, W.-M. He, *Green Chem.* **2020**, *22*, 433-438.

(5) G. O. Schenck, C. H. Krauch, *Angew. Chem. Int. Ed.* **1962**, 74, 510.

(6) C. S. Foote, J. W.Peters, *J. Am. Chem. Soc.* **1971**, *93*, 3795-3796.

(7) E. Skolia, P. L. Gkizis, C. G. Kokotos, *ChemPlusChem* **2022**, *87*, e202200008.

(8) S. M. Bonesi, S. Crespi, D. Merli, I. Manet, A. Albini, *J. Org. Chem.* **2017**, *82*, 9054-9065.

(9) E. Skolia, P. L. Gkizis, N. F. Nikitas, C. G. Kokotos, *Green Chem.* **2022**, *24*, 4108-4118.

(10) P. K. Roy, Y. Hitomi, *Asian J. Org. Chem.* **2023**, *12*, e202300378.

(11) X. Lang, W. Hao, W. R. Leow, S. Li, J. Zhao, X. Chen, *Chem. Sci.* **2015**, *6*, 5000-5005.

(12) X. Lang, J. Zhao, X. Chen, , *Angew. Chem. Int. Ed.* **2016**, *128*, 4775-4778.

(13) Y. Xu, Z.-C. Fu, S. Cao, Y. Chen, W.-F. Fu, *Catal. Sci. Technol.* **2017**, *7*, 587-595.

(14) W. Zhao, C. Yang, J. Huang, X. Jin, Y. Deng, L. Wang, F. Su, H. Xie, P. K. Wong, L. Ye, *Green Chem.* **2020**, *22*, 4884-4889.

(15) H. Wei, Z. Guo, X. Liang, P. Chen, H. Liu, H. Xing, *ACS Appl. Mater. Interfaces* **2019**, *11*, 3016-3023.

(16) X. Lan, Q. Li, Y. Zhang, Q. Li, L. Ricardez-Sandoval, G. Bai, *Appl. Catal. B: Environ.* **2020**, *277*, 119274.

(17) X. Dong, H. Xu, H. Hao, W. Sheng, X. Lang, *J. Coll. Interface Sci.* **2022**, *608*, 882-892.

# PART 2

# Electrochemical Transformation of Alkenes

# Chapter 1

# Electrochemical Epoxidation Catalyzed by Manganese Salen Complex and Carbonate with Boron-Doped Diamond Electrode

## Abstract

Epoxides are essential precursors for epoxy resins and other chemical products. In this study, I investigated whether electrochemically oxidizing carbonate ions could produce percarbonate to promote an epoxidation reaction in the presence of appropriate metal catalysts, although Tanaka and co-workers had already completed a separate study in which the electrochemical oxidation of chloride ions was used to produce hypochlorite ions for electrochemical epoxidation. I found that epoxides could be obtained from styrene derivatives in the presence of metal complexes, including manganese(III) and oxidovanadium(IV) porphyrin complexes and manganese salen complexes, using a boron-doped diamond as the anode. After considering various complexes as potential catalysts, I found that manganese salen complexes showed better performance in terms of epoxide yield. Furthermore, the substituent effect of the manganese salen complex was also investigated, and it was found that the highest epoxide yields were obtained when Jacobsen's catalyst was used. Although there is still room for improving the yields, this study has shown that the in situ electrochemical generation of percarbonate ions is a promising method for the electrochemical epoxidation of alkenes.

## Introduction

Epoxide functional groups are essential not only in the chemical and pharmaceutical industries but also in nature. In the chemical and pharmaceutical industries, epoxide-containing compounds are used as versatile intermediates in the manufacture of many chemical products, including epoxy resins, fragrances, and pharmaceuticals. In nature, many natural products have epoxide groups and are used for medical purposes or as essential compounds for organic synthesis because they are highly reactive. Epoxide can be synthesized using different reactions,

including the chlorohydrin method, but is often prepared through the transfer of oxygen atoms to alkenes using peroxides such as *tert*-butyl hydroperoxide, peracetic acid, and *m*-chloroperoxybenzoic acid.[1-3] Such reagents are difficult to handle and produce undesirable stoichiometric by-products, except for hydrogen peroxide.[4,5] These problems can be avoided if the compounds that are by-products of the reaction between the alkene and the oxygen additive can be oxidized and the oxygen additive can be synthesized again.[6-13] For example, the two-electron reduction of oxygen can produce hydrogen peroxide. It should be noted that Collman and co-workers pioneered the epoxidation of alkene using manganese *meso*-tetraphenylporphyrin catalysts with hydrogen peroxide generated through the electrochemical reduction of oxygen using polymer-coated electrodes.[11] Electrocatalytic epoxidation using manganese salen complexes also has been performed through reductive dioxygen activation.[14,15] It is also possible to synthesize hydrogen peroxide, alky or acyl peracids, or oxygen-transfer reagents by electrode oxidation using water as an oxygen source, as shown in Figure 1. Recently, Manthiram and co-workers reported a new electrochemical method for the epoxidation of an alkene substrate using water as the sole source of oxygen atoms and monodisperse manganese oxide nanoparticles as catalysts.[6] Based on electro-kinetic studies, they proposed the formation of manganese(IV) oxo species as the resting state as well as the oxidizing species for alkene epoxidation. In addition, photochemical epoxidation using various metal complexes with water as the oxygen source have been investigated.[8-10,16] For example, chemical oxidants such as potassium hexachloroplatinate and visible light irradiation activate ruthenium(II) porphyrins have been used to form ruthenium oxo species using water as the oxygen atom source, which can transfer oxygen to alkene substrates to form epoxides. Similarly, the photosensitizer tris(2,2'-bipyridyl)ruthenium(II) chloride in combination with the one-electron oxidant pentaamminechlorocobalt(III) chloride produces metal–oxygen species that have been used as catalysts for alkene epoxidation. [(bTAML)Fe$^{III}$-OH$_2$]$^-$ (bTAML = biuret-modified tetraamido macrocyclic ligand), [(*R,R*-BQCN)Mn$^{II}$]$^{2+}$ (*R,R*-BQCN = *N,N'*-dimethyl-*N,N*-bis(8-quinolyl)cyclohexanediamine), and [Ru (TMP)(CO)] (TMP = tetramesitylporphyrin) catalysts have shown high selectivity and yield in photochemical epoxidation. Torii and co-workers produced electrochemical alkene epoxidation reactions using the acetonitrile–water–sodium bromide water–organic solvent biphasic system.[12] In their system, the electrolysis of the bromide ions in the water produces hypobromite ions, which transfer an oxygen atom to the alkene substrates, and the water is an oxygen source for epoxide formation. Tanaka and co-workers subsequently carried out the electrochemical epoxidation of styrene derivatives using *N,N'*-bis(3,5-di-*tert*-butylsalicylidene)-1,2-

cyclohexanediaminomanganese(III) chloride (Figure 2, Mn(L1-*t*-Bu), known as Jacobsen's catalyst) in a dichloromethane–water–sodium chloride water–organic solvent biphasic system.[17] In this new system, the electrolysis of the chloride ions in the water produces hypochlorite ions, and Jacobsen's catalyst promotes the epoxidation reaction of the styrene derivatives with the hypochlorite ions in a water–organic solvent biphasic system. Thus, Jacobsen's catalyst may produce manganese-oxo species which can serve as the active species for alkene epoxidation.[18] These excellent results demonstrate that water is an attractive and safe source of oxygen atoms in electrochemical and photochemical epoxidation reactions. With this in mind, I re-investigated and checked the scope and limitations of the method for the electrochemical epoxidation of alkenes reported by Tanaka and co-workers.[17] Firstly, cyclooctene was electrochemically epoxidized in the dichloromethane and aqueous sodium chloride solution system using the same catalyst, Jacobsen's catalyst Mn(L1-*t*-Bu), according to the procedure reported by Tanaka and co-workers.[17] As a result, I found that, besides the desired epoxide, an undesired product that chlorinated at the allylic position of the cyclooctene was generated (Figure 3). It is known that the electrochemical oxidation of chloride ions in water produces active chlorine species such as $Cl_2$ and $Cl_2O$[19] which may cause chlorination at the allylic position of cyclooctene. I therefore searched for a suitable chemical species to replace the chloride ions in electrochemical epoxidation reactions in order to avoid the allylic halogenation of alkenes.

Carbonates have often been used as activators for oxidation reactions with hydrogen peroxide, including epoxidation reactions.[20-24] It has been reported that percarbonate is involved in manganese-catalyzed alkene epoxidation reactions using hydrogen peroxide in carbonate or bicarbonate aqueous solutions.[20,21,24-26] Burgess and co-workers proposed the involvement of manganese $\eta^2$-peroxycarbonate complexes to facilitate the cleavage of the O–O bonds of percarbonate ions. A similar iron(III) $\eta^2$-percarbonate complex was isolated and characterized using X-ray crystallography.[27] Percarbonate is generated through the equilibrium reaction between carbonate ions and hydrogen peroxide.[28] Therefore, the formation of percarbonate is the same as the formation of hydrogen peroxide. It has been reported that percarbonate can be generated via the oxidative electrolysis of carbonate ions using a platinum anode[29-38] or a boron-doped diamond (BDD)[32-38] electrode. Compared with other electrodes, a BDD has a higher overpotential for water oxidation,[39,40] which is suitable for the electro-synthesis of oxidants in aqueous media. Recently, Wenderich, Mei, and co-workers reported that BDDs are promising tools for anodic hydrogen peroxide production, which is greatly

improved by using sodium carbonate as an electrolyte.[41] In this study, I aimed to utilize the electrochemically generated percarbonate ions on a BDD electrode.
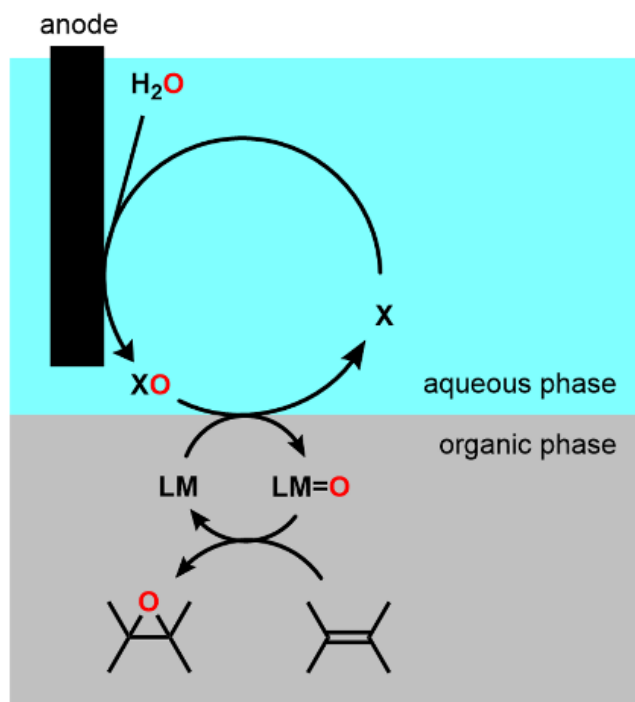


**Figure 1**. Epoxidation reaction with the electrochemical oxidative generation of an oxidizing agent (XO).



Jacobsen's catalyst, Mn(**L1-*t*-Bu**)

X = MeO (**L1-OMe**), *t*-Bu (**L1-*t*-Bu**), H (**L1-H**), Cl (**L1-Cl**), NO$_2$ (**L1-NO$_2$**)

X = *t*-Bu (**L2-*t*-Bu**), H (**L2-H**)
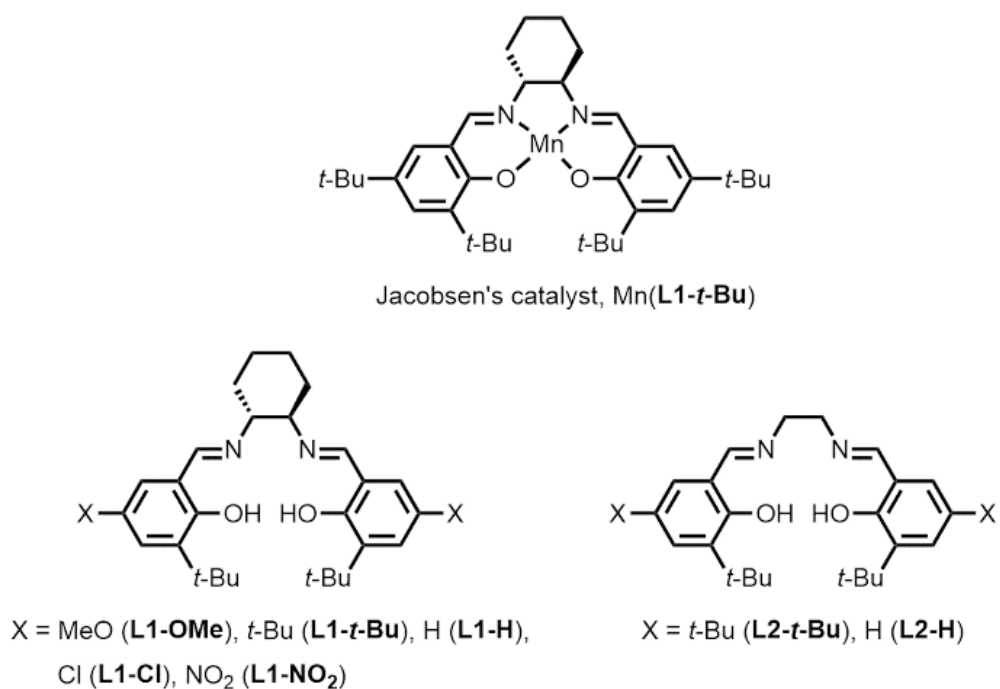
**Figure 2**. Jacobsen's catalyst and salen ligands (and their abbreviations).
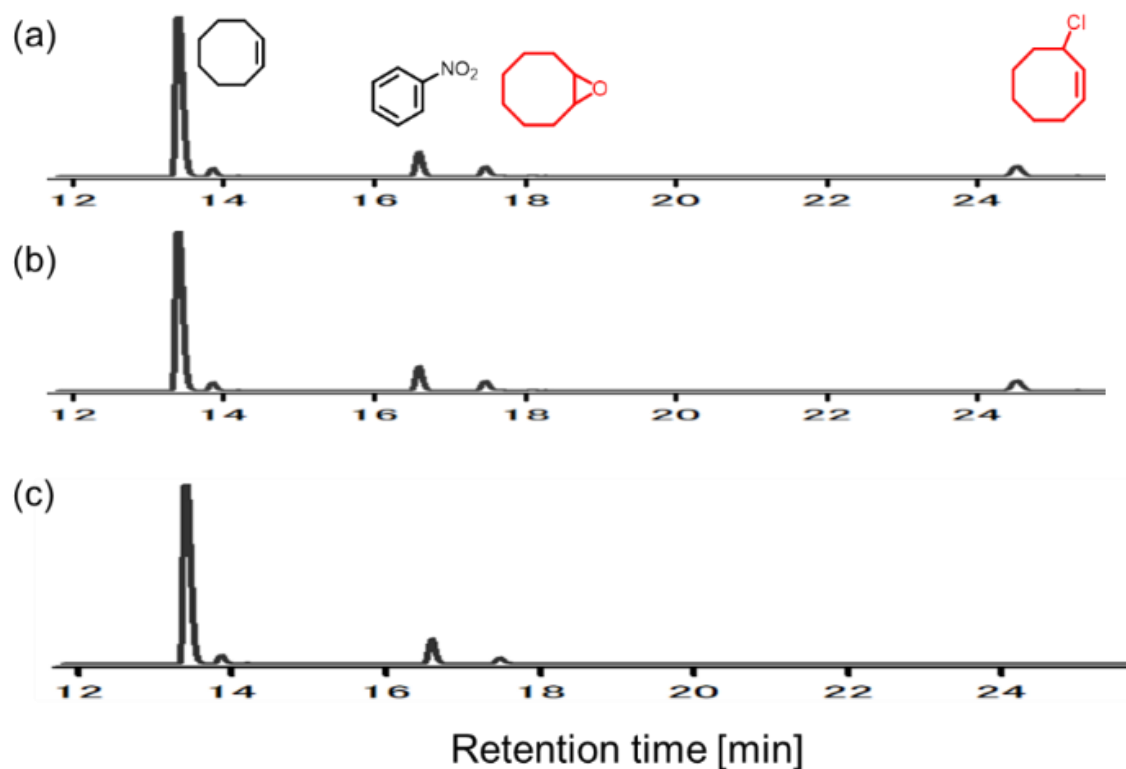
**Figure 3**. Gas chromatograms for electrochemical cyclooctene epoxidation catalyzed by Mn(L1-*t*-Bu) under different reaction conditions. (**a**) $CH_2Cl_2$/1 M NaCl aq. (1:9), (+)Pt/(−)Pt, (**b**) $CH_2Cl_2$/1 M NaCl aq. (1:9), (+)BDD/(−)Pt, and (**c**) $CH_2Cl_2$/1 M $Na_2CO_3$ aq. (1:9), (+)BDD/(−)Pt. Other reaction conditions: substrate (0.25 mmol), catalyst (0.05 mmol), 2.5 V vs Ag/AgCl, in undivided cell, 0°C (bath temp.), 90 min.

Electrocatalysis employing metal complexes has attracted a great deal of attention in the field of organic synthesis and has shown significant progress in recent years.[42-45] In this study, inspired by Tanaka's work,[17] I have examined electrochemical epoxidation via in situ electrochemical generation of percarbonate by using various metal complexes, including manganese salen complexes and manganese and vanadium porphyrin complexes as a mediator in an organic solvent–aqueous carbonate two-phase system in a simple undivided cell. As I expected, the electrochemical epoxidation of styrene derivatives proceeded when a BDD was used as an anode. The reaction optimization was performed in detail.

## Results and discussion

### Electrochemical epoxidation using a BDD

First, to examine whether percarbonate-mediated electrochemical epoxidation can proceed using a BDD, glassy carbon, graphite, or platinum anode, I performed the electrochemical epoxidation of *trans*-β-methylstyrene in a biphasic system containing 1 M sodium carbonate aqueous solution and a solution of Jacobsen's catalyst Mn(L1-*t*-Bu) in dichloromethane under conditions similar to those used in Tanaka's work.[17] After 30 min of electrolysis using a BDD as an anode with a voltage of 2.50 V vs. Ag/AgCl at a bath temperature of −5 °C, the epoxide of the *trans*-β-methylstyrene was obtained with a yield of 18.5%, while the electrolysis experiments conducted using the other electrodes (glassy carbon, graphite, or platinum anodes) gave yields lower than 2.2% (Table 1). Thus, the BDD anode showed the best performance in the electrochemical epoxidation of the *trans*-β-methylstyrene. It is thought that the oxidation of water to oxygen is easier with electrodes other than BDDs.[39,46] However, yields decreased with longer reaction times using BDDs. Interestingly, the same product yields were observed under air and nitrogen. When sodium sulfate and sodium chloride were used as an electrolyte instead of sodium carbonate, the yields of the corresponding epoxide of the *trans*-β-methylstyrene were lower than 6%.

**Table 1**. Epoxidation of *trans*-β-methylstyrene catalyzed by Mn$^{III}$(L1-*t*-Bu)[a]

| Anode (3 cm$^2$) | Epoxide yield (%) |
|:---:|:---:|
| BDD | 18.5 |
| glassy carbon | 2.2 |
| platinum | 1.8 |
| graphite | 1.8 |

[a] Reaction conditions: substrate (0.25 mmol), catalyst (0.05 mmol), CH$_2$Cl$_2$/1 M Na$_2$CO$_3$ aq. (1:9), (−)Pt, 2.5 V vs Ag/AgCl, in undivided cell, −5 °C (bath temp.), 30 min, under air.

Next, I investigated the effects of applied oxidation voltage vs. Ag/AgCl, bath temperature, and type of electrolyte on electrochemical epoxidation. The applied oxidation voltage was very sensitive to the epoxidation reaction of the *trans*-β-methylstyrene. The yields of the corresponding epoxide were 5.7%, 18.5%, and 6.2% for the electrolysis using a BDD electrode at 2.25 V, 2.50 V, and 2.75 V vs. Ag/AgCl, respectively. These results suggest that the production of percarbonate requires more than 2.50 V vs. Ag/AgCl, but that the higher

applied voltage may result in unwanted side reactions. The reactions were performed at three different bath temperatures. The yields of the corresponding epoxide from the *trans*-β-methylstyrene were 9.6, 17.5, and 18.5 at bath temperatures of 5 °C, 0 °C, and −5 °C, respectively. Thus, the lower bath temperatures afforded higher epoxide yields, probably due to the suppression of unwanted side reactions at higher temperatures. I also conducted the electrochemical epoxidation of *trans*-β-methylstyrene in different water–organic solvent systems (i.e., water–ethyl acetate, water–acetonitrile, and water–toluene), where the water phase was 1 M sodium carbonate and a BDD electrode was used as an anode with a voltage of 2.50 V vs. Ag/AgCl at a bath temperature of −5 °C. The epoxide yields from the *trans*-β-methylstyrene were lower than 1.3% when ethyl acetate, acetonitrile, and toluene were used, yields which are lower than that obtained in the water–dichloromethane biphasic system (18.5%). In the water–dichloromethane biphasic system, the BDD anode contacts the upper aqueous layer, not the lower dichloromethane phase containing Jacobsen's catalyst Mn(L1-*t*-Bu) and the *trans*-β-methylstyrene. This alignment allows the efficient production of percarbonate in the aqueous phase and avoids the direct oxidation of the *trans*-β-methylstyrene, which should be one of the key factors in promoting the electrochemical epoxidation reaction in the water–dichloromethane biphasic system.

Next, I examined the electrochemical epoxidation of *cis*-β-methylstyrene, cyclooctene, *trans*-stilbene, and cyclohexene under the optimized conditions using a BDD anode. The epoxide yields are listed in Table 2. I compared the obtained yields with their corresponding alkene ionization because a clear correlation between the alkene ionization potential and the epoxidation rate constants for the iron(IV)-oxo porphyrin cation radical complexes has been reported.[47] As expected, the results show that as the ionization energy of the alkenes increased, the epoxide yield decreased, except in the case of the *trans*-stilbene. The exceptionally low yield we observed may be attributable to the two bulky phenyl groups of the *trans*-stilbene. The correlation between the epoxide yields and the alkene ionization potentials suggests that the epoxidation step should take longer than the formation of percarbonate ions through electrolysis on the BDD anode. As control experiments, I performed epoxidation reactions of the alkenes without using the BDD electrode by adding one equivalent of hydrogen peroxide as an oxidant to a biphasic system containing 1 M sodium carbonate aqueous solution and a solution of Jacobsen's catalyst Mn(L1-*t*-Bu) in dichloromethane. The epoxide yields obtained via the conventional epoxidation reaction using hydrogen peroxide with sodium carbonate are listed in the right column in Table 2. The epoxide yields obtained using the hydrogen peroxide

showed a similar trend to those observed with electrochemical epoxidation. The results suggest that hydrogen peroxide is generated through electrolysis using a BDD anode. In carbonate aqueous solutions, there should be an equilibrium between hydrogen peroxide and percarbonate. Therefore, it is not easy to distinguish between the generation of hydrogen peroxide and the generation of percarbonate. However, it is likely that percarbonate is first generated through the oxidation of carbonate, as reported by Richardson and co-workers, based on their kinetic study using $^{13}$C-labeled bicarbonate solutions.[48]

**Table 2**. Mn(L1-*t*-Bu)-catalyzed epoxidation of a series of alkenes[a]

| Substrate [Ionization energy] | Epoxide yield (%) | |
| :---: | :---: | :---: |
| | **Electrochemical generation** | **H$_2$O$_2$/Na$_2$CO$_3$** [b] |
| *trans*-β-methylstyrene (8.08 eV) | 18.5 | 26.4 |
| *cis*-β-methylstyrene (8.48 eV) | 19.8 [85:15][c] | 22.3 [84:16][c] |
| cyclooctene (9.02 eV) | 5.6 | 1.4 |
| *trans*-stilbene (7.70 eV) | 1.6 | 1.0 |
| cyclohexene (9.12 eV) | 0.3 | 0.4 |

[a] Reaction conditions: substrate (0.25 mmol), catalyst (0.05 mmol), CH$_2$Cl$_2$/1 M Na$_2$CO$_3$ aq. (1:9), (+)BDD/(−)Pt, 2.5 V vs Ag/AgCl, in undivided cell, −5 °C (bath temp.), 30 min. [b] H$_2$O$_2$ (0.25 mmol), CH$_2$Cl$_2$/1 M Na$_2$CO$_3$ aq. (1:9), −2 °C (bath temp.). [c] *trans*/*cis*.

When *cis*-β-methylstyrene is used as a substrate for an epoxidation reaction, *cis*-to-*trans* isomerization occurs.[49,50] Tanaka and co-workers reported that when the electrochemical epoxidation of *cis*-β-methylstyrene is catalyzed by Jacobsen's catalyst Mn(L1-*t*-Bu) in the dichloromethane and sodium chloride aqueous solution biphasic system, a corresponding epoxide was obtained with a *cis* to *trans* ratio of 87:13. In our case, under the electrochemical epoxidation conditions, the *cis* to *trans* ratio of the corresponding epoxide obtained from the *cis*-β-methylstyrene was 85:15. A similar *cis* to *trans* isomerization value was observed for the conventional epoxidation reaction of *cis*-β-methylstyrene catalyzed by Jacobsen's catalyst Mn(L1-*t*-Bu) using hydrogen peroxide. A comparable extent of *cis*-to-*trans* isomerization from

*cis*-β-methylstyrene has been observed following an epoxidation reaction with sodium hypochlorite and Jacobsen's catalyst Mn(L1-*t*-Bu).[49,50] Electrochemical epoxidation using an optically active (*R,R*)-Jacobsen's catalyst Mn(L1-*t*-Bu) afforded the desired *cis*-(1*R*,2*S*)-epoxide with an enantiomeric excess (ee) of 87%, which was comparable to the reported ee values.[17] The results suggest that the same oxidizing species derived from Jacobsen's catalyst Mn(L1-*t*-Bu) are formed in the cases of electrochemical epoxidation using chloride ions and carbonate ions as well as conventional epoxidation using hydrogen peroxide with carbonate ions and sodium hypochlorite.

**Exploration of More Efficient Catalysts**

Next, I examined whether other catalysts could be used for electrochemical epoxidation. In this study, I focused on catalysts that have been reported to be effective in the epoxidation of alkenes with hydrogen peroxide. Lane and Burgess have reported that manganese sulfate catalyzes the epoxidation of alkene using aqueous hydrogen peroxide in the presence of sodium bicarbonate.[51] They assumed that percarbonate ions are formed from hydrogen peroxide and that bicarbonate ions react in situ with manganese ions to give the active intermediate for the epoxidation reactions of alkenes. Qi and co-workers have reported that manganese oxide has superior properties for converting styrene to epoxide with aqueous hydrogen peroxide in a bicarbonate solution.[52] Based on these reports, I conducted the electrochemical epoxidation of *trans*-β-methylstyrene under the optimal conditions with a BDD electrode as an anode with a voltage of 2.50 V vs. Ag/AgCl at a bath temperature of −5 °C, using manganese sulfate or manganese oxide as a catalyst. However, these two reactions using manganese sulfate or manganese oxide instead of Jacobsen's catalyst Mn(L1-*t*-Bu) afforded negligible amounts of epoxide from the *trans*-β-methylstyrene. I further examined whether conventional epoxidation using hydrogen peroxide proceeds in the 1 M sodium carbonate–dichloromethane biphasic system containing manganese sulfate or manganese oxide as a catalyst. However, the yields of the corresponding epoxide were negligible. These results indicate that my biphasic system is not suitable for epoxidation reactions using manganese sulfate or manganese oxide as a catalyst, probably because these catalysts are water soluble or hydrophilic.

Dar and co-workers have reported that the electron-deficient oxidovanadium(IV) porphyrin catalyst β-octabromo-meso-tetrakis(2,6-dibromo-3,5-dimethoxyphenyl)porphyrinatooxidovanadium (VO(L1)) efficiently promotes the epoxidation of styrene using hydrogen peroxide in acetonitrile–water containing sodium bicarbonate.[53]

Nishihara and co-workers have carried out electrochemical cyclooctene epoxidation with manganese(III) porphyrin complexes using hydrogen peroxide generated from polymer-coated electrodes in dichloromethane containing 1-methylimidazole and benzoic acid.[11]



**VO(TPP)**
yield 5.3%

**VO(L1)**
yield 0.6%

**VO(L2)**
yield 9.6%

**Mn(TPP)**
yield 6.2%

**Mn(TDCPP)**
yield 1.4%

**Mn(L2)**
yield 0.8%
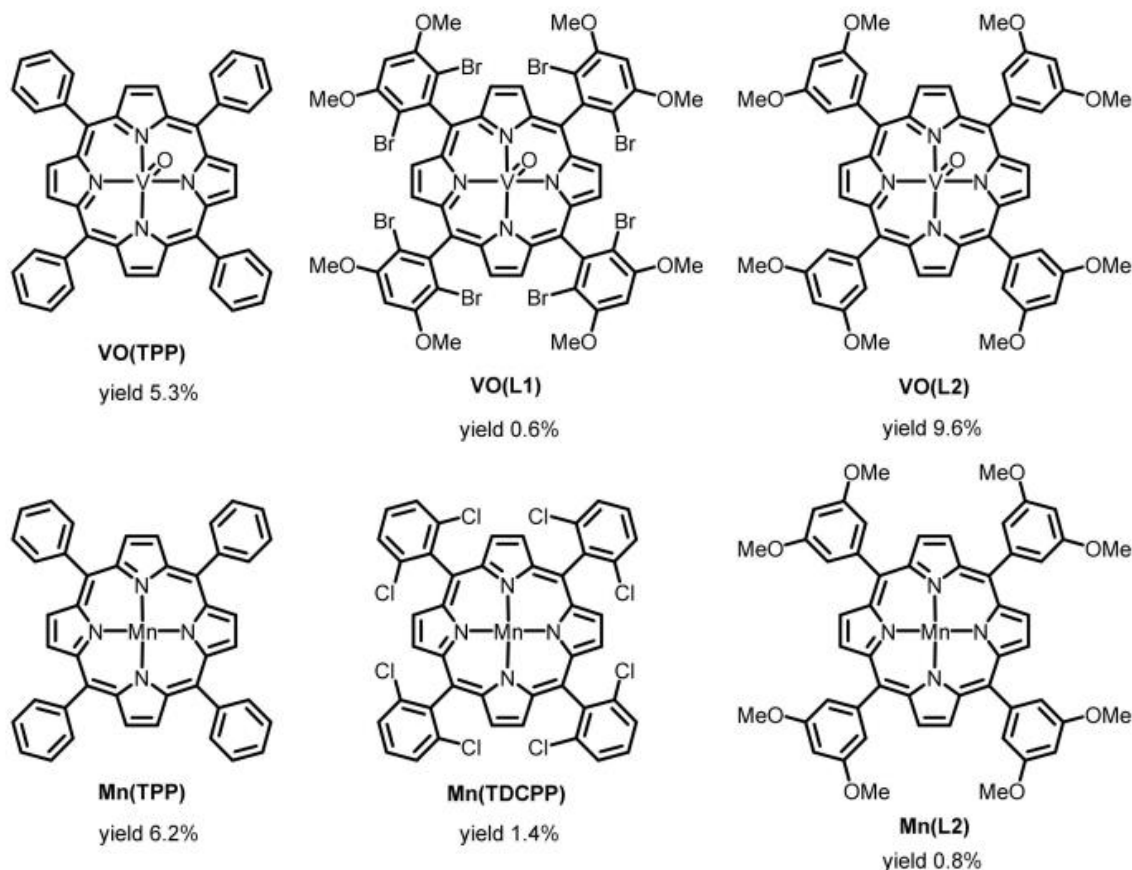
**Figure 4**. Oxidovanadium(IV) porphyrin and manganese porphyrin catalysts are shown with the yields of epoxide obtained from the *trans*-β-methylstyrene under the electrochemical conditions.

Thus, some oxidovanadium(IV) porphyrin and manganese(III) complexes promote the chemical epoxidation of alkenes with hydrogen peroxide in the presence of bicarbonate or electrochemical epoxidation. Therefore, I examined the electrochemical epoxidation of *trans*-β-methylstyrene under the optimal conditions for Jacobsen's catalyst Mn(L1-*t*-Bu), i.e., using a BDD electrode as an anode with a voltage of 2.50 V vs. Ag/AgCl at a bath temperature of −5 °C, with manganese(III) and oxidovanadium(IV) tetraphenylporphyrin derivatives as a catalyst. I prepared six metalloporphyrins for this purpose in accordance with the literature:[53] manganese tetraphenyl porphyrin, Mn(TPP), manganese 5,10,15,20-tetrakis(2,6-dichlorophenyl)porphyrin, Mn(TDCPP), 5,10,15,20-tetrakis(3,5-dimethoxyphenyl)porphyrin,

Mn(L2), oxidovanadium(IV) tetraphenylporphyrin, VO(TPP), oxidovanadium(IV) 5,10,15,20-tetrakis(2,6-dibromo-3,5-dimethoxyphenyl)porphyrin VO(L1), and oxidovanadium(IV) 5,10,15,20-tetrakis(3,5-dimethoxyphenyl)porphyrin, VO(L2). The chemical structures of the catalysts are shown in Figure 4 together with the epoxide yields obtained from the *trans*-β-methylstyrene.

Among the oxidovanadium(IV) porphyrins, electron-deficient oxidovanadium(IV) porphyrin VOL1 showed the lowest epoxide yield derived from the *trans*-β-methylstyrene (0.6%), probably because of its low solubility in 1 M sodium carbonate–dichloromethane biphasic solution. VOTPP and VOL2 showed respective epoxide yields of 9.6% and 5.3% derived from the *trans*-β-methylstyrene. Among the manganese porphyrin complexes, MnTPP produced the highest yield (6.2%). Mn(TDCPP) is known as a more robust oxidation catalyst than Mn(TPP). Regardless, I found that the use of MnL2 as a catalyst produced only negligible amounts of epoxide, probably due to its lower solubility in 1 M sodium carbonate–dichloromethane biphasic solution. Oxidovanadium(IV) porphyrins are neutral compounds, but manganese(III) porphyrins are cationic. This difference may affect their solubility in the biphasic solution. For example, VO(L2) showed a higher yield (9.6%) compared with its manganese counterpart, MnL2 (0.8%). Thus, my catalyst survey disclosed that Jacobsen's catalyst Mn(L1-*t*-Bu), a manganese salen complex, is superior to oxidovanadium(IV) and manganese porphyrins.

**Optimization of Manganese Salen Complexes**

Next, I decided to optimize the structures of the manganese salen complexes for the electrochemical epoxidation reaction, I established in this study. For this purpose, I prepared eight manganese complexes, including Jacobsen's catalyst Mn(L1-*t*-Bu).[54] The manganese salen complexes had *trans*-1,2-cyclohexanediamine or 1,2-ethylenediamine as a backbone, and a methoxy-, chloride-, nitro-, and *tert*-butyl group at the 4-position of the phenol moieties, whose chemical structures are shown in Figure 2. The epoxide yields derived from *trans*-β-methylstyrene after a 30 min reaction under the optimal electrochemical epoxidation conditions are listed in Table 3. For comparison, I also performed conventional chemical epoxidation using hydrogen peroxide as an oxidant in the same 1 M sodium carbonate and dichloromethane biphasic system. A similar trend in the substituent effect was observed for all the manganese complexes in both the electrochemical and conventional epoxidation reactions. Among them, Jacobsen's catalyst Mn(L1-*t*-Bu) showed the highest yield for both types of epoxidation

reaction. The redox potentials of the manganese complexes had been evaluated and were reported to be in the order: Mn(L1-OMe) < Mn(L1-*t*-Bu) < Mn(L1-Cl).[54] In terms of the redox potentials, the manganese-oxo species of Mn(L1-Cl) should have been more reactive for the epoxidation than Mn(L1-*t*-Bu), but the epoxide yield observed with Mn(L1-Cl) was much lower than that of Mn(L1-*t*-Bu). Thus, the reactivity of the oxidizing species of manganese salen complexes cannot explain the epoxide yields. This opposite trend could be attributable to the formation step of the oxidizing species of manganese salen complexes. I speculated that Mn(L1-Cl) could not react with percarbonate to form the corresponding manganese-oxo species due to the electron-withdrawing groups on the phenyl groups. Therefore, according to the established procedure, I performed the epoxidation reaction using a more potent oxidizing agent, sodium hypochlorite, only in dichloromethane.[18] The data are listed in the right column of Table 3. Jacobsen's catalyst Mn(L1-*t*-Bu) gave the highest yield, a result observed for the electrochemical epoxidation with carbonate as well as for the conventional epoxidation using the hydrogen peroxide with carbonate system. However, the epoxidation reaction using the other manganese salen complexes and sodium hypochlorite only in dichloromethane and sodium hypochlorite showed higher epoxide yields than the reactions in the 1 M sodium carbonate and dichloromethane biphasic system. These results demonstrate the uniqueness of Jacobsen's catalyst Mn(L1-*t*-Bu) as a useful and practical epoxidation catalyst. I speculate that its electronic structure, bulky functional groups, rigid backbone, and high solubility in organic solvents all contribute to its catalytic capability.

**Table 3**. Mn(L1-*t*-Bu)-catalyzed epoxidation of *trans*-β-methylstyrene.[a]

| Catalyst | Epoxide yield (%) | | |
|:---:|:---:|:---:|:---:|
| | **Electrochemical generation** | **$H_2O_2$/$Na_2CO_3$** [b] | **NaOCl** [c] |
| Mn(L1-OMe) | 5.3 | 2.1 | 45.5 |
| Mn(L1-*t*-Bu) | 18.5 | 26.4 | 74.1 |
| Mn(L1-H) | 2.2 | 13.2 | 59.8 |
| Mn(L1-Cl) | 1.8 | 3.3 | 60.9 |
| Mn(L1-NO$_2$) | 1.8 | 1.8 | 53.8 |
| Mn(L2-*t*-Bu) | 7.3 | 1.5 | – |
| Mn(L2-H) | 0.5 | 0.8 | – |
| none | 0.7 | 0.5 | 8.4 |

a) Reaction conditions: substrate (0.25 mmol), catalyst (0.05 mmol), CH$_2$Cl$_2$/1 M Na$_2$CO$_3$ aq. (1:9), (+)BDD/(−)Pt, 2.5 V vs Ag/AgCl, in undivided cell, −5 °C (bath temp.), 30 min. b) H$_2$O$_2$ (0.25 mmol), CH$_2$Cl$_2$/1 M Na$_2$CO$_3$ aq. (1:9), −2°C (bath temp.). c) Reaction conditions: substrate (0.2 mmol), catalyst (0.01 mmol), NaOCl (0.72 mmol), CH$_2$Cl$_2$/H$_2$O (1:2), 0 °C (bath temp.), 16 h.

Next, I examined epoxidation reactions involving cyclooctene using the above manganese salen complexes. The cyclooctene epoxide yields obtained by electrochemical epoxidation are listed in Table 4, together with the cyclooctene epoxide yields obtained using hydrogen peroxide. Cyclooctene is a less reactive substrate than *trans*-β-methylstyrene. The cyclooctene epoxide yields were 5.6% and 6.8% after 30 min and 90 min, respectively (Tables 3 and 4), which are lower than that observed with *trans*-β-methylstyrene (18.5%) after 30 min. A similar trend was observed in the epoxidation yield of cyclooctene as that observed with *trans*-β-methylstyrene. Jacobsen's catalyst Mn(L1-*t*-Bu) gave the highest yield in both electrochemical epoxidation and epoxidation with hydrogen peroxide with carbonate. Overall, it is clear that the epoxide yields are not dependent simply on the electronic properties of Mn salen complexes. These results again illustrate that Jacobsen's catalyst Mn(L1-*t*-Bu) is an excellent electrochemical epoxidation catalyst. I tentatively concluded that the bulkiest catalyst, Jacobsen's catalyst Mn(L1-*t*-Bu), favors the formation of the active mononuclear manganese-oxo species because four *tert*-butyl groups on Jacobsen's catalyst prevent the formation of inactive μ-oxo dimers, resulting in a higher effective concentration of the active catalyst in solution compared with other less bulky Mn(salen) complexes.[55] The lower yields observed with Mn(L2-*t*-Bu) and Mn(L2-H) also suggest the substantial role of the cyclohexane moiety of L1 in the epoxidation reaction.

**Table 4**. Cyclooctene epoxidation catalysed by manganese salen complexes.[a)]

| Catalyst | Epoxide yield (%) | |
| --- | --- | --- |
| | Electrochemical generation | H$_2$O$_2$/Na$_2$CO$_3$ [b)] |
| Mn(L1-OMe) | 6.8 | 8.6 |
| Mn(L1-*t*-Bu) | 9.9 | 9.3 |
| Mn(L1-H) | 7.7 | 8.1 |
| Mn(L1-Cl) | 8.0 | 7.6 |
| Mn(L1-NO$_2$) | 8.1 | 6.3 |

## Experimental

### Chemicals and Equipment

Cyclohexene and cyclooctene were passed through a short alumina column prior to their use. Except for Mn(L1-*t*-Bu), the Mn(salen) complexes were prepared according to the reported procedure.[54] All other chemicals and solvents, including the Mn(L1-*t*-Bu), were purchased and used without further purification. The oxidation products of *trans*-stilbene were analyzed using ^{1}H NMR measurements obtained with a JEOL JMN-A500 NMR spectrometer. The other products were analyzed using Shimadzu GC-2014 and GCMS-QP2020 NX spectrometers equipped with a GL Science Inert Cap 1701 capillary column (60 m × 0.25 mm).

### General Procedure for Electrochemical Epoxidation

Electrochemical epoxidation was performed using IKA ElectraSyn2.0 in a 5 mL vial equipped with a BDD plate as an anode and Pt as a cathode. A mixture of olefin (0.25 mmol), metal complex (0.05 mmol), dichloromethane (0.5 mL), and 1 M Na$_2$CO$_3$ (4.5 mL) was placed in the 5 mL vial. The vessel was immersed in an alcohol bath, whose temperature was kept at −5 °C with a cooling system (Techno Sigma, Okayama, Japan, UCR-150N-S). The mixture was electrolyzed for the indicated reaction time at a constant voltage, typically 2.5 V vs. Ag/AgCl (3 M NaCl), at a low temperature under air, and with gentle stirring so that the two phases were retained. After the reaction, *p*-nitrotoluene or nitrobenzene (0.1 mmol) was added to the resulting mixture as an internal standard. The product yields and *cis/trans* ratios were determined using GC analysis of authentic samples. The ee% was determined using HPLC.

### General Procedure for Epoxidation with Hydrogen Peroxide

A mixture of olefin (0.25 mmol), metal complex (0.05 mmol), dichloromethane (0.5 mL), and 1 M Na$_2$CO$_3$ (4.5 mL) was placed in the 5 mL vial. The bath temperature was kept at −2 °C with a cooling system (Techno Sigma, UCR-150N-S). Hydrogen peroxide (0.25 mmol) was then added to the mixture. After the reaction, *p*-nitrotoluene (0.1 mmol) was added to the resulting mixture as an internal standard.

## Conclusions

In conclusion, I confirmed that electrochemical alkene epoxidation proceeds using a BDD electrode, Jacobsen's catalyst, and carbonate as a mediator in a 1 M sodium carbonate and dichloromethane biphasic system. It should be noted that unwanted chlorination at the allylic position of the alkene does not occur in my method. Epoxide yields were higher than those obtained from electrochemical epoxidation with chloride ions as the mediator when a BDD was used as an anode. I believe that carbonate ions are better mediators for electrochemical epoxidation than chloride ions. Cyclooctene epoxide yields were still low even after prolonged reactions under optimal conditions. I am currently attempting to improve the reaction conditions for carbonate-mediated electrochemical epoxidation.

## References

(1)     M. Yan, Y. Kawamata, P. S. Baran, *Chem. Rev.* **2017**, *117*, 13230-13319.

(2)     Q.-H. Xia, H.-Q. Ge, C.-P. Ye, Z.-M. Liu, K.-X. Su, *Chem. Rev.* **2005**, *105*, 1603-1662.

(3)     R. H. Holm, *Chem. Rev.* **1987**, *87*, 1401-1449.

(4)     C. Kim, T. G. Traylor, C. L. Perrin, *J. Am. Chem. Soc.* **1998**, *120*, 9513-9516.

(5)     V. G. Dryuk, *Tetrahedron* **1976**, *32*, 2855-2866.

(6)     K. Jin, J. H. Maalouf, N. Lazouski, N. Corbin, D. Yang, K. Manthiram, *J. Am. Chem. Soc.* **2019**, *141*, 6413-6418.

(7)     D. Tatsumi, T. Tsukamoto, R. Honna, S. Hoshino, T. Shimada, S. Takagi, *Chem. Lett.* **2017**, *46*, 1311-1314.

(8)     B. Chandra, K. K. Singh, S. S. Gupta, *Chem. Sci.* **2017**, *8*, 7545-7551.

(9)     D. Shen, C. Saracini, Y.-M. Lee, W. Sun, S. Fukuzumi, W. Nam, *J. Am. Chem. Soc.* **2016**, *138*, 15857-15860.

(10)    S. Funyu, T. Isobe, S. Takagi, D. A. Tryk, H. Inoue, *J. Am. Chem. Soc.* **2003**, *125*, 5734-5740.

(11)    H. Nishihara, K. Pressprich, R. W. Murray, J. P. Collman, *Inorg. Chem.* **1990**, *29*, 1000-1006.

(12)    S. Torii, K. Uneyama, H. Tanaka, T. Yamanaka, T. Yasuda, M. Ono, Y. Kohmoto, *J. Org. Chem.* **1981**, *46*, 3312-3315.

(13)    S. Torii, K. Uneyama, M. Ono, H. Tazawa, S. Matsunami, *Tetrahedron Lett.* **1979**, *20*, 4661-4662.

(14)     J.-C. Moutet, A. Ourari, *Electrochim. Acta.* **1997**, *42*, 2525-2531.

(15)     P. Guo, K.-Y. Wong, *Electrochem. Commun.* **1999**, *1*, 559-563.

(16)     A. Ishikawa, S. Sakaki, *J. Phys. Chem. A* **2011**, *115*, 4774-4785.

(17)     H. Tanaka, M. Kuroboshi, H. Takeda, H. Kanda, S. Torii, *J. Electroanal. Chem.* **2001**, *507*, 75-81.

(18)     E. N. Jacobsen, W. Zhang, M. L. Guler, *J. Am. Chem. Soc.* **1991**, *113*, 6703-6704.

(19)     M. Pourbaix, *Atlas of Electrochemical Equilibria in Aqueous Solutions*; National Association of Corrosion Engineers: Houston, TX, USA, **1974**.

(20)     B. Hincapie, S. M. Llano, H. F. Garces, D. Espinal, S. L. Suib, L. J. Garces, *Adsorpt. Sci. Technol.* **2018**, *36*, 9-22.

(21)     A. M. Garcia, V. Moreno, S. X. Delgado, A. E. Ramírez, L. A. Vargas, M. Á. Vicente, A. Gil, L. A. Galeano, *J. Mol. Catal. A Chem.* **2016**, *416*, 10-19.

(22)     H. H. Monfared, V. Aghapoor, M. Ghorbanloo, P. Mayer, *Appl. Catal. A Gen.* **2010**, *372*, 209-216.

(23)     H. Yao, D. E. Richardson, *J. Am. Chem. Soc.* **2000**, *122*, 3220-3221.

(24)     B. S. Lane, M. Vogt, V. J. DeRose, K. Burgess, *J. Am. Chem. Soc.* **2002**, *124*, 11946-11954.

(25)     V. A. Drozd, R. V. Ottenbacher, K. P. Bryliakov, *Molecules* **2022**, *27*, 2538.

(26)     V. Escande, E. Petit, L. Garoux, C. Boulanger, C. Grison, *ACS Sustain. Chem. Eng.* **2015**, *3*, 2704-2715.

(27)     K. Hashimoto, S. Nagatomo, S. Fujinami, H. Furutachi, S. Ogo, M. Suzuki, A. Uehara, Y. Maeda, Y. Watanabe, T. Kitagawa, *Angew. Chem. Int. Ed.* **2002**, *41*, 1202-1205.

(28)     D. E. Richardson, H. Yao, K. M. Frank, D. A. Bennett, *J. Am. Chem. Soc.* **2000**, *122*, 1729-1739.

(29)     J. Zhang, C. W. Oloman, *J. Appl. Electrochem.* **2005**, *35*, 945-953.

(30)     G. Manoharan, M. Muthu Mohamed, N. S. Raghavendran, K. C. Narasimham, *Trans. SAEST (Soc. Adv. Electrochem. Sci. Technol.)* **2000**, *35*, 69-72.

(31)     P. Wiel, L. J. J. Janssen, J. G. Hoogland, *Electrochim. Acta* **1971**, *16*, 1217-1226.

(32)     Irkham, A. Fiorani, G. Valenti, N. Kamoshida, F. Paolucci, Y. Einaga, *J. Am. Chem. Soc.* **2020**, *142*, 1518-1525.

(33)     C. P. Chardon, T. Matthée, R. Neuber, M. Fryda, C. Comninellis, *ChemistrySelect* **2017**, *2*, 1037-1040.

(34)     E. J. Ruiz-Ruiz, Y. Meas, R. Ortega-Borges, J. L. Jurado Baizabal, *Surff. Eng. Appl. Electrochem.* **2014**, *50*, 478-484.

(35)    S. Velazquez-Peña, C. Sáez, P. Cañizares, I. Linares-Hernández, V. Martínez-Miranda, C. Barrera-Díaz, M. A. Rodrigo, *Chem. Eng. J.* **2013**, *230*, 272-278.

(36)    E. J. Ruiz, R. Ortega-Borges, J. L. Jurado, T. W. Chapman, Y. Meas, *Electrochem. Solid-State Lett.* **2008**, *12*, E1-E4.

(37)    M. S. Saha, T. Furuta, Y. Nishiki, *Electrochem. Commun.* **2004**, *6*, 201-204.

(38)    M. S. Saha, T. Furuta, Y. Nishiki, *Electrochem. Solid-State Lett.* **2003**, *6*, D5-D7.

(39)    S. Mavrikis, M. Göltz, S. Rosiwal, L. Wang, C. Ponce de León, *ACS Appl. Energy Mater.* **2020**, *3*, 3169-3173.

(40)    Y. Einaga, *Bull. Chem. Soc. Jpn.* **2018**, *91*, 1752-1762.

(41)    K. Wenderich, B. A. M. Nieuweweme, G. Mul, B. T. Mei, *ACS Sustain. Chem. Eng.* **2021**, *9*, 7803-7812.

(42)    M. Ghosh, V. S. Shinde, M. Rueping, *Beilstein J. Org. Chem.* **2019**, *15*, 2710-2746.

(43)    C. Ma, P. Fang, Z.-R. Liu, S.-S. Xu, K. Xu, X. Cheng, A. Lei, H.-C. Xu, C. Zeng, T.-S. Mei, *Sci. Bull.* **2021**, *66*, 2412-2429.

(44)    L. F. T. Novaes, J. Liu, Y. Shen, L. Lu, J. M. Meinhardt, S. Lin, *Chem. Soc. Rev.* **2021**, *50*, 7941-8002.

(45)    N. Kaeffer, W. Leitner, *JACS Au* **2022**, *2*, 1266-1289.

(46)    S. Mavrikis, S. C. Perry, P. K. Leung, L. Wang, C. Ponce de León, *ACS Sustain. Chem. Eng.* **2021**, *9*, 76-91.

(47)    M. A. Sainna, S. Kumar, D. Kumar, S. Fornarini, M. E. Crestoni, S. P. de Visser, *Chem. Sci.* **2015**, *6*, 1516-1529.

(48)    E. V. Bakhmutova-Albert, H. Yao, D. E. Denevan, D. E. Richardson, *Inorg. Chem.* **2010**, *49*, 11287-11296.

(49)    W. Zhang, E. N. Jacobsen, *J. Org. Chem.* **1991**, *56*, 2296-2298.

(50)    E. N. Jacobsen, W. Zhang, A. R. Muci, J. R. Ecker, L. Deng, *J. Am. Chem. Soc.* **1991**, *113*, 7063-7064.

(51)    B. S. Lane, K. Burgess, *J. Am. Chem. Soc.* **2001**, *123*, 2933-2934.

(52)    B. Qi, L.-L. Lou, K. Yu, W. Bian, S. Liu, *Catal. Commun.* **2011**, *15*, 52-55.

(53)    T. A. Dar, B. Uprety, M. Sankar, M. R. Maurya, *Green Chem.* **2019**, *21*, 1757-1768.

(54)    T. Kurahashi, H. Fujii, *J. Am. Chem. Soc.* **2011**, *133*, 8307-8316.

(55)    E. M. McGarrigle, D. G. Gilheany, *Chem. Rev.* **2005**, *105*, 1563-1602.

# GENERAL CONCLUSION

I focused on the generation of α-thioalkyl radicals via single electron transfer (SET) oxidation and subsequent deprotonation of thioanisole derivatives through light irradiation and utilizing these α-thioalkyl radicals to construct C-C bond formation reactions. Moreover, I described the studies on electrochemical epoxidation reactions involving the generation of percarbonate ions by using DBB electrode, which was an effective electrode for electrochemical epoxidation reactions. I proposed the plausible reaction mechanisms of these works on the basis of absorption spectra, control experiments and DFT calculations. Major achievements are summarized as follows.

In Chapter 1 of Part 1, I develop a protocol for generating α-thioalkyl radicals. It highlights the induction of such radicals by blue light irradiation of thioanisole within a charge transfer or electron donor acceptor (EDA) complexes, illustrating the delicate control achieved over radical generation and their utility in bond-forming reactions. This study also brings to light the criticality of the thioanisole framework for EDA-mediated photo-induced C-C bond formation. However, the lack of reactivity with aliphatic thioethers implies that focusing on the thioanisole framework and its unique properties may be necessary for future studies in this area.

In Chapter 2 of Part 1, I found that the addition of titanium dioxide significantly enhanced the C-C bond formation reactions. Generation of α-thiomethyl radical from thioanisoles by one-electron oxidation of thioanisole to the conduction band of $TiO_2$ under blue light irradiation and subsequent generation of α-thioalkyl radicals through deprotonation occurs. In addition, maleimide can form annulation products under photocatalytic radical addition/cyclization reactions, leading to the rapid synthesis of intricate structures like thiochromenopyrrolediones. However, the significant advantage of the present reaction is that it does not require such leaving groups, thanks to the addition of an appropriate solvent $CH_3CN$ and titanium dioxide photocatalyst. Overall, the findings provide a solid foundation for further exploration and optimization in thioether chemistry, especially regarding the synthesis and functionalization of these valuable compounds.

In Chapter 3 of Part 1, I have delved into the highly selective synthesis of sulfoxides from the oxidation of thioanisole derivatives using 2, 2, 2-trifluoroethanol solvent utilizing a 370 nm ultraviolet LED lamp. The major advantages of this protocol are used green oxidant such as dioxygen, gram-scale production, and no use of metals or metal complex catalysts. These results will play an important role in future studies in the field of thioether oxidation.

In Chapter 1 of Part 2 documents my research on the efficient electrochemical epoxidation of styrene derivatives, influenced by seminal efforts from pioneers such as Tanaka. Utilizing a manganese-salen catalyst within a biphasic system and producing percarbonate ions on a boron-doped diamond electrode not only reflects but also potentially exceeds previous approaches regarding efficiency and eco-friendliness, signifying a breakthrough in electrochemical synthesis.

Finally, the extensive body of research undertaken, encompassing the generation of radical species and their ensuing chemical transformations, evidences my substantial contributions to the fields of photocatalysis and organic synthesis. These innovations underpin future progress in sustainable chemistry and materials science.

# LIST OF PUBLICATIONS

1.  Electrochemical Epoxidation Catalyzed by Manganese Salen Complex and Carbonate with Boron-Doped Diamond Electrode
    Pijush Kanti Roy, Keisuke Amanai, Ryosuke Shimizu, Masahito Kodera, Takuya Kurahashi, Kenji Kitayama, and Yutaka Hitomi, *Molecules* (28/4), 1797 (**2023**).

2.  A Simple Method for the Formation of α-Thioalkyl Radicals and the Promotion of Carbon-Carbon Bond Formation by Photoirradiation of Electron Donor-Acceptor Complexes
    Pijush Kanti Roy and Yutaka Hitomi, *Asian Journal of Organic Chemistry* (12/10), e202300378 (**2023**).

3.  Blue Light-Promoted Synthesis of Thiochromenopyrroledione Derivatives via Titanium Dioxide-Catalyzed Dual Carbon–Carbon Bond Formation with Thioanisole and Maleimide Derivatives

    Pijush Kanti Roy, Sayuri Okunaka, Hiromasa Tokudome and Yutaka Hitomi, *Advanced Synthesis and Catalysis* (365/24), 4556-4561 (**2023**).

4.  Solvent-Dependent Photocatalytic Synthesis of Sulfoxides: Trifluoroethanol-Enhanced Conversion of Thioethers and Application in Ricobendazole Production

    Pijush Kanti Roy and Yutaka Hitomi, *Journal of Sulfur Chemistry*, submitted.